SHEAR STRENGTH OF REINFORCED CONCRETE BEAMS

MADE WITH RECYCLED COARSE AGGREGATE

by

Abdullah Mohsin Sagher

A Thesis Presented to the Faculty of the
American University of Sharjah
College of Engineering
in Partial Fulfillment
of the Requirements
for the Degree of

Master of Science in
Civil Engineering

Sharjah, United Arab Emirates

July 2016

Approval Signatures

We, the undersigned, approve the Master's Thesis of Abdullah Mohsin Sagher.

Thesis Title: Shear Strength of Reinforced Concrete Beams Made with Recycled Coarse Aggregate.

Signature	**Date of Signature** (dd/mm/yyyy)
_____	_____
Dr. Sami Tabsh Professor, Department of Civil Engineering Thesis Advisor	
_____	_____
Dr. Rami Haweeleh Associate Professor, Department of Civil Engineering Thesis Committee Member	
_____	_____
Dr. Lotfi Romdhane Professor, Department of Mechanical Engineering Thesis Committee Member	
_____	_____
Dr. Aliosman Akan Head, Department of Civil Engineering	
_____	_____
Dr. Mohamed Guma El-Tarhuni Associate Dean, College of Engineering	
_____	_____
Dr. Leland Blank Dean, College of Engineering	
_____	_____
Dr. Khaled Assaleh Interim Vice Provost for Research and Graduate Studies	

Acknowledgment

I would like to present my sincere gratitude to my thesis advisor Dr. Sami Tabsh. His door was always open for me. I thank him for his guidance, kindness and for sharing his knowledge and experience with me.

I would also like to thank all my friends who helped me throughout the laboratory work. Special gratitude is extended to Senior Lab Instructor Mr. Arshi Faridi and Lab Technician Mr. Mohammed Ansari for helping out in conducting the experimental tests in the laboratory.

Furthermore, thanks to the department of civil engineering for helping me with the graduate teaching assistantship. Special thanks to Head of the Civil Engineering department, Dr. Aliosman Akan, for helping me whenever needed.

My family has been always the rock that I rely on. For that and everything, I thank them.

Abstract

The Bee'ah's Waste Management Complex in the Emirate of Sharjah, UAE, has been producing aggregate from construction and demolition wastes for quite some time. However, such a product has not been utilized in structural applications. This research focuses on the concrete shear strength, which is a major component of the total shear resistance of reinforced concrete elements. Therefore, the objectives of this study are to investigate the behavior and develop design recommendations for the shear strength of reinforced concrete beams made with locally produced coarse aggregate. To do that, laboratory experiments on fifteen half-scale beams and associated theoretical predictive methods are utilized. The experimental part of the study addresses beams with different concrete compressive strengths, recycled coarse aggregate replacement percentages in the concrete mix, shear span-to-depth ratios and effective flexural steel reinforcement ratios. The experimental results are compared with corresponding findings from reinforced concrete beams employing natural aggregate. The theoretical part of the study considers available codified procedures for predicting the shear strength of concrete beams, such as the ACI 318 and CSA 23.3, as well as the strut-and-tie procedure, modified compression field theory and fracture mechanics approach. Results of the study showed that North American codes can adequately predict the shear strength provided by concrete when the shear span-to-depth ratio is large, but over-estimates it when the applied load is very close to the support. The strut-and-tie model predicted the shear strength of the tested beams much better than the other methods. The recycled concrete beams showed lower shear strength when the coarse aggregate replacement ratio was 50% and comparable shear strength when the replacement ratio was 100% than corresponding beams made with natural aggregate. The influence of concrete compressive strength on the shear capacity is much more predominant in the beams that were made with natural aggregate than those that were made with recycled aggregate. The effect of the flexural reinforcement ratio was not as significant in the beams made with concrete utilizing recycled aggregate as those made with natural aggregate. Until more tests on concrete beams made from different batches of recycled aggregate from Bee'ah become available, a 30% reduction factor is suggested to be incorporated into the shear strength equations in the relevant codes.

Search terms: *Concrete, Recycled Material, Aggregate, Reinforced Beams, Shear.*

Table of Contents

List of Figures

List of Tables

Chapter 1: Introduction

In this chapter, background information on the subject is provided, as well as the problem statement, objectives and scope of the study. Organization of the thesis into chapters is also included.

1.1. Introduction and Research Significance

The exponential increase in the number of people living on earth is increasing the need for building new houses and expanded infrastructure. This is particularly true in the UAE, where the economy is flourishing once again following the economic slowdown less than a decade ago, despite of the recent drop in oil prices [1]. Currently, reinforced concrete is considered to be the most suitable and economical building construction material. Thus, it is being produced in huge quantities to meet the construction sector's need of the Gulf Countries Council (GCC), where demand for concrete in the Kingdom of Saudi Arabia is set to reach over $30.5 billion this year. The UAE follows the Kingdom with an estimated requirement of $4 billion, while Qatar and Kuwait will be active in the market as well [2]. As coarse aggregate consists around 75% of concrete mixes by volume, it is the main contributor to the strength and performance of the concrete. The main source for aggregates is mining, which is done by blasting blocks of rocks from mountains and then crushing them to the required size, as shown in Figure 1. This process endangers the environment by various ways, such as destroying mountains, disturbing the habitations of wild animals, eroding soils, and producing huge quantities of Carbon Dioxide into the air [3]. Moreover, concrete wastes from construction demolition and precast concrete plants rejects dumped in landfills lay further burden on the environment. In Sharjah, Bee'ah's Waste Management Complex has among other facilities a Construction and Demolition Waste (CDW) recycling facility, shown in Figure 2 [4]. Such a facility is responsible for processing more than 6,000 tonnes of construction waste made up of concrete, bricks, wood, insulation and asphalt daily. This busy facility is responsible for waste reduction and recycling of construction, demolition and land clearing debris resulting from the construction industry. Using specialized machines, large pieces and

blocks of concrete and debris are broken down under great pressure and processed into fine and coarse aggregate.

Figure 1: Ready Rocks Quarries in Fujairah, UAE [5]

The coarse byproduct is then reused as aggregate for roads, pavements and walkways, or for landscaping. This process saves huge amount of natural resources, conserves energy, and lessen the burden on dump sites.

According to Bee'ah's Waste Management Complex, no structural use of the recycled coarse aggregate has been tried in the past, although recycled concrete has been used in Europe, North America and Australia for a long time. This makes the UAE construction industry somewhat lagging behind in this regard, although recently approved regulations in the Emirates of Dubai are in place regarding applying green building specifications on all new buildings in the Emirate of Dubai as per Circular No. 198 [6]. In the Emirate of Abu Dhabi, Plan 2030 launches a vision for sustainability as the foundation of any new development occurring in the capital. The guiding force behind this initiative is Estidama, which establishes a framework for quantitatively measuring the performance of sustainability beyond the planning and construction phases. It ensures that sustainability is always addressed through four important aspects: environmental, economic, social and cultural [7].

Figure 2: Bee'ah's Construction and Demolition Waste recycling facility [4]

1.2. Problem Statement

There have been many published studies in the global literature on the mix design, mechanical properties, and durability of concrete made with recycled materials [8-12]. The corresponding work on recycled concrete material in the region and has been compiled by Abdelfatah and Tabsh [13]. Work on structural behavior, structural member strength characteristics, and structural design recommendations lacks far behind research work at the material level. The flexural strength of reinforced concrete beams does not depend much on the mechanical properties of the concrete. The axial capacity of reinforced concrete tied or spiral columns can be somewhat predicted from the steel and concrete material strengths. However, shear strength of concrete inside structural elements is a very complex phenomenon that often cannot be extrapolated from the properties of the involved materials with ease. This can be demonstrated by comparing the shear strength of two concrete mixes having the same compressive strength but one made with normal-weight aggregate while the other is made with light-weight aggregate. Of course, the concrete which is made with normal-weight aggregate will always give higher shear strength than the corresponding that is made with light-weight aggregate. Based on the above, there is a need to investigate the shear strength of reinforced concrete members made with locally produced coarse aggregate from Bee'ah.

1.3. Objectives of Study

The main objectives of this study are to:

1- Investigate experimentally the shear strength behavior of reinforced concrete beams without stirrups made with locally produced recycled coarse aggregate from Bee'ah's plant in Sharjah.

2- Compare the shear strength behavior of the recycled concrete tested beams with corresponding beams made with natural coarse aggregate.

3- Use theoretical approaches to predict the shear behavior of reinforced concrete sections made with recycled coarse aggregate.

4- Provide practical guidelines and recommendations regarding the shear strength of reinforced concrete beams utilizing locally produced recycled coarse aggregate in the concrete mix.

1.4. Scope of Study

The scope of the study addresses the shear strength of beams without stirrups made with recycled coarse aggregate produced by Bee'ah. The research involves both experimental and theoretical studies. The experimental part consists of laboratory tests up to failure of 1500mm-long simply-supported beams with 150mmx300mm cross-sections that are flexurally reinforced with steel rebars in the tension zone. The beams are tested in the AUS structural laboratory inside a Universal testing machine (UTM), where the actuator's load and extension are recorded. Two percentages of recycled coarse aggregate replacement, 50% and 100%, are considered, in addition to the control (0%). Two concrete compressive strengths are targeted in the study, one about 25 *MPa* and another about 35 *MPa*, and two shear span-to-depth ratios are investigated, a/d = 1.15 and 2.50. In addition, two effective flexural steel reinforcement ratios, ρ= 0.0103 and 0.016 are utilized. Instrumentation of the tested beams consists of strain gauges installed on the steel rebars and concrete surface in compression at the location of maximum moment, plus linear variable differential transformers (LVDT) installed diagonally across the expected inclined crack in the maximum shear region to monitor the crack width with the increase in load. The theoretical part of the study involves the use of North American structural concrete code equations to predict the shear strength of concrete in beams without stirrups. Furthermore, more comprehensive shear strength predictive models available from the

literature, such the strut-and-tie, modified compression field theory and fracture mechanics are considered. The ultimate goal of the study is to make recommendations with regard to the potential of using recycled coarse aggregate in concrete beams subject to high shear forces without stirrups.

1.5. Organization of the Thesis

This thesis is organized into seven chapters. Chapter 1 introduces the subject matter, defines the problem, provides objectives, and suggests a methodology for solving the problem. Chapter 2 presents a brief history about shear design guidelines for reinforced concrete structures and introduces the outcomes of researches and codes' equations and models that are used to predict the shear strength of such structures. In Chapter 3, studies that have discussed the use of recycled concrete aggregate in concrete beams subjected to shear are presented along with their findings. Then, Chapter 4 explains the experimental program, tests setup, material properties, mix design and the preparation and casting of the beams used in this study. Chapter 5 presents the experimental results and observations. In Chapter 6, these results and findings are discussed thoroughly and compared with theoretical equations and models available in the literature that predict the shear strength of reinforced concrete structures. Finally, Chapter 7 summarizes the outcomes of this study, presents the conclusions and suggests recommendations for future studies on the subject.

Chapter 2: Background of Shear Strength

In this chapter, a brief history on shear design guidelines for reinforced concrete (RC) structures is presented, together with findings of studies on the shear behavior of such structures.

2.1. Shear Design History of RC

Numerous studies have been published in the literature to predict the shear strength behavior of RC members. Unlike flexure, the shear design guidelines of RC members are mainly empirically-based due to the complexity of the problem. Many researchers tried to come up with analytical methods to determine the shear strength of an RC structure that accounts for all the variables, but till now we have only what can be called semi-empirical methods. Empirical methods are usually cumbersome and require long hand-calculations. Moreover, using these methods require preserving the conditions and the assumption that were present during the experiments' implementation.

Failure of RC members due to shear is brittle and sudden, thus various safety factors are incorporated in the design equations to prevent this type of failure from happening. The shear behavior can be influenced by many factors such as the depth of the member, concrete compressive strength, nature of the aggregate and shear span-to-depth ratio (a/d), dowel action of the flexural reinforcement, etc. Throughout the second half of the past century, significant advances have been introduced to the structural codes design guidelines with regard to shear. To put that in perspective, prior to 1963 the ACI 318 code shear design procedure consisted of only four equations compared to around 40 equation in 2000 [14]. Most of the new equations were introduced to ACI in 1963 and 1971 after the famous incidence of Air-Force warehouses shear failure in 1955 [15].

Before the year 1900, there was a notion among a group of researches that shear failure in RC members is caused by the horizontal shear stress as shown in Figure 3. That idea came from their experience with wooden structures and shear-keys action

where the horizontal shear stress for a homogeneous beam is calculated using Equation (1):

$$v = \frac{VQ}{Ib} \tag{1}$$

v : Horizontal shear stress

V: Applied shear force

Q: Static moment of cross-section area, above or below the level being investigated for shear

I: Moment of Inertia

b: Width of cross-section

Thus, reinforced concreted was being considered as a continuation of the same material (i.e. wood) and that it can only resist low shear stress without transverse stirrups, see Figure 4. Based on that, stirrups were assumed to work as shear keys to resist higher shear stress [16].

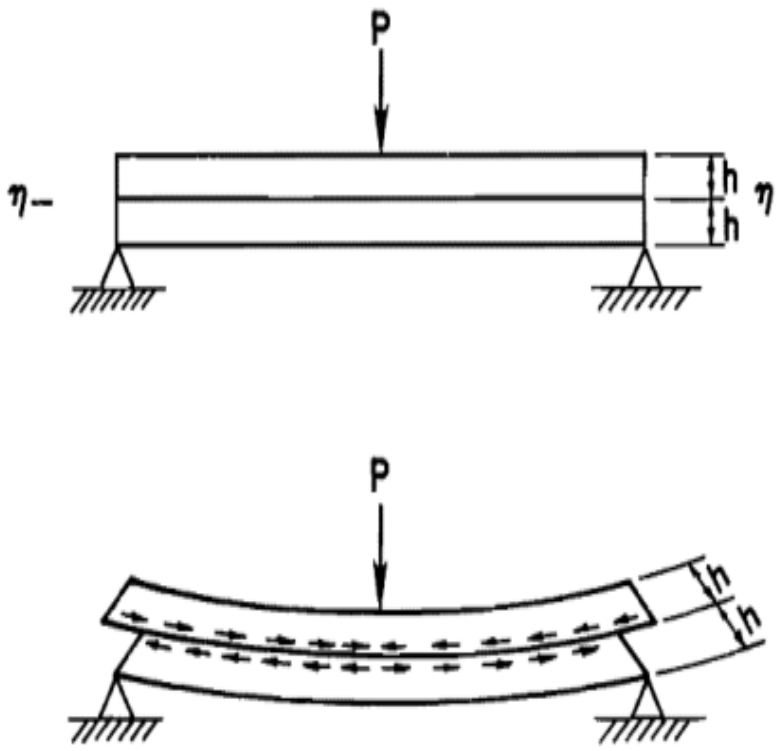

Figure 3: Horizontal shear stress thought to be the cause of shear failure [16]

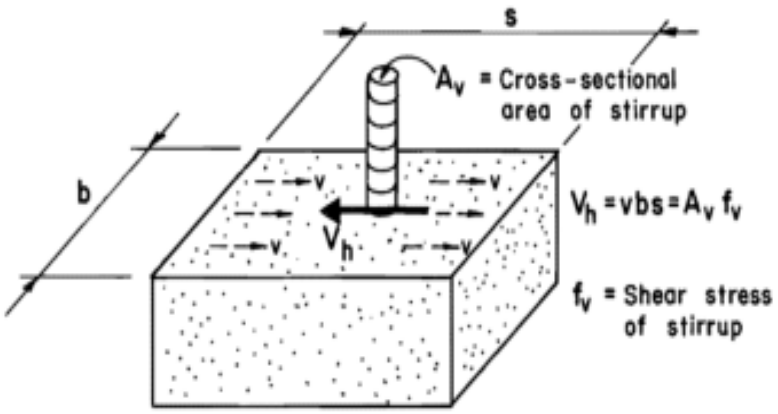

Figure 4: The role of stirrups in resisting horizontal shear [16]

Ritter, in 1899, came up with the first truss model to approximate the shear behavior in beams believing that the shear failure is due to diagonal tension in concrete [17]. He assumed that when a beam is subject to external shear force, it behaves like a truss where the concrete in the top will act as compression chord, the bottom longitudinal steel will act like tension chord and the concrete between the cracks will be acting like diagonal struts, as shown in Figure 5. He also assumed that the diagonal cracks are inclined by 45º and he neglected the tensile stresses between them. That led to very conservative results when compared to experimental results. The debate between the horizontal shear theory and the diagonal stress theory was ended mainly by the effort of Morsch in 1920s. He proved that the shear failure is caused by diagonal tension. Like Ritter, Morsch also proposed the truss analogy for the shear design and introduced the use of truss model for torsion.

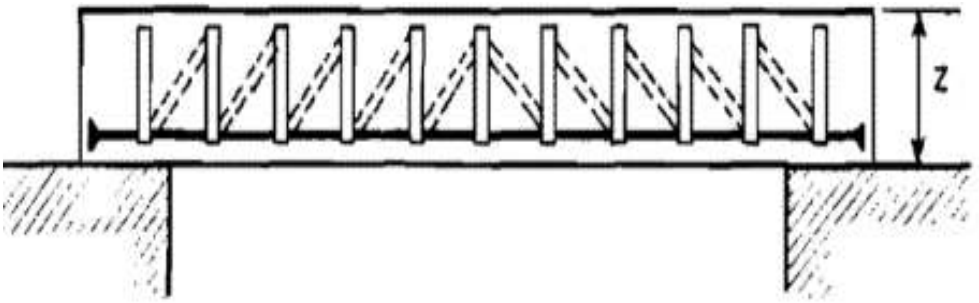

Figure 5: Ritter Truss Model [16]

The truss model neglects the tension in the concrete, and the amount of the transverse steel reinforcement continued to be calculated based on Ritter's truss model till the 1950's. By that time, factors other than concrete compressive strength (f'_c), were being investigated as shear failure contributors. A. P Clark introduced the span-to-depth ratio (*a/d*) in 1951, where "*a*" is the distance from the shear force to the support and "*d*" is the effective beam depth [18]. He noticed that the shear strength of beams having smaller (*a/d*) ratio is higher than the shear strength in the beams having larger (*a/d*). That can explained by the fact that the regions under the concentrated shear force and at the support are subjected to local compression. This local state of compression delays the appearance of the diagonal tension cracks which leads to increasing the shear strength. Thus, the shorter the distance between the external concentrated load and the support, the more difficult it is for the diagonal cracking to happen as depicted Figure 6.

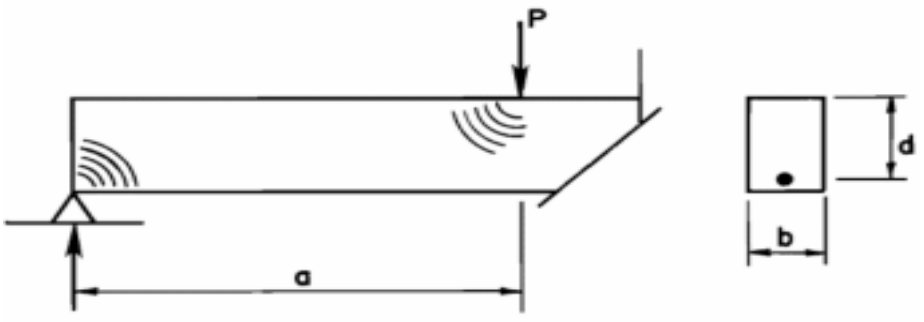

Figure 6: (*a/d*) ratio and local compression concept [18]

In 1962, the ACI committee 326 introduced an equation to calculate the shear strength that a member without transverse reinforcement can carry. The equation is:

$$V_c = \left(0.16\sqrt{f_c'} + 17\rho_w \frac{V_u d}{M_u}\right) b_w d \leq 0.29\sqrt{f_c'} b_w d \qquad (2)$$

where V_u is the factored shear force (*N*) at the required section, M_u is the corresponding factored bending moment (*N-mm*) at the same section, f'_c is the concrete compressive strength (*MPa*), b_w is narrowest width of the beam, $\rho_w = \frac{A_s}{b_w d}$ is

the reinforcement ratio, and the ratio ($V_u d/M_u$) shall not exceed unity. ACI 318 code of 1963 adopted the above V_c equation, but also added a new equation, Equation (3), for calculating the area of the required transverse steel reinforcement [19].

$$A_v = \frac{V_s * S}{f_y * d} \tag{3}$$

where V_s is the difference between the ultimate shear strength of a member and the shear strength that is carried by the concrete as per Equation (2). In the following versions of ACI 318 code, the shear design procedure remained almost the same with minor modifications, particularly related to use of lightweight concrete [20, 21].

Several other models were proposed to understand how shear transfer through the RC members without transverse reinforcement. Most of them fall in three main categories [22]:

1. Mechanical or physical models for structural behavior and failure.
2. Fracture mechanics approaches.
3. Nonlinear finite element analysis.

In the first category lie models such as the truss model and strut-and-tie model used in this study. Three different models based on fracture mechanics are discussed and used in chapter 6. The nonlinear analysis is not utilized in this research.

Kani played a pioneer role when he proposed "Kani Tooth Model" in 1964 and introduced the term "Size Effect" [23]. In the 1970s, Fenwick, and Paulay deduced that a great percentage of shear resistance is a results of aggregates interlocking [24]. Great steps for understanding shear behavior of RC members were accomplished in 1980s when the Modified Compression Field Theory (MCFT) was introduced at the University of Toronto by Vecchio and Collins [25].

2.2. Shear Strength Models

Important methods for predicting the shear strength of RC members, such as the truss analogy, Tooth model, strut-and-tie model, and MCFT, are discussed in the following sections. International building codes are mainly based on the mentioned

approaches and models. For example, the shear design approach used in the ACI 318 building code, which will be discussed later, is based on the truss analogy with 45 degree-inclined struts. Because the actual angle of inclination is usually less than 45º, the ACI 318 predictions are usually thought to be very conservative. While in Europe, the strut-and-tie model has more influence on the building codes.

2.2.1. Truss analogy. One of the earliest proposed models was Ritter Model or Truss Model [26]. Although this model was proposed by Ritter in 1899, it still renders the basis of shear design provisions for many modern building codes around the world. The model assumes that the concrete resists no tension at all and that the cracked beam behaves like a truss. A simple beam in positive bending under the application of shear force will have the concrete on top resists compression and the longitudinal reinforcement at the bottom resists tension. The inclined struts, which may be assumed to be at 45° angle, will be compressed while the vertical stirrups will take the tension imposed by the shear forces [27] as shown in Figure 7. Based on the latter assumptions and from the equilibrium along the vertical direction shown in Figure 8, we can find that the shear strength of the stirrups is:

$$V_s = n * A_s * f_y \tag{4}$$

where '*n*' is number of stirrups that crosses an inclined shear crack (which can be assumed equal to *d/S*, where *S* is the spacing of the stirrups and d is the effective depth of flexural reinforcement), A_s is the cross-sectional area of the legs and f_y is the yielding stress of the transverse reinforcement [28].

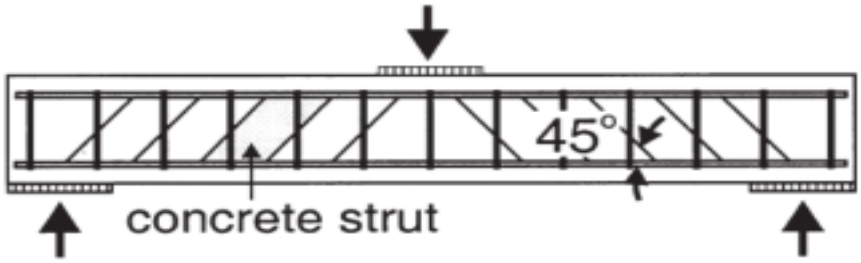

Figure 7: Truss Model [28]

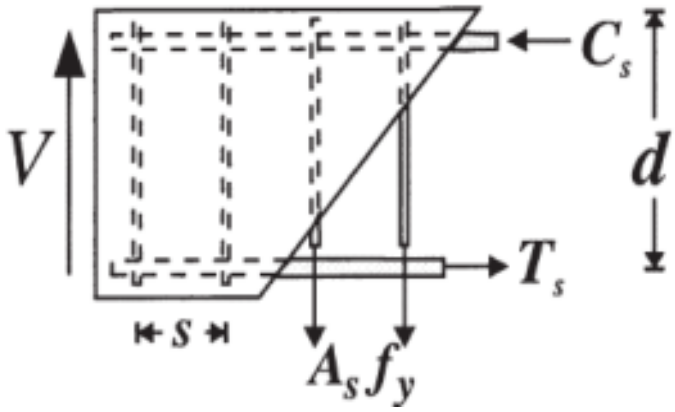

Figure 8: Free Body Diagram [28]

Experience proved that this model gives very conservative predictions. And because of that, the ACI code introduced the term "concrete contribution" V_c which was defined as the shear value at the commencement of the first diagonal crack in the beam [27]. Thus, the total shear strength of the beam was equal to the sum of the shear resistance in the transverse steel reinforcement plus the shear resistance from concrete contribution as shown in see Equation (5).

$$V = V_c + V_s \tag{5}$$

2.2.2. Tooth model. The Tooth Model was introduced by Kani as a trial to come up with a "Rational Theory" of shear in 1964 [23]. He proposed that the concrete between two adjacent cracks are analogous to tooth of a comb and they act like cantilevers attached to the compressed concrete zone in the beam as depicted in Figure 9. These teeth are loaded horizontally by the shear force from the boned reinforcement. He explains, based on that assumption, that the secondary cracks are result of bending of the "teeth".

Fenwick and Paulay and then Taylor , evaluated Kani's Model. They pointed out that the teeth are restricted by the friction between the cracks' surface and by the dowel action of the longitudinal reinforcement and can't bend freely [17]. Many other researchers further investigated and developed Kani's Model. They studied the flexure shear cracking mechanism for RC slender beams without web reinforcement.

Figure 9: Kani's Model "Tooth Model" [23]

Reineck in 1991, derived a formula for the ultimate shear force for members without axial neither pre-stress forces [29]. His formula includes in the dowel action from the longitudinal reinforcement and the friction between the cracks. The results that are derived from this theoretically derived formula are very comparable to test results as well as many other empirically derived formulas [17].

2.2.3. Strut-and-Tie model. Strut-and-Tie model (STM) was developed based on the Low-Bound Theorem of Plasticity [30].

The model is an extension of the truss model for beams with uniform diagonals' inclination. It requires minimum amount of reinforcement, distributed in both direction; longitudinally and vertically. That will ensure the redistribution of the internal stresses post cracking. In this model, shear is transferred to the support directly through diagonally compressed strut as shown in Figure 10. Both, longitudinal and vertical, reinforcement hold the concrete on both sides of the crack and tie them together to prevent the beam from failing due to shear. Thus, the concrete will resist the compression in the region where the stresses are being transferred to the support, and the reinforcement will be under tension trying to restrain the diagonal crack from further opening. As the depth of the beam increases, more shear will be transferred through the compression strut. It means that this model is more suitable for deep beams. Walraven and Lehwalter further investigated the model and introduced the factor "Size effect" [31]. Experimental results show that deep beams with (*a/d*) less than 2.5 usually fail in two mechanisms: splitting of the

diagonal crack or crushing of concrete [32]. The model might also be used for finding shear strength of slender beams; however the results are feared to be unsafe.

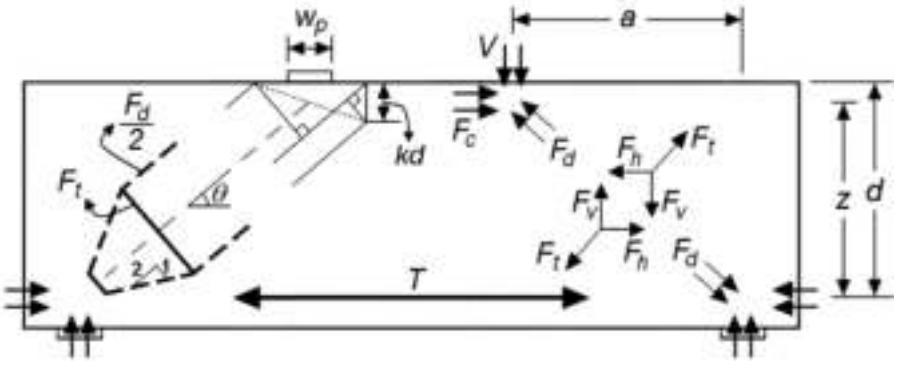

Figure 10: Strut-And-Tie Model [32]

2.2.4. Modified compression field theory. The Truss Model assumes that the diagonal compression strut to be inclined by 45º with respect to the horizontal reinforcement. However, in order to make accurate calculations, the angle should be defined precisely.

Wagner, in 1929, experimented with thin-web metal girders studying post-buckling shear resistance [33]. He assumed that the angle of principle tensile stain would be known by knowing the angle of the diagonal tensile stress. This assumption is known as Tension Field Theory.

In 1974, Collins and Mitchell [34, 35], using the compatibility condition, the equilibrium equation and the stress-strain relationship of concrete and steel, proposed an approach to predict the behavior of a beam subjected to shear and called it the Compression Field Theory (CFT). The CFT deals with cracked concrete as a new material that has its own stress-strain relationship characteristics. However, CFT did not account for the tensile stresses in the concrete between the cracks which caused its predictions to be somewhat conservative. In 1986, Vecchio and Collins [25] modified CFT to include the tensile stresses in the concrete between the cracks and employed experimental results to make average stress–average strain relationship for the cracked concrete and called their new method the Modified Compression Field

Theory (MCFT). They used, in their experimental study, concrete element reinforced orthogonally with steel in X and Y directions as shown in Figure 11.

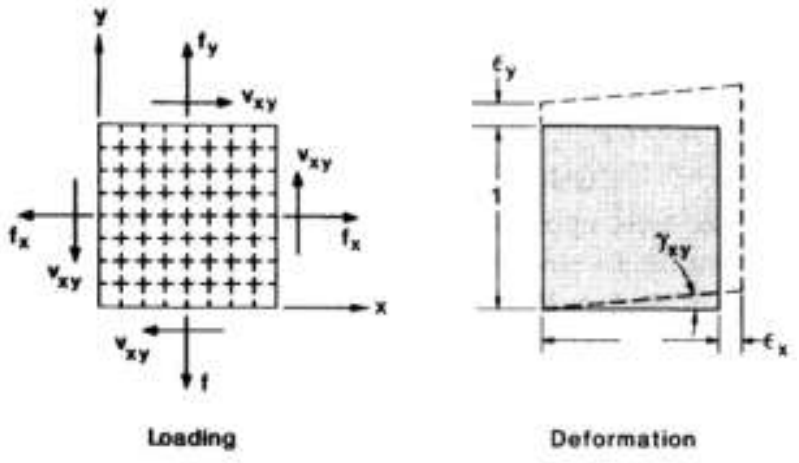

Figure 11: Membrane Element [25]

The element was subjected to uniform axial stresses f_x and f_y and uniform shear stress v_{xy} on its edges. It is assumed that the edges remain straight and parallel when the element is deformed. The deformation is defined by normal strains $\varepsilon_x, \varepsilon_y$ and the shear strain γ_{xy} as shown in Figure 12.

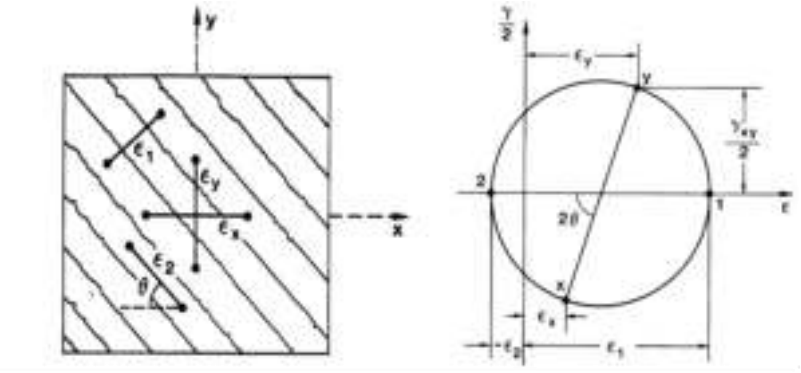

Figure 12: Normal strains in concrete element [25]

The objective was to relate the stresses in-plane (f_x, f_y and v_{xy}) to the strains in-plane (ε_x, ε_y and γ_{xy}). To do that, they used the three conditions mentioned earlier. The first condition is the compatibility and it states that any deformation in the concrete matches the same deformation in the reinforcement and any change in strain in the concrete is accompanied by equal change in strain in the reinforcement. Therefore:

$$\varepsilon_{sx} = \varepsilon_{cx} = \varepsilon_x \tag{6}$$

and

$$\varepsilon_{sy} = \varepsilon_{cy} = \varepsilon_y \tag{7}$$

Knowing the three strains (ε_x, ε_y and γ_{xy}) and using Mohr's Circle, the strain in any direction can be known form geometry. Hence, Equations (8), (9) and (10) can be derived:

$$\gamma_{xy} = \frac{2\,(\varepsilon_x - \varepsilon_2)}{tan\theta} \tag{8}$$

$$\varepsilon_x + \varepsilon_y = \varepsilon_1 + \varepsilon_2 \tag{9}$$

and

$$tan^2\theta = \frac{\varepsilon_x - \varepsilon_2}{\varepsilon_y - \varepsilon_2} = \frac{\varepsilon_1 - \varepsilon_y}{\varepsilon_1 - \varepsilon_x} = \frac{\varepsilon_1 - \varepsilon_y}{\varepsilon_y - \varepsilon_2} = \frac{\varepsilon_x - \varepsilon_2}{\varepsilon_1 - \varepsilon_x} \tag{10}$$

Equilibrium condition is the second condition. The stresses in the concrete and in the reinforcement resist the applied external forces. From the free-body diagram shown in Figure 13, we find, in *X* direction:

$$f_x = f_{cx} + \rho_{sx}.f_{sx} \tag{11}$$

and in *Y* direction:

$$f_y = f_{cy} + \rho_{sy}.f_{sy} \tag{12}$$

and

$$v_{xy} = v_{cx} + \rho_{sx}.v_{sx} \tag{13}$$

$$v_{xy} = v_{cy} + \rho_{sy}.v_{sy} \tag{14}$$

assuming that:

$$v_{cx} = v_{cy} = v_{cxy} \tag{15}$$

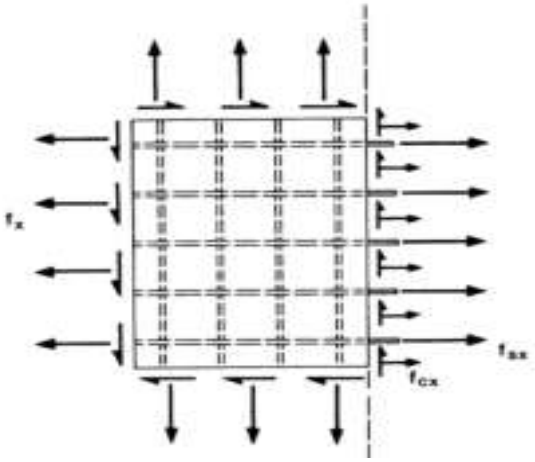

Figure 13: Free-Body Diagram [25]

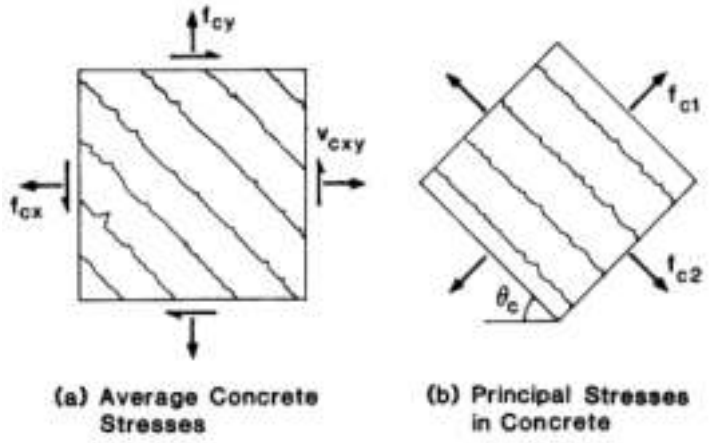

Figure 14: Average and principal stresses in concrete [25]

From Mohr's circle for the average stresses in concrete in Figure 15:

$$f_{cx} = f_{c1} - v_{cx}/tan\theta_c \tag{16}$$

$$f_{cy} = f_{c1} - v_{cx} \,.\, tan\theta_c \tag{17}$$

and

$$f_{c2} = f_{c1} - v_{cxy}.\left(tan\theta_c + \frac{1}{tan\theta_c} \right) \tag{18}$$

The third condition they used is Stress-Strain Relationship. A relationship is needed to relate the average stresses and the average strains in both, concrete and reinforcement. Even though, the average stress-average strain relationships for the concrete and for the reinforcement are not independent of each other, they are assumed to be so for simplicity. It was also assumed that the axial stress in the reinforcement is due only to the axial strain in the reinforcement and that it does not resist shear stress on the plane normal to the reinforcement.

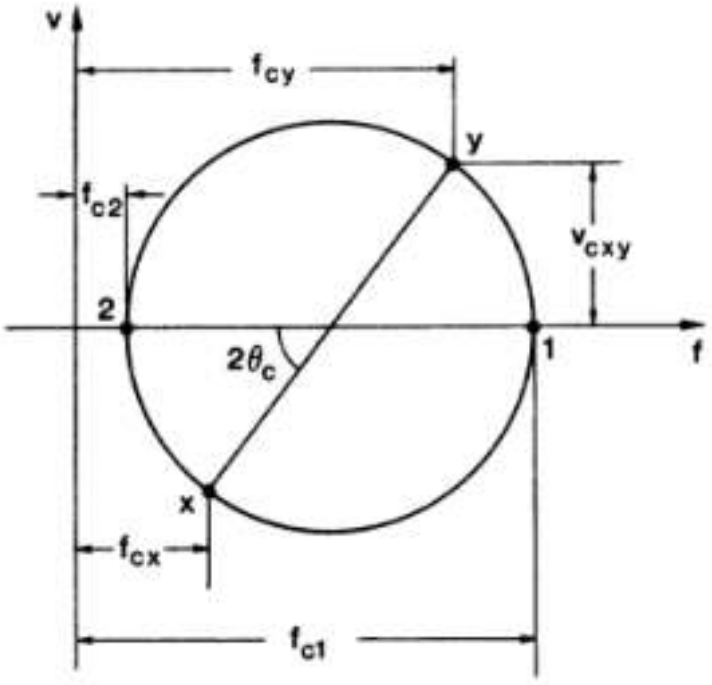

Figure 15: Mohr's Circle for the average concrete stresses [25]

The relations in Figure 16 will be adopted:

$$f_{sx} = E_s \,.\, \varepsilon_x \;\leq\; f_{yx} \tag{19}$$

$$f_{sy} = E_s \,.\, \varepsilon_y \;\leq\; f_{yy} \tag{20}$$

$$v_{sx} = v_{sy} = 0 \tag{21}$$

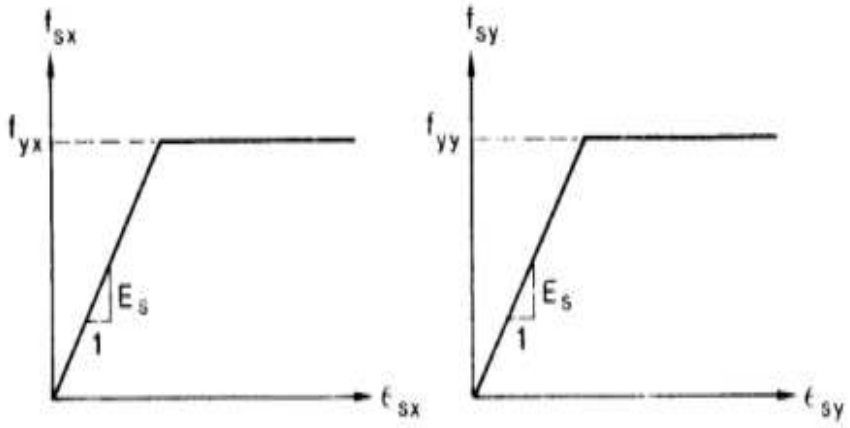

Figure 16: Stress-Strain Relationship for reinforcement [25]

For the concrete, they assumed reasonably that the stress axes coincide with the strain axes. And after the analyzing the test data, they found out that the principle compressive stress in the concrete (f_{c2}) is not only a function of the principle compressive strain (ε_2), but also a function of the co-existing principle tensile strain (ε_1). In other words, the cracked concrete subjected to high tensile strain in the direction perpendicular to the compressive strain is weaker than concrete in standard cylinder test. Hence, they suggested the following relationships:

$$f_{c2} = f_{c2max} \cdot \left[2\left(\frac{\varepsilon_2}{\varepsilon'_c}\right) - \left(\frac{\varepsilon_2}{\varepsilon'_c}\right)^2\right] \tag{22}$$

$$\frac{f_{c2max}}{f'_c} = \frac{1}{0.8-0.34\,\varepsilon_1/\varepsilon'_c} \leq 1.0 \tag{23}$$

The principle tensile stress (f_{c1}) in concrete has linear relationship to the principle tensile strain (ε_1) prior to cracking. After that it, the relationship becomes inverse where f_{c1} decreases with the increase of ε_1. They suggested the following relationship prior to cracking:

$$f_{c1} = E_C \,.\, \varepsilon_1 \tag{24}$$

where $E_C = 2\, f'_c \,/\varepsilon'_c$

After cracking, the relationship becomes:

$$f_{c1} = \frac{f_{cr}}{1+\sqrt{200\,\varepsilon_1}} \tag{25}$$

in which $\varepsilon_1 > \varepsilon_{cr}$

All the previous stress and strain relationships use average stress and average strain. They don't describe the local variations of stresses and strains. Vecchio and Collins found that the tensile stresses in the reinforcement at the crack are higher than the average, and those in the reinforcement at the mid-distance between the cracks are less. On the other hand, the tensile stress in the concrete at the crack is zero, but it is higher than the average at the mid-distance between the cracks Figure 18.

Their observation indicates that the reinforcement ability to transfer the tensile strength at the crack may govern the ultimate strength of the shear. Hence:

$$f_{sxcr} \leq f_{yx} \tag{26}$$

$$f_{sycr} \leq f_{yy} \tag{27}$$

Vecchio and Collins presented a solution technique in their paper that one can refer to for a step-by-step procedure for determining the response of a stressed element.

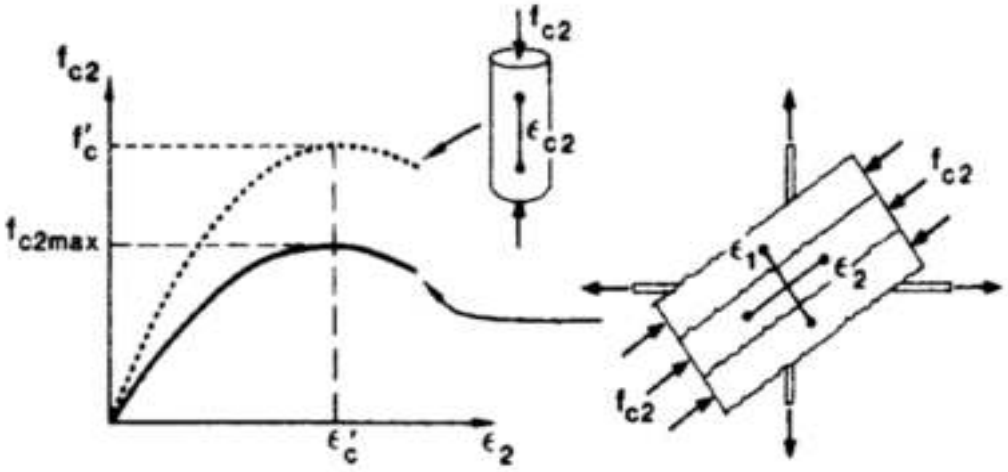

a) Stress-Strain relationship for cracked concrete in compression

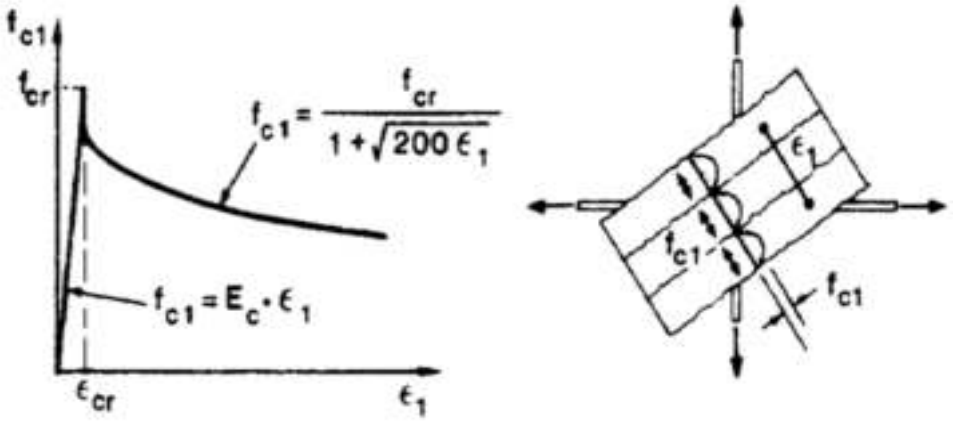

b) Stress-Strain relationship for cracked concrete in tension

Figure 17: Average Stress-Strain relationship for cracked concrete [25]

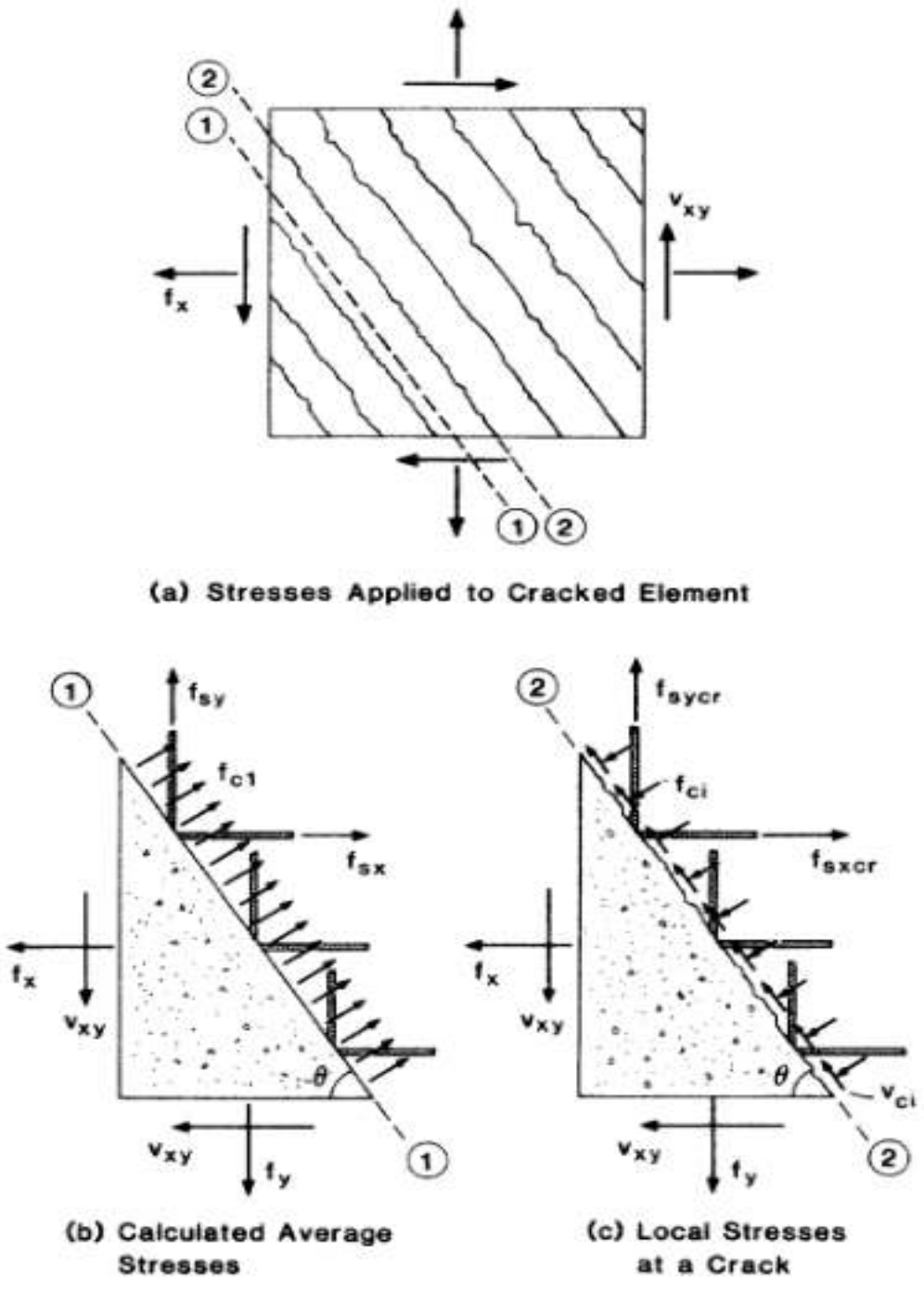

Figure 18: Local stresses at crack and calculated average stresses [25]

Chapter 3: Literature Review

In this chapter, a literature review on reinforced concrete beams made with recycled aggregate and subjected to shear forces is presented. The literature review considers recently published research on the subject. Both experimental and theoretical studies are considered.

Gonzalez and Fernando considered beams made with 50% RA and with different amount of shear reinforcement in their study [36]. The recycled aggregate were obtained from a single source. The beam had a cross-section of 200*mm* x 350*mm*, and they were tested with a span-to-depth ratio of 3.3 as shown in Figure 19.

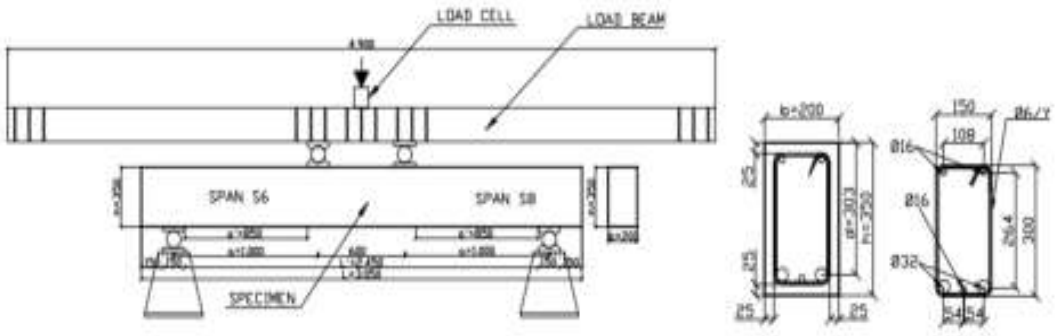

Figure 19: Typical beam and testing setup of Gonzalez et al. [36]

The testing setup maintained two spans for each beam, where each span had a different shear reinforcement (one of them had stirrups of 6*mm* or no shear reinforcement and the other had stirrups of 8*mm*). As expected, the flexure cracks started to appear near the center of the beams. Then, flexure cracks appeared away from the center until one of them propagated as a diagonal crack. The beams without shear reinforcement failed abruptly after the diagonal crack extended towards the loading point, while the beams with shear reinforcement showed more load-carrying capacity. The test results were compared to the prediction of Response-2000 software package -which is based on the MCFT- and with various codes, such as the Spanish code (EHE), Canadian code (CSA 23.3), American code (ACI 318) and the Australian code (AS3600). All the predictions were conservative and thus the codes used are

feasible to predict shear strength of recycled aggregate beam. They reported that the equations of the codes gave closer results when the beams were without shear reinforcement. On the other hand, the MCFT gave better predictions for the beams with shear reinforcement. They concluded that, there is no significant difference in the shear strength and the deflection of NA beams and the 50% RA beams.

Ajdukiewicz and Kliszczewicz [37] conducted a comparative study between beams and columns made from either RA or NA, both of them coming from different sources. They tested 16 series of beams, each one of them consists of three beams. The beams in each series contain the same amount of reinforcement, but each beam is prepared using different percentage of RA. The 16 series differ in three characteristics; the source of the RA (i.e. river gravel, crushed granite and crushed basalt), the combination and the type (natural or recycled) of fine and coarse aggregates and the concrete compressive strength (low, medium and high). The cross-section and the longitudinal view of the beams are presented in Figure 20.

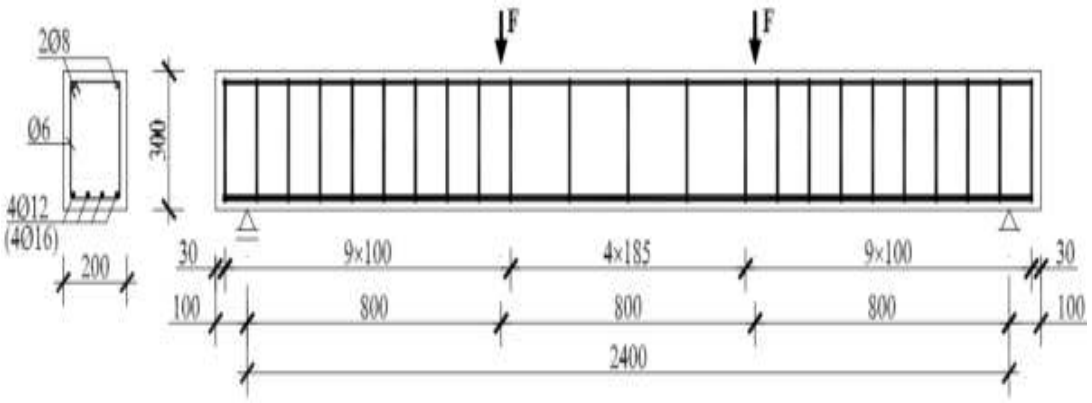

Figure 20: Typical Beam dimensions and detailing [37]

As expected, the flexure-type beams failed due to yielding of reinforcement steel with minor damage in the compressed concrete. Also, with the increase of replacement percentage (R%), the modulus of elasticity decreases and deformability of a beam increases. On the other hand, the beams that were designed to study shear had the initial cracks appearing due to flexure, but then after, the shear cracks started to appear till the shear failure happened as appears in Figure 21.

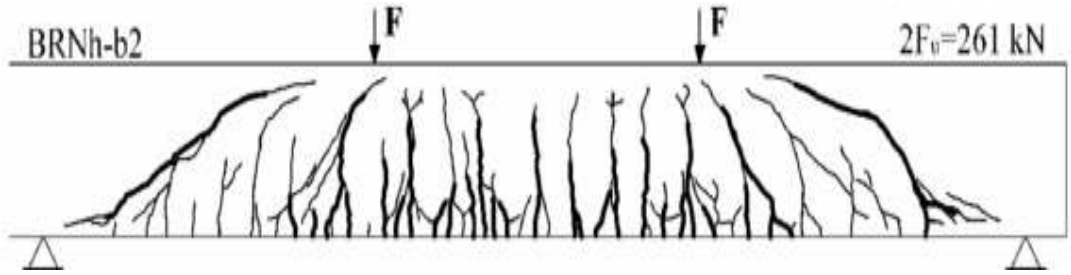

Figure 21: Typical shear failure and the cracks propagation [37]

The load-deflection relationships of two beam series in shear up to failure are shown in Figure 22. The first series (*m*) refers to medium strength concrete beams, whereas the second series (*h*) denotes high strength. To understand the labeling of the beams, '*B*' stands for basalt as the source of the aggregates, the first and the second '*N*'s indicates that the fine and the coarse aggregates, respectively, are natural. If '*R*' is used in lieu of '*N*', that means the aggregate is recycled. The '*b*' indicates that this is a beam (not a column); while number '*1*' means that the bottom reinforcement of the beam is (*4Ø12*) as opposed to number '*2*' which means that the bottom reinforcement of the beam is (*4Ø16*). As can be noticed in Figure 22, the authors' conclusion was that the difference observed in the behavior of beams made from RA and NA beams is insignificant regardless to the replacement ratio R%. Hence, it is possible to use good quality RA, both fine and coarse, in structural members; however, the serviceability should be taken in consideration.

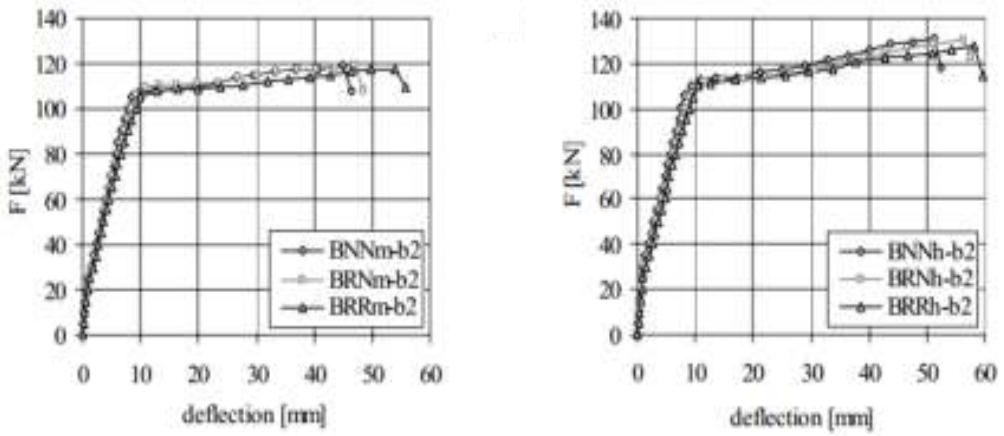

(a) Medium-strength beams (b) High-strength beams

Figure 22: Load-Deflection relationships of two beam series [37]

Fathifazl et al. published a paper in 2010 about the shear strength of RC beams made with RA and without stirrups [38]. In that paper, they argued that the reduction in the strength and properties of RC beams made with recycled aggregate is not inherited. In their opinion, the cause of the reduction is due to the use of conventional method of mixing, which replaces the amount of the natural aggregate in a mix with recycled aggregate directly. Those methods of mixing neglect the residual mortar around the recycled aggregates, causing the concrete made with RA to have more mortar when the new mortar is added compared to the NA concrete. In other words, the shear plane go through less aggregate and more mortar in the RA concrete due to the presence of the residual mortar. So, the lack of aggregate in RA concrete is the reason behind the reduction in shear strength reported by some researchers. To validate their proposition, they made two types of concrete mixes. The first is a mix made with natural aggregate and proportioned as per ACI code method. The second is a mix made with RA and the proportions were calculated using their proposed method which is called Equivalent Mortar Volume (EMV). Also, their study included other parameters such as shear span-to-depth ratio and beam size. Twenty beams were tested and all of them had no shear reinforcement. They concluded that the failure mode was very similar in both RA concrete and NA concrete. Moreover, using EMV method increases the aggregate interlock mechanism and consequently the shear resistance. Thus, the international building codes, particularly the ACI-318, the CSA23.3-04 and Eurocode 2, can be used to predict the shear strength of RC beams made with RA irrespective to (a/d) and the depth of the beam.

Schubert et al. used RA to cast and study the shear of RC slabs without shear reinforcement [39]. Fourteen slabs were casted and tested in four-point setup. A section of the slabs is shown in Figure 23 where the width was 500mm. The compared the experimental results to various models, such as Swiss Standard, Eurocode 2. The results indicated that the shear strength of RC beams made with RA are promising and very close to those made with NA, and that it can be predict using the utilized building standards.

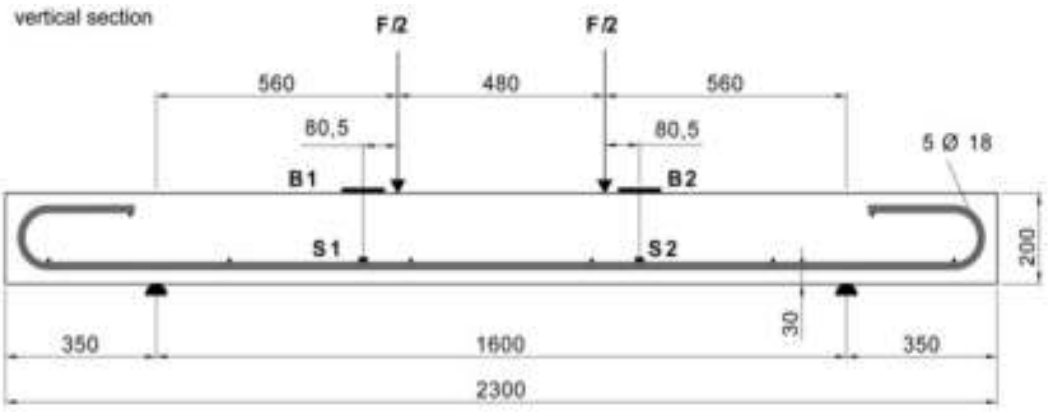

Figure 23: Schubert et al. utilized slab section [39]

Some studies reported that the RA that were obtained from high strength concrete, can be used to produce new concrete that have shear strength comparable or superior to concrete made with NA. To examine these reports, Lian et al experimentally studied beams made with 25% RA along with beams made with NA [40]. The recycled aggregate were from a crushed concrete of strength 25-30 *MPa*. They made three beams from each concrete mix with dimensions of 150*mm* x 200*mm* x 1200*mm*. The typical beam detailing and the testing setup are shown in Figure 24. The shear span-to-depth ratio varied in the tested beams, namely *a/d* =1.0, 1.5 and 2.0.

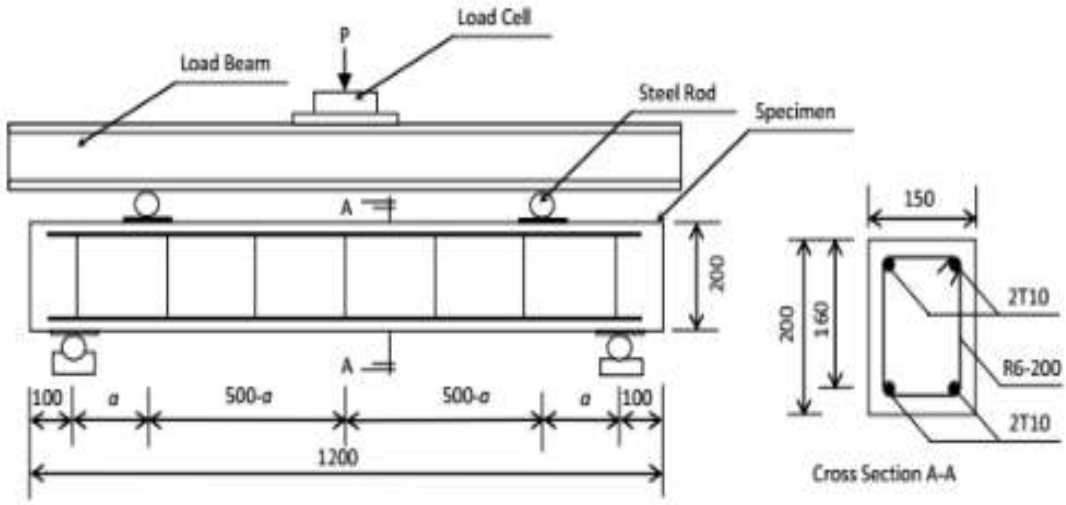

Figure 24: Typical beam and testing setup of Lian et al. [40]

Their results suggested that the RA beams performed very well or even slightly better for *a/d*= 1.5 and 2.0.However, they shear strength was less when *a/d*= 1.0 when compared to the NA beams. Regarding the effect of shear span-to-depth ratio, their conclusions matched the existing literature which proved the decrease in the shear strength when the *a/d* is increased. Finally, upon comparing their experimental results with the existing codes; such as ACI 318, AS3600 and the Eurocode-2, they found that all the predictions were conservative and that the ACI 318 predictions were the closest.

Significant research about shear strength of RC with 100% replacement (by volume) of RA was done by Arezoumandi et al. [41]. They casted six beams using convectional concrete with the help of local ready-mix supplier. Those same beams were crushed, after being tested, to produce the RA that were used in the RA concrete beams for results comparison purposes. The compressive strength of both concrete types was taken as the average of three standard cylinders. Also, splitting tensile strength and flexure strength were tested and all the results are presented in Table 1. All the beams had a cross-sectional area of (300*mm* x 460*mm*) and length of 4300 *mm*. The targeted compressive strength of both mix designs was 35 *MPa*. To study the effect of the longitudinal reinforcement ratio (r) on shear strength, they used three different values; ρ= 1.27%, ρ = 2.03% and ρ = 2.71%. However, all the beams were without transverse reinforcement within the test regions, the beams detailing are shown in Figure 25.

Table 1: Fresh and hardened concrete results [41].

Property	CC-1	CC-2	RAC-1	RAC-2
Slump (mm)	140	205	210	130
Air content (%)	8.5	9.0	6.5	5.0
Unit weight (kg/m^3)	2330	2340	2180	2220
Compressive strength* (MPa)	37.2	34.2	30.0	34.1
Split tensile strength* (MPa)	3.48	2.97	2.55	2.65
Flexural tensile strength** (MPa)	3.45	2.90	2.81	2.76

The testing of beams was done in a load frame that has two 490-kN servo-hydraulic actuators to apply load at two points on the beam. The load was applied with displacement control method using 0.5 *mm*/minute load.

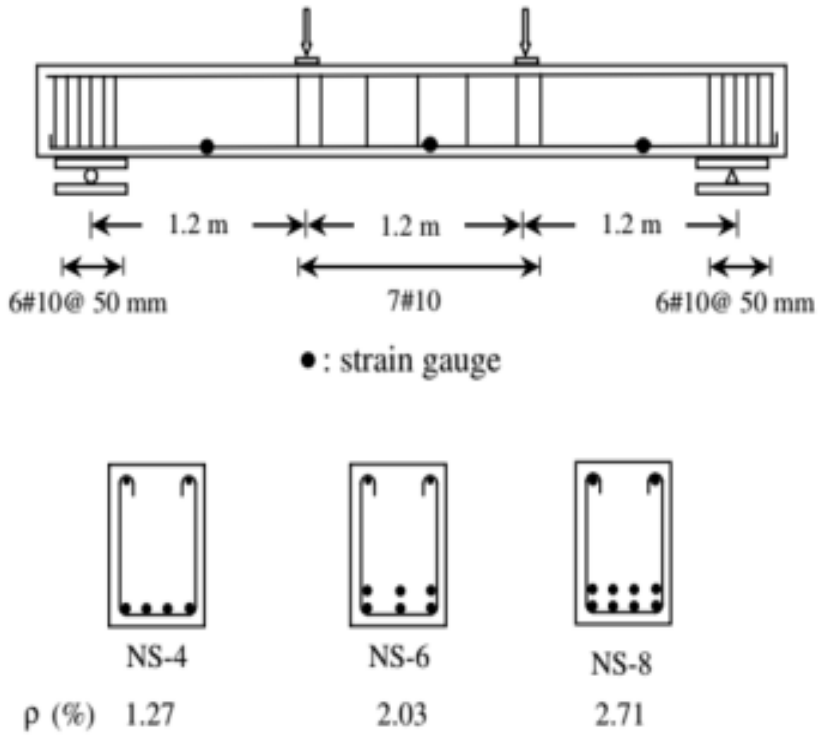

Figure 25: Beams detailing and test setup [41]

The test results are presented in Table 2. The deflection at mid-span results showed that the beams behaved elastically till the first flexure crack occurred. Increasing the load forced the beams to develop flexure-shear cracks. It is noted that the propagation of cracks in both CC and RA concrete was similar. The beams with higher reinforcement ratio had higher capacity, as expected. They attributed that to the increase in the dowel action and tightened cracks which led to higher aggregate interlock. The shear strength results of the beams were compared to the shear strength predicted from various codes as shown in Table 3. The range of V_{test}/V_{code} for the CC was from 0.80 to 1.54, while it was 0.76 to 1.38 for the RA concrete, see Table 3. It is noted that the ratio of the RA is lower than the ratio of CC. Furthermore, the author used fracture mechanics approach to predict the shear strength. They used three

different equations; Bazant equation, Gastebled equation and Xu equation, [42-44]. Those equations will be discussed further in Chapter 6.

Table 2: Arezoumandi et al. test results summary [41]

Sections		f'_c (MPa)	V_{test} (kN)	$v_{test} = V_{test}/b_w d$ (MPa)	$v_{test}/\sqrt{f'_c}$
CC					
NS-4	1	37.3	121.2	1.0	0.16
	2	34.2	129.9	1.1	0.18
NS-6	1	37.3	143.2	1.3	0.21
	2	34.2	167.0	1.5	0.25
NS-8	1	37.3	173.5	1.5	0.25
	2	34.2	170.8	1.5	0.26
RAC					
NS-4	1	30.0	114.8	0.9	0.17
	2	34.1	113.0	0.9	0.16
NS-6	1	30.0	143.2	1.3	0.23
	2	34.1	124.1	1.1	0.19
NS-8	1	30.0	131.4	1.2	0.21
	2	34.1	140.3	1.2	0.21

Table 3: V_{test}/V_{code} for the selected codes [41]

Section		AASHTO	ACI	AS-3600	CSA	Eurocode 2	JSCE
CC							
NS-4	1	0.82	0.98	0.97	0.80	0.90	1.09
	2	0.95	1.10	1.07	0.93	0.99	1.21
NS-6	1	0.94	1.24	1.02	0.92	0.96	1.16
	2	1.23	1.51	1.23	1.20	1.15	1.39
NS-8	1	1.11	1.50	1.12	1.09	1.16	1.28
	2	1.13	1.54	1.14	1.11	1.17	1.29
Ave.		1.03	1.31	1.09	1.01	1.05	1.24
COV (%)		14.7	18.2	8.4	14.8	11.5	8.5
RAC							
NS-4	1	0.85	1.04	0.99	0.83	0.91	1.11
	2	0.78	0.96	0.93	0.76	0.86	1.05
NS-6	1	1.05	1.38	1.10	1.03	1.03	1.25
	2	0.81	1.12	0.91	0.79	0.85	1.04
NS-8	1	0.84	1.27	0.92	0.83	0.94	1.04
	2	0.86	1.27	0.94	0.85	0.97	1.06
Ave.		0.87	1.17	0.96	0.85	0.93	1.09
COV (%)		11.0	13.6	7.4	11.2	7.2	7.5

Table 4 shows the latter results comparison. It was found out that Xu equation gave the best accuracy. They also, compared the test results with the MCFT which is incorporated in several codes such as the AASHTO LRFD-10 and CSA 23.3-04. The ratio (V_{test}/V_{MCFT}) shows that the MCFT method underestimates the shear strength of all beams. Also, the load-deflection behavior shows good agreement when compared between the experimental results and the MCFT results. They concluded that all the methods that were used to predict shear strength in their study are feasible and can be applied on beams made with 100% recycled aggregate.

Table 4: Comparison with fracture mechanics and MCFT [41]

Section		V_{test}/V^{b}	V_{test}/V^{b}	V_{test}/V^{c}	V_{test}/V_{MCFT}
CC					
NS-4	1	1.20	1.05	1.02	1.08
	2	1.32	1.16	1.13	1.19
NS-6	1	1.26	1.23	1.20	1.17
	2	1.51	1.48	1.45	1.48
NS-8	1	1.37	1.45	1.40	1.32
	2	1.38	1.47	1.44	1.33
Ave.		1.34	1.31	1.27	1.26
COV (%)		8.1	14.2	14.5	11.3
RAC					
NS-4	1	1.21	1.07	1.06	1.09
	2	1.14	1.01	1.00	1.02
NS-6	1	1.35	1.33	1.32	1.25
	2	1.12	1.10	1.08	1.01
NS-8	1	1.11	1.18	1.18	1.05
	2	1.14	1.21	1.19	1.08
Ave.		1.18	1.15	1.14	1.08
COV (%)		7.6	10.0	10.0	8.1

In recent study, Knaack and Kurama studied the flexure and shear behavior of 12 twin pairs of normal strength concrete beams [45]. They used the direct volume replacement method (DVR) to produce two mix designs; R = 50%, in addition to the conventional concrete mix R =0%. The RA source was foundations of 1920s plant. The targeted compressive strength was 40 *MPa* with (*w/c*) ratio = 0.44. The casted beams were 2.0m length with a cross-section area of 150*mm* x 230*mm*, reinforced with either critical flexure or critical shear reinforcement as shown in Figure 26. The

beams were loaded monotonically until their failure using four-points test setup with loading rate of 2.5 *mm*/minute, see Figure 27. During the test, the initial cracks and their propagation were observed. For the shear critical-section beams, the initial cracks were due to flexure since the beams were slender. Then, diagonal cracks started to appear and propagate causing a sudden failure when the shear strength was reached. The results showed that increasing R% had more reduction effect of the initial stiffness of RA beams than on their flexure and shear strength.

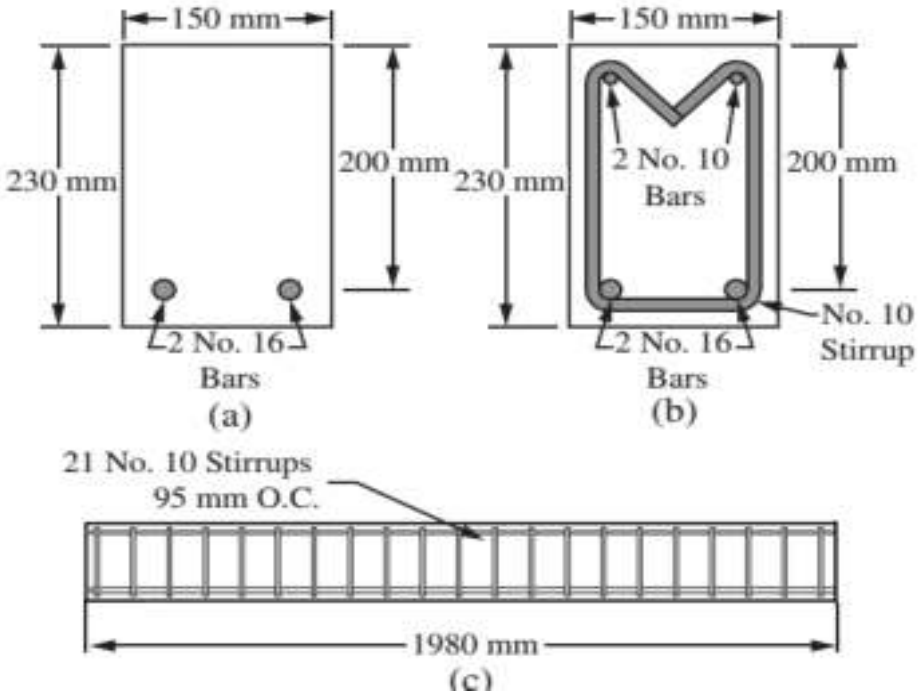

Figure 26: (a) Shear-critical section (b) Flexure-critical section (c) Beam [45]

Furthermore, in their efforts to predict the behavior of the beams, they used DRAIN-2DX software package [46] to model the beams. They also did the convectional analysis using ACI-318. Comparing all the results (i.e. experimental, from DRAIN-2DX and the ACI-318 analytical results), a good agreement was found among them as shown in Figure 28. Hence, they concluded that the existing design standards are applicable for the design of RA concrete. An interesting note by the authors was that even though each pair of the beams was saw-cut in half from longer beam, the load-deflection behavior was different between them. That renders how the

concrete material is so complex and shows the inherit variability in the behavior of concrete members.

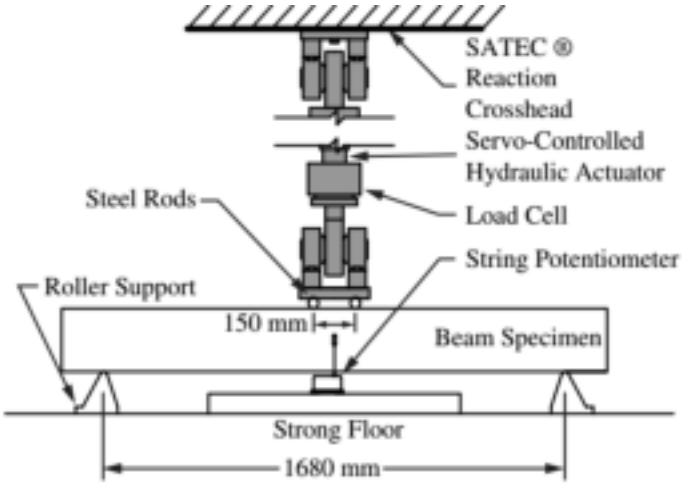

Figure 27: Testing setup [45]

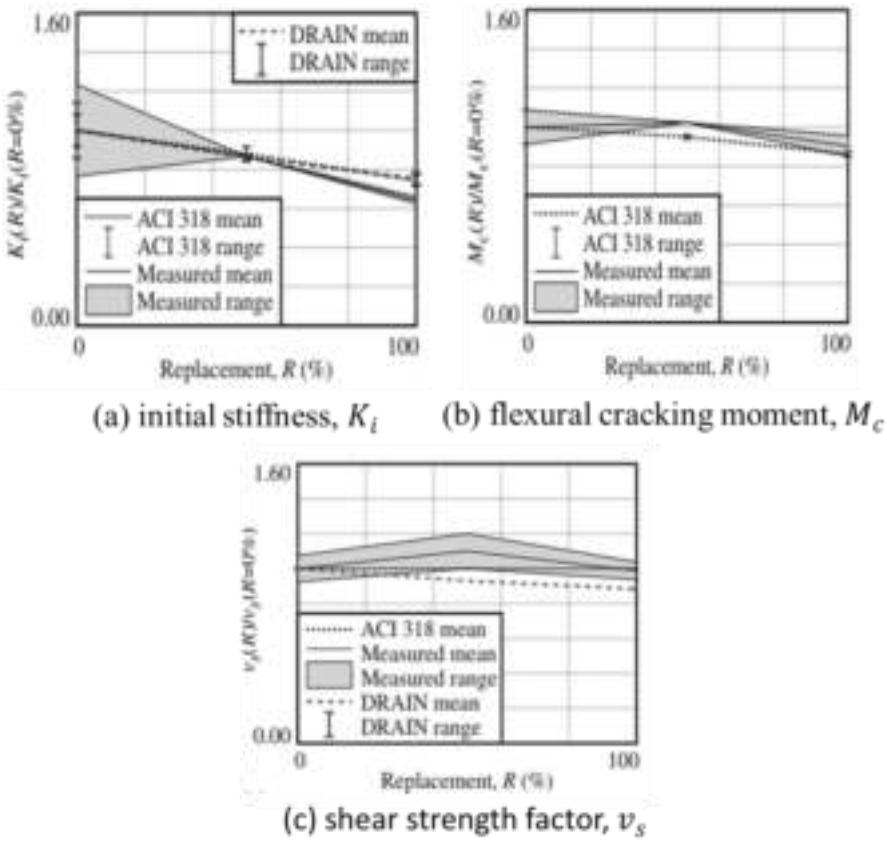

Figure 28: Effect of RCA on shear-critical beam behavior [45]

Arezoumandi et al. extended his previously mentioned study in another paper discussing the RA replacement ratio on the shear strength of RC beams [47]. In addition to the 100% RA mix and the NA mix, they used 50% RA mix. The experimental results were compared to the results obtained from the methods mentioned in the earlier paper. The conclusions were that the shear strength of beams made with 100% RA is less by 11% than the beams made with NA. However, beams made with 50% RA gave similar shear strength to the beams made with NA. Nevertheless, all the methods that were used were able to predict the shear strength for all beams with conservancy regardless to the RA replacement ratio.

Rahal and Alrefaei did an experimental study in which they used different RA replacement ratios and investigated their effect on the shear strength of RC beams [48]. They tested five beams with target compressive strength of 50 *MPa*. The RA replacement ratios were 0%, 10%, 20%, 35% and 100%. The detailing of the beams is shown in Figure 29.

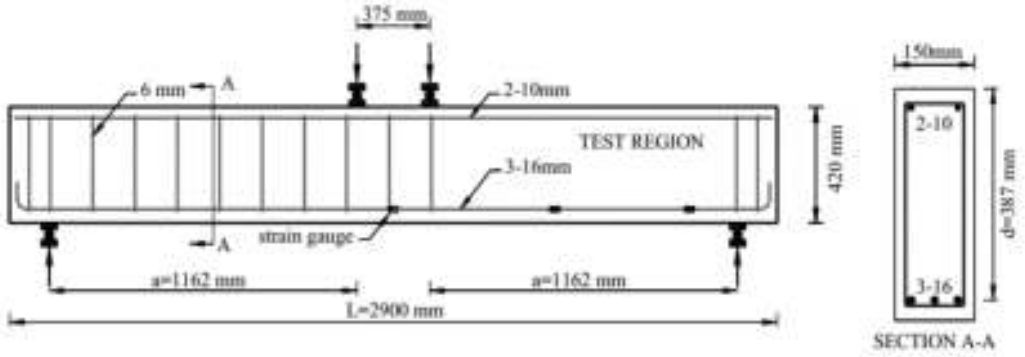

Figure 29: Detailing of the beams in Rahal and Alrefaei study [48]

The shear strength was normalized with respect to the compressive strength of each beam. The results showed that the shear strength in RA concrete beams was in fact higher than the control beam. But, they also found that the modulus of elasticity was reduced in the RA beams by up to 14%. However, they recommended that these conclusions should be interpreted carefully with respect to the testing variations. The results are presented in Figure 30 and Figure 31.

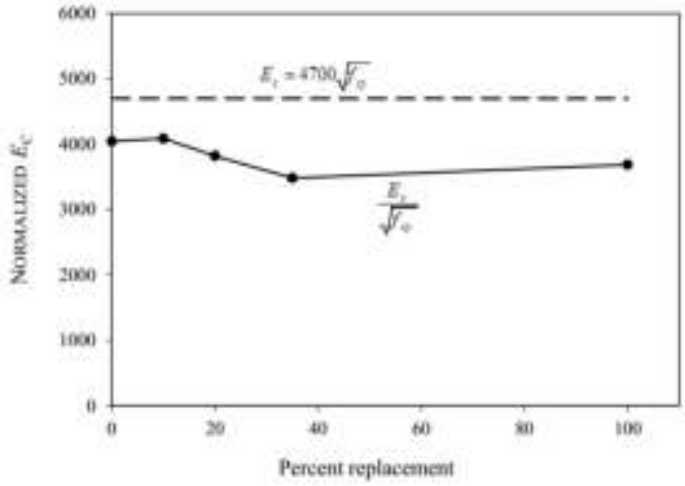

Figure 30: Effect of replacement ratio on Modulus of Elasticity [48]

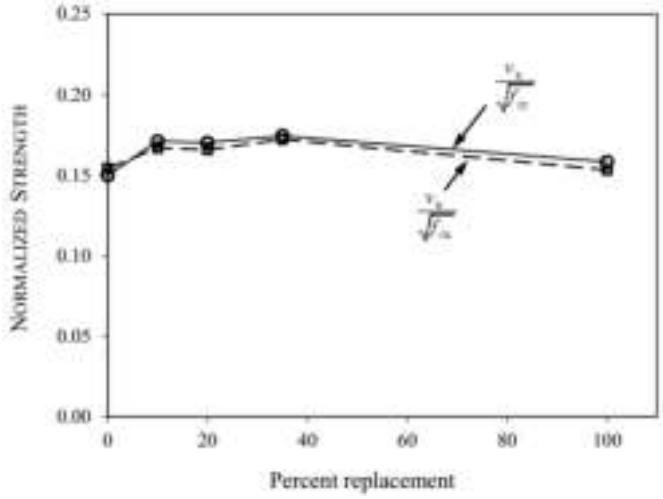

Figure 31: Effect of replacement ratio on normalized shear strength [48]

Snag-Woo et al. found similar results in their study [49]. They tested 15 beams made with different replacement ratios. To study the size effect on the beams, their width was varied from 200*mm* to 400*mm* and their effective depth from 300*mm* to 600*mm*. Their results showed that the change in the width had no size effect on the beams made with RA; however, the shear strength decreased with the increase of the effect depth regardless to the replacement ratio. More importantly, they found out that the shear reduction and the crack pattern in RA beams were similar to those made with NA.

Also, similar conclusions were reached in a study that was done by Deng et al. [50], in which they considered nine beams with three different coarse aggregate

replacement ratios equal to 0%, 50% and 100%. They found out that the shear strength is slightly affected in the RA beams when compared to NA beams, if the compressive strength among the beams was maintained constant among the beams.

In addition to the considered studies in this chapter, there have been a few other less significant research studies addressing the shear strength behavior of RC beams made with recycled coarse aggregate and subjected to shear. Such studies include the work of Choi et al. in 2010 [51], Al-Zahraa et al. [52], Ikponmwosa and Salau [53] in 2011, Wang et al. in 2013 [54], and Yu and Yin in 2015 [55].

Chapter 4: Experimental Program

The experimental program is introduced in this chapter, which includes the test beams properties, notations, test machine characteristics, and test setup.

4.1. Laboratory Work

A well-planned experimental program is essential for yielding good results and practical design recommendations. Since shear strength of concrete is a complex phenomenon, the best way to study it is by experimental laboratory studies, complemented later by some theoretical work. The experimental part of this study consists of fabricating and casting fifteen half scale beams of length 1.5 m and a cross-section of 150*mm* x 300*mm*. All beams were reinforced with two No. 10 bars at the top and two No. 16 (or two No. 20) bars at the bottom, as shown in Figure 32.

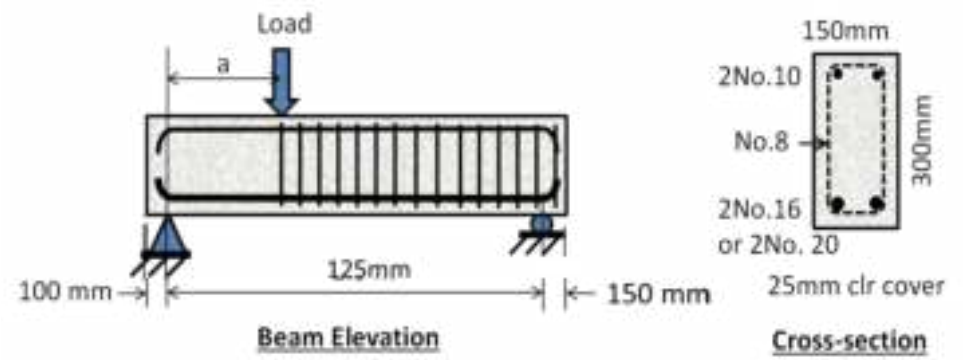

Figure 32: Dimensions and reinforcement details of the test beams

The instrumented region of the beam that is subjected to high shear was free from stirrups; whereas, the remaining region had No. 8 stirrups at 100*mm* spacing in order to protect that region from premature failure. The beams were tested inside the 2,500 kN Instron UTM in the AUS structural lab. They were simply-supported at a span of 1.3m or 1.25m and subjected to a single concentrated load in a displacement-controlled environment at a rate of 0.5 *mm*/minute. Strain gauges were installed on the longitudinal bottom rebars and top surface of the concrete beam to record the tensile

strain in the steel and compressive strain in the concrete at the location of maximum moment as the load was increased. One LVDT was mounted at the bottom of the beams at the location of the applied load to measure the vertical deflection. Another LVDT was installed diagonally on the side of the tested beams across the expected inclined cracks in the maximum shear region to monitor the average crack width with the increase in load. The test setup and instrumentation are summarized in Figure 33.

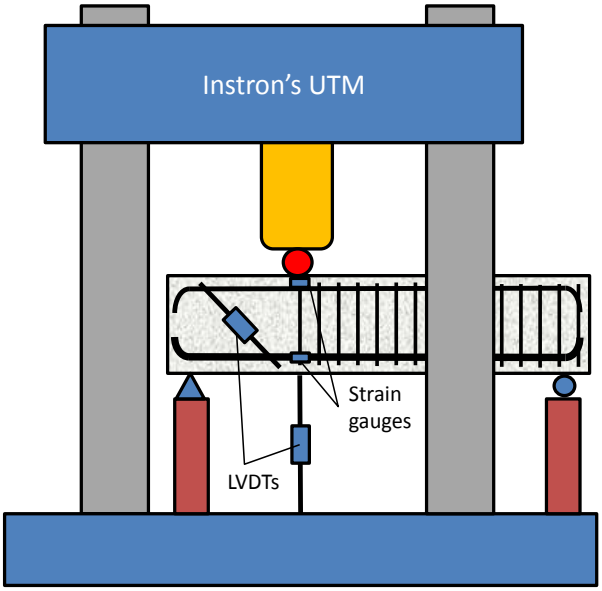

Figure 33: Test setup and instrumentation

The testing program consists of 15 beams, some of which had 25 *MPa* targeted compressive strength and some 35 *MPa*. For each compressive strength group, three beams were made with 50% recycled coarse aggregate, three with 100% recycled coarse aggregate, and the remaining three were made with natural aggregate. One of the most important parameters in shear behavior of reinforced concrete beams is the shear span-to-depth ratios, *a/d*. The experimental program considered two different locations of the applied load on the test beams, such that *a/d* = 1.15 or 2.5. Furthermore, some of the test's beams had an effective flexural steel reinforcement ratio ρ_w= 0.0103; whereas, the remaining beams had ρ_w= 0.016. A summary of the experimental test program is presented in Figure 34 and the labeling of the 15 test beams is shown in Table 5.

At every load increment, the results of the experimental program included the applied load, beam deflection, concrete strain, steel strain, and average crack opening. The obtained data allowed for the developing plots involving: (1) Load-deflection relationship, (2) Shear-deflection relationship, (3) Shear-average shear strain relationship, (4) Moment-curvature relationship, and others. Such plots help in determining the shear strength, ductility, and residual strength beyond ultimate capacity of concrete beams made with recycled aggregate. The results of the test program were studied, analyzed, compared with available data from past literature and discussed later. Video recording was utilized throughout the experimental test program to identify the first flexural crack, first shear crack, pattern of the observed crack development and mode of failure at the end.

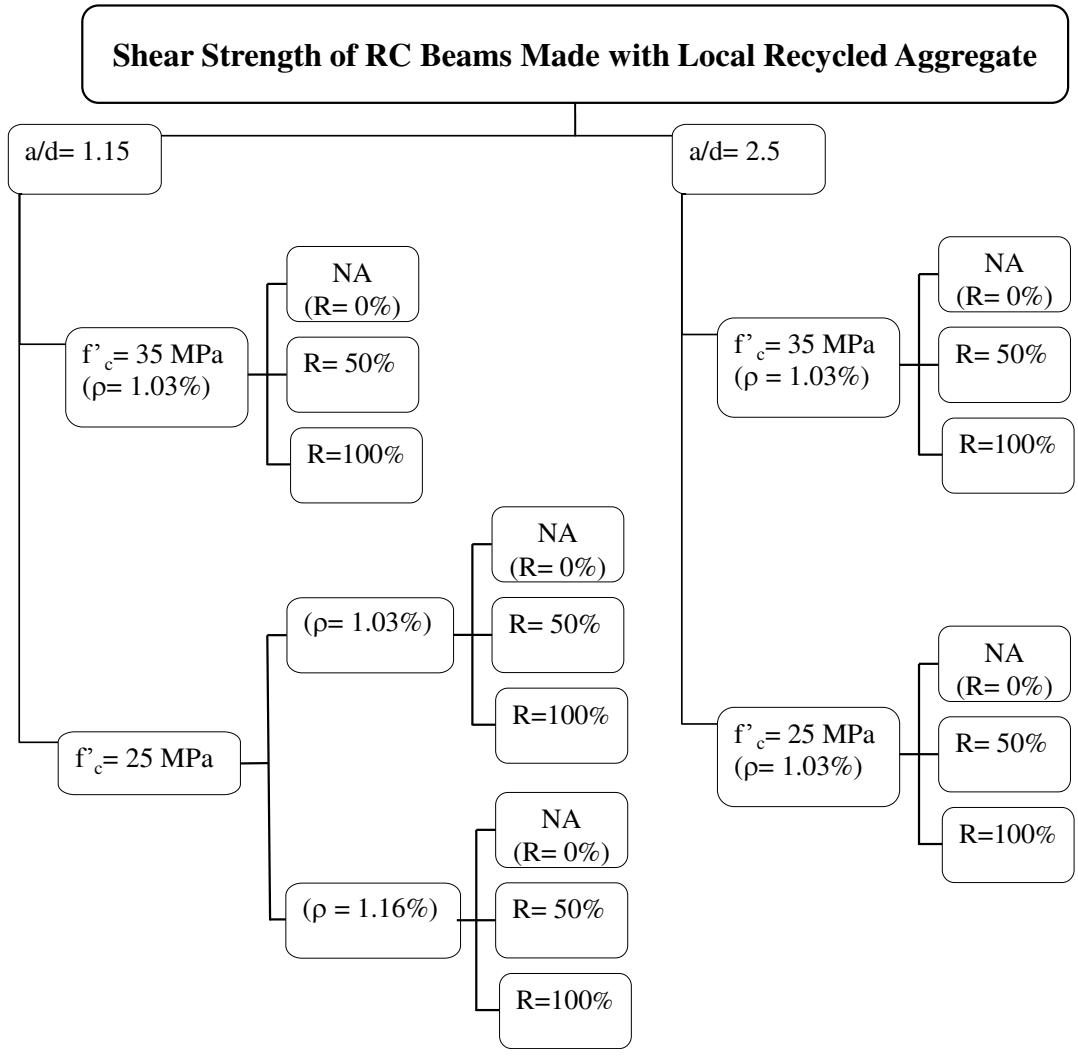

Figure 34: Summary of the experimental test program

Table 5: Beams properties and notations

Serial No.	Beam ID*	*a/d*	Target f'_c (*MPa*)	% Coarse Aggregate Replacement	ρ
1	NA-L-1-HR	1.15	25	0	0.016
2	NA-L-1-LR		25	0	0.0103
3	NA-M-1-LR		35	0	0.0103
4	R50-L-1-HR		25	50	0.016
5	R50-L-1-LR		25	50	0.0103
6	R50-M-1-LR		35	50	0.0103
7	R100-L-1-HR		25	100	0.016
8	R100-L-1-LR		25	100	0.0103
9	R100-M-1-LR		35	100	0.0103
10	NA-L-2.5-LR	2.5	25	0	0.0103
11	NA-M-2.5-LR		35	0	0.0103
12	R50-L-2.5-LR		25	50	0.0103
13	R50-M-2.5-LR		35	50	0.0103
14	R100-L-2.5-LR		25	100	0.0103
15	R100-M-2.5-LR		35	100	0.0103

* NA=natural aggregate, R=recycled aggregate, LR = low ρ, HR = high ρ, L=low f'_c, and M= medium f'_c

4.2. Material

4.2.1. Concrete. ASTM type I Ordinary Portland cement was brought from Sharjah cement factory and was used in all concrete mixes. Since this research is focusing on coarse aggregate influence on shear strength of RC beams, all the fine aggregate that were used were natural aggregate. Two types of fine aggregates were utilized: dune sand and crushed sand. In concrete mixes where the target compressive strength was 25 *MPa*, the percentile of dune sand and crushed sand were 35% and 65% of the total fine aggregate weight, respectively. While in the mixes where 35 *MPa* was the target compressive strength, the dune sand was 40% and the crushed sand was 60% of the total weight of the fine aggregate. The Fineness Modulus of the

fine aggregate is presented in Table 6. On the other hand, two coarse aggregate sizes were used: 10*mm* and 20*mm*. In all mixes, the 10*mm* maximum size aggregate constituted 35% of the coarse aggregate total weight. The remaining 65% percent were 20*mm* maximum size aggregate. The properties of both, natural aggregate and recycled aggregate, are shown in Table 7. The concrete mixes proportions are presented in Table 8. The RA concrete mixes were prepared by directly replacing the NA aggregate in the concrete mix, with the same weight of RA. Everything else was kept the same to prevent introducing any additional parameters to the study.

Table 6: Fineness Modulus of the natural fine aggregate

	Dune Sand	Crushed Sand	Combined Dune and Crushed Sand
F.M	0.74	3.51	2.03

Table 7: Coarse aggregate properties

Aggregate Type	Size (*mm*)	Bulk S.G	Apparent S.G	Absorption	Moisture	LA Abrasion	Crushing Value
Natural	10	2.84	2.7	3.99	1.18	24	19.1
	20	2.64	2.73	1.16	0.78	18.6	19.8
Recycled	10	2.36	2.72	5.61	1	27.3	21.5
	20	2.4	2.71	4.72	1.83	31.9	24.1

Table 8: Concrete mix proportions

Mix	Crushed Sand (*Kg*)	Dune Sand (*Kg*)	NA coarse Aggregate (Kg)		RA coarse Aggregate (Kg)		Cement (*Kg*)	Water (*Kg*)
			10 *mm*	20 *mm*	10 *mm*	20 *mm*		
NA-L	579	314	336	614	-	-	293	171
RA-L	579	314	-	-	336	614	293	171
NA-M	391	257	358	693	-	-	500	229
RA-M	391	257	-	-	358	693	500	229

For each beam, two cylinders (300*mm* x 150*mm*) and two cubes (150*mm* x 150*mm* x 150*mm*) were casted to test the compressive strength at the beam testing day. Testing of cylinders and cubes samples is shown in Figure 35 and Figure 36, respectively. Two compressive strengths were targeted, low and medium, since common RC structures rarely employ high-strength concrete. For each of them, the mix proportions were kept the same regardless of the aggregate replacement ratio. In other words, for the beams that have compressive strength target of 25 *MPa*, the mix proportions were kept the same whether the beam has R=0%, R=50% and R=100%. The natural fine and coarse aggregate (10*mm* and 20*mm*) were brought from local supplier as well. As mentioned, the recycled coarse aggregate were brought from Bee'ah's recycling plant in Sharjah. It was noticed during the casting of the beams that with the increase of the replacement ratio of the coarse aggregate, the workability of the concrete decreased. That's why super-plasticizer was added in order to increase the workability without adding more water; so that, the water/cement ratio was constant for the same type of beams.

Typical stress-strain curves for the targeted low and medium strength concrete made with recycled coarse aggregate are presented in Figure 37 and for the natural aggregate concrete in Figure 38. As expected, the relationships show that the modulus of elasticity for the recycled aggregate concrete is slightly lower than that for the natural aggregate concrete.

Figure 35: Testing cylinders and a crushed sample

Figure 36: Testing cubes and a crushed sample

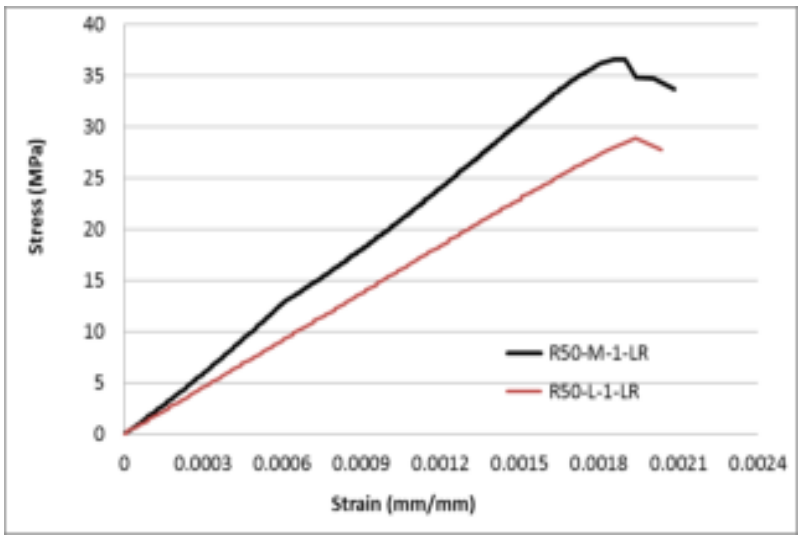

Figure 37: Stress-Strain relationships for the recycled aggregate concrete

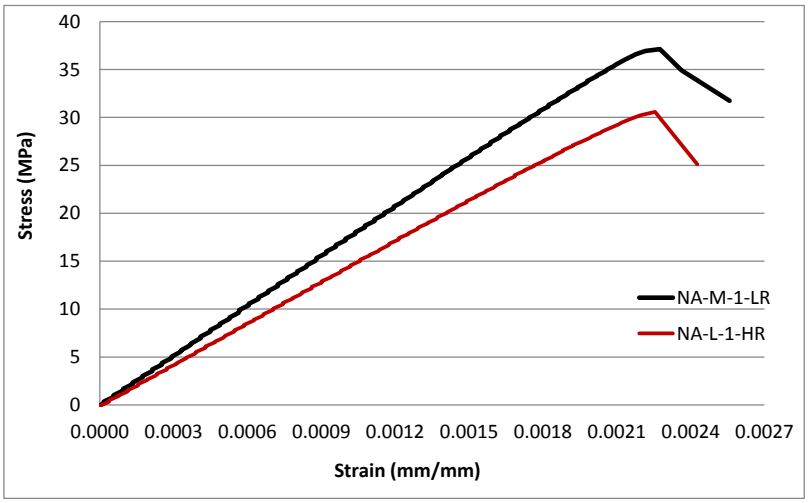

Figure 38: Stress-Strain relationships for the natural aggregate concrete

4.2.2. Steel. As shown in Figure 32, steel reinforcement bars with different diameters were used, 8*mm*, 10*mm*, 16*mm* and 20*mm*. Samples from the steel bars were tested in tension using a small capacity UTM machine in the AUS laboratory to determine their actual yielding strength. Figure 39 shows the stress-strain relation of two samples having different sizes. The actual yield strength, f_y, of both samples was about 600 *MPa*.

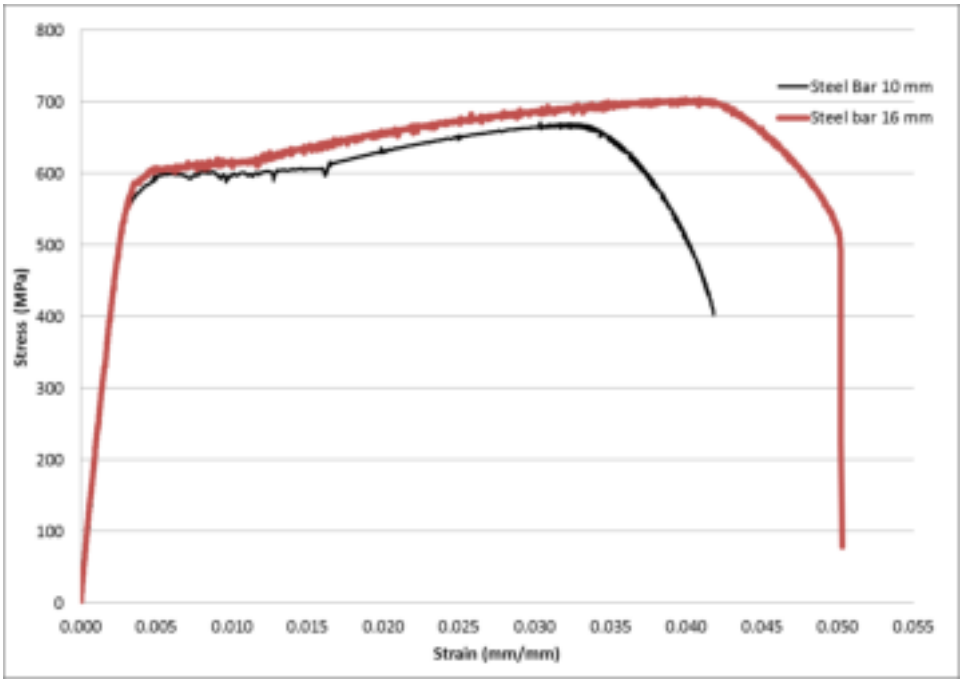

Figure 39: Steel bars Stress-Strain relationship

4.3. Beams Preparations and Casting

All the preparations and casting of the beams were done at the AUS lab except the fabrication of the steel cages. As mentioned earlier, the stirrups were not present in the instrumented and tested part of all beams as shown in Figure 40 and Figure 41.

To install the strain gauges on the bottom steel bars, the surface at the desired location was grinded, smoothed and cleaned first. Then, the strain gauge was glued on the surface as shown in Figure 42. After that, the strain gauge was coated with water-proofing martial (see Figure 43). Standard plywood of thickness 18*mm* was cut and the pieces were joined in the lab to prepare the form work of the beams, as shown in Figure 44.

Figure 40: Steel reinforcement of (*a/d*=2.5) beam

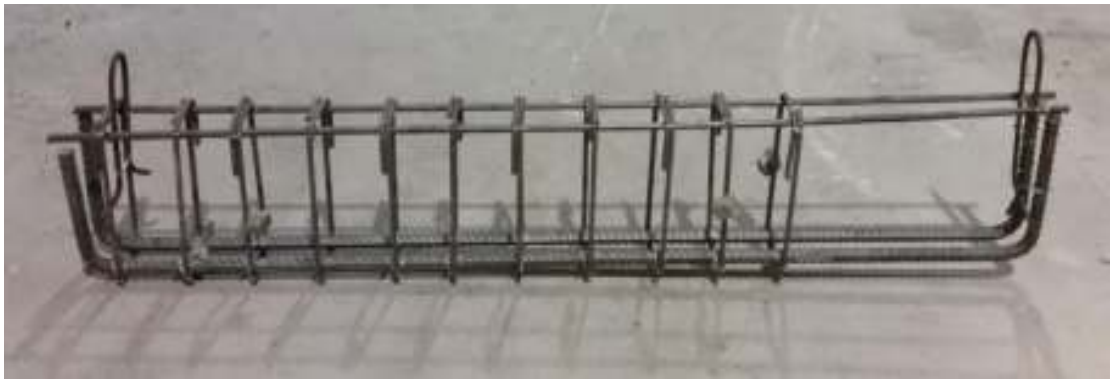

Figure 41: Steel reinforcement of (*a/d*=1.15) beam

Figure 42: Surface preparation and mounting the strain gauge

Figure 43: Surrounding the strain gauge with water-proofing material

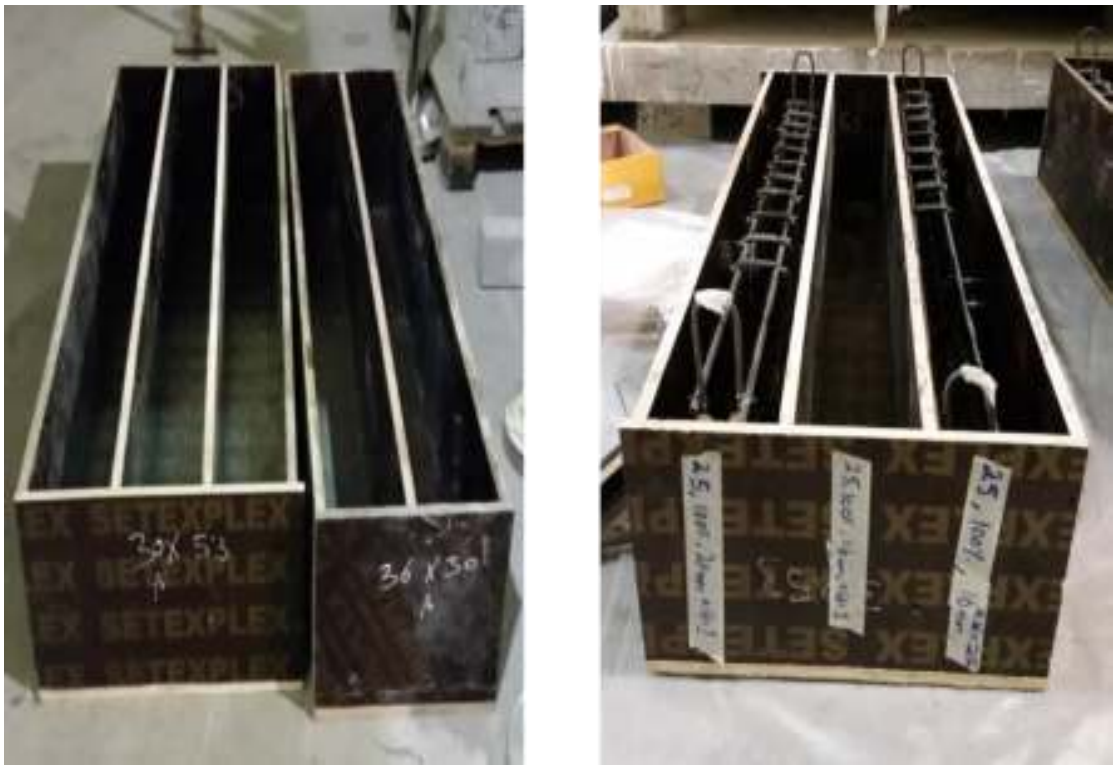

Figure 44: Preparation of beams' form work

Prior to each mix, the cement, water, coarse aggregate and fine aggregate were weighed as per each mix design. The mixing was done using mechanical rotation mixer in the AUS lab as shown in Figure 45. The fresh concrete was tested for its slump and then poured into the beam's form work. A mechanical vibrator was used to ensure good compacting and to prevent honeycombing in the finished product, as depicted in Figure 46.

Figure 45: Mixing concrete proportions in the lab

Figure 46: Compacting fresh concrete using mechanical vibrator

The casted beams and their companion specimens were, then, cured at ambient temperature for one week. They were covered with hessian cloth and watered daily to compensate for the evaporated water from concrete as shown in Figure 47.

Figure 47: Curing of beams

One day before the testing of any beam, two concrete strain gauges were mounted on the top surface of the beam as explained earlier. Moreover, to measure the average crack width, an LVDT was placed on the surface of the concrete crossing the expected shear crack using steel angles and epoxy. Another LVDT was mounted beneath the beam at the load location to measure the vertical deflection as shown in Figure 48 and Figure 49.

Figure 48: Concrete strain gauges and vertical LVDT setup

Figure 49: Mounting the inclined LVDT on the concrete surface

Chapter 5: Experimental Results

In this chapter, the shear strength of the beams from the experimental results is presented and compared to the predicted shear strength obtained by theoretical different methods available either in design codes or existing literature.

5.1. Experimental Results of Shear Strength

Each of the fifteen beams was subjected to displacement-controlled loading at a rate of 0.5 *mm*/minute till failure. Failure is defined when the load drops to about 70% of the ultimate load. The load-deflection relationships for all the tested beam specimens are presented in Figure 50 to Figure 64. The deflection is recorded at the location of the load. The figures depict the pre-cracking stage, post-cracking stage, and cracking pattern at ultimate. As expected, most load-deflection relationships show a reduction in the stiffness of the beam just after cracking. The deflection at instant of first crack varied depending on the nature of the coarse aggregate and location of concentrated load along the beam. For the beams with *a/d* ratio of 1.15, the deflection at first crack was 1-1.5 *mm*, with the lower value associated with beams having natural coarse aggregate. For the beams with *a/d* ratio of 2.5, the deflection at first crack averaged around 0.5 *mm* for both natural and recycled coarse aggregate beams. The deflection at which the beams reached their maximum shear strength for the case of *a/d*=1.15 was within a narrow range of 3-4 *mm* for the natural aggregate beams, and a wide range of 2-4 *mm* for recycled aggregate beams. The corresponding deflection at maximum shear capacity for the case of *a/d*=2.5 was in the range of 2-5 *mm* for the natural aggregate beams and in the range 2.5-4.5 *mm* for the recycled aggregate beams. The observed residual shear strength beyond the ultimate capacity was not consistent among the tested RC beams, as some of the natural aggregate and recycled aggregate beams had some residual strength while others did not show any. The shear strength (V_c) was calculated using the recorded ultimate load value (P) from the UTM machine. The general shear and moment diagrams for beams with shear span-to-depth ratios of 1.15 and 2.5 are respectively shown in Figure 65 and Figure 66. The shear strength results along with the cylinder concrete compressive strength of each beam on testing day are presented in Table 9.

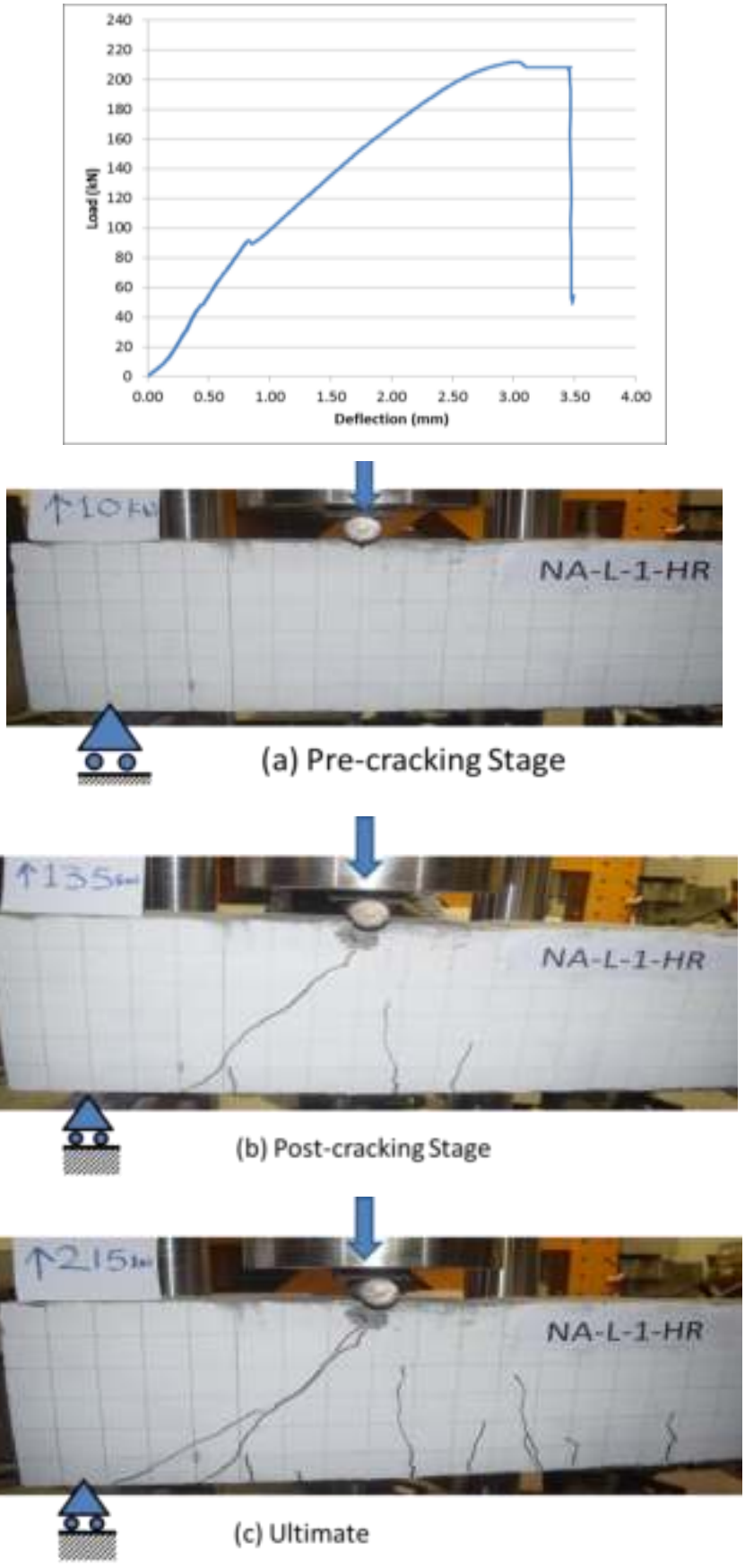

Figure 50: Load- Deflection curve and cracking pattern of beam NA-L-1-HR

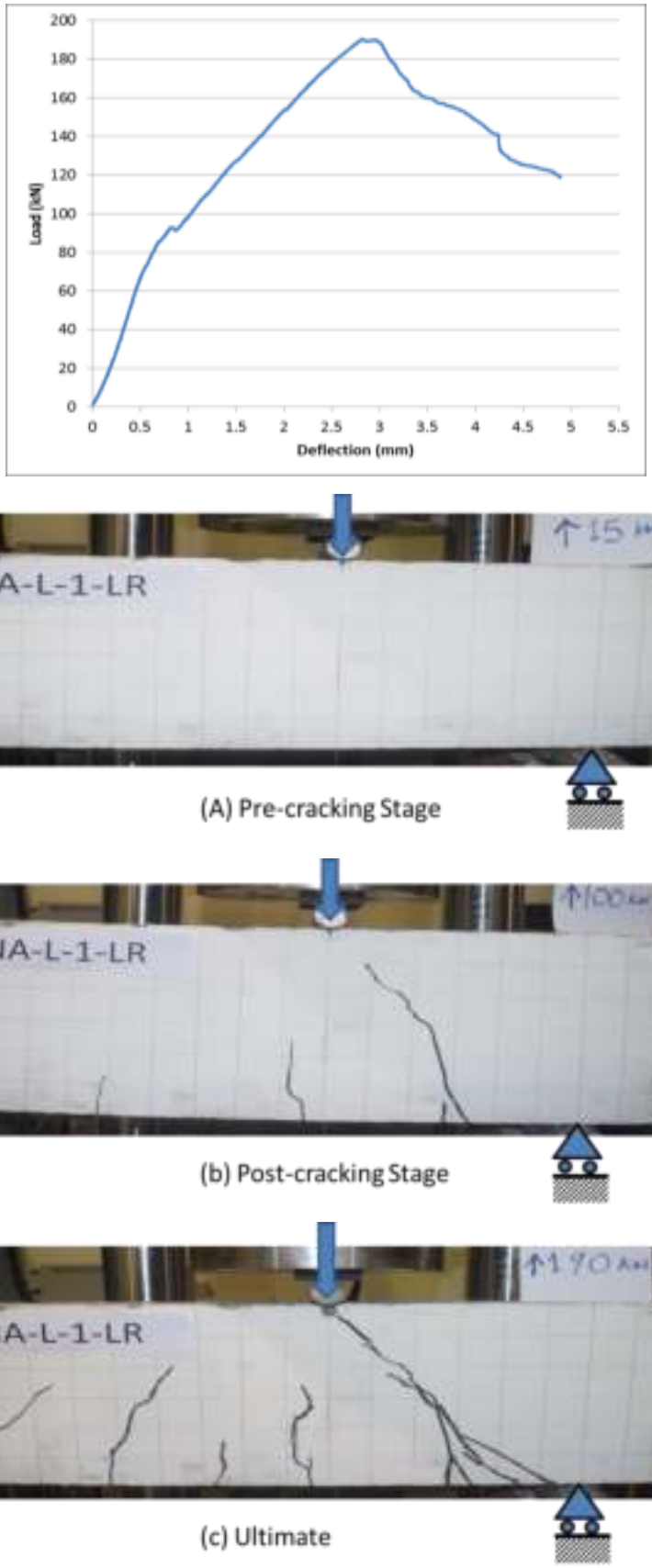

Figure 51: Load- Deflection curve and cracking pattern of beam NA-L-1-LR

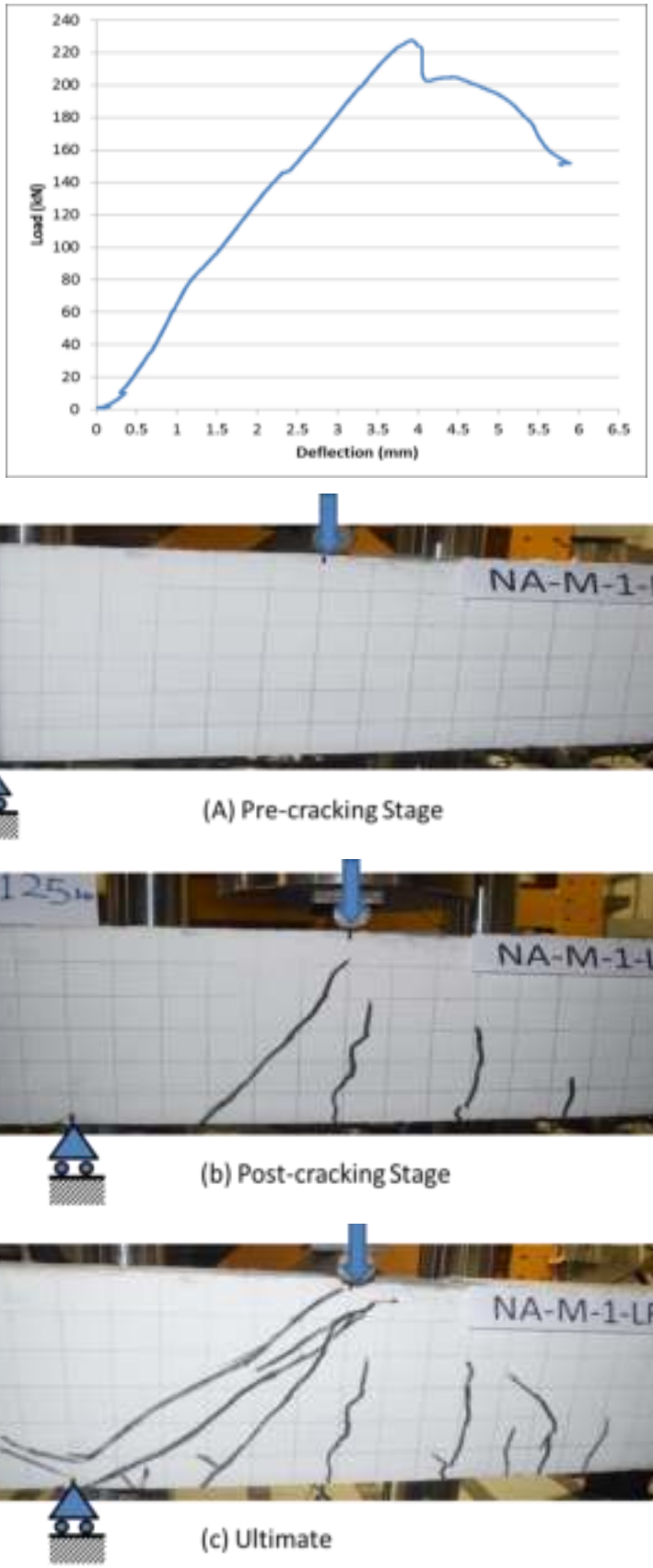

Figure 52: Load- Deflection curve and cracking pattern of beam NA-M-1-LR

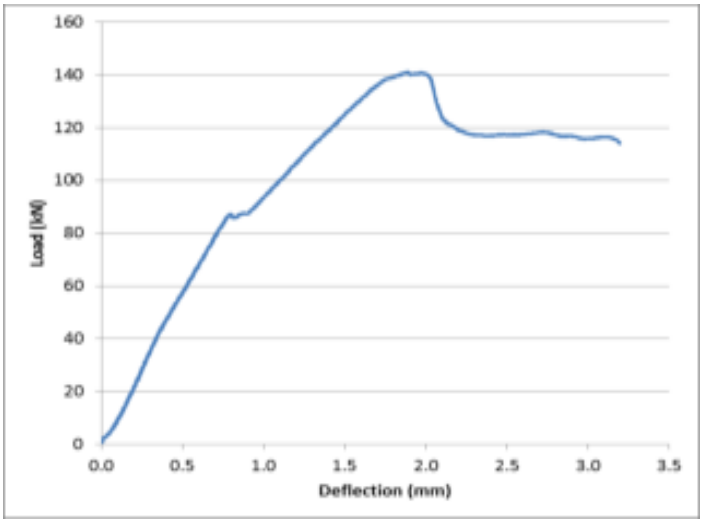

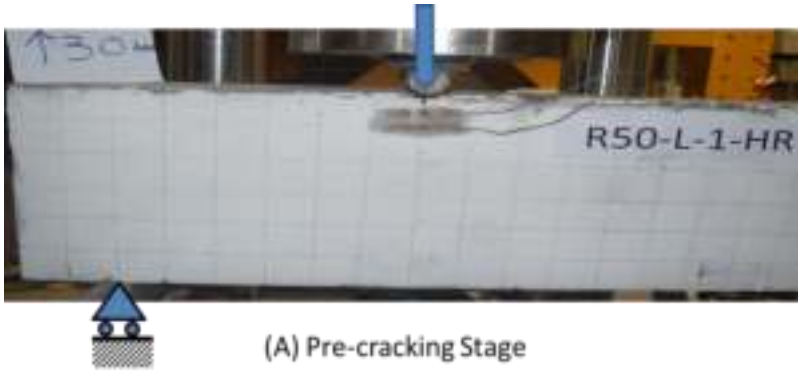

(A) Pre-cracking Stage

(b) Post-cracking Stage

(c) Ultimate

Figure 53: Load- Deflection curve and cracking pattern of beam R50-L-1-HR

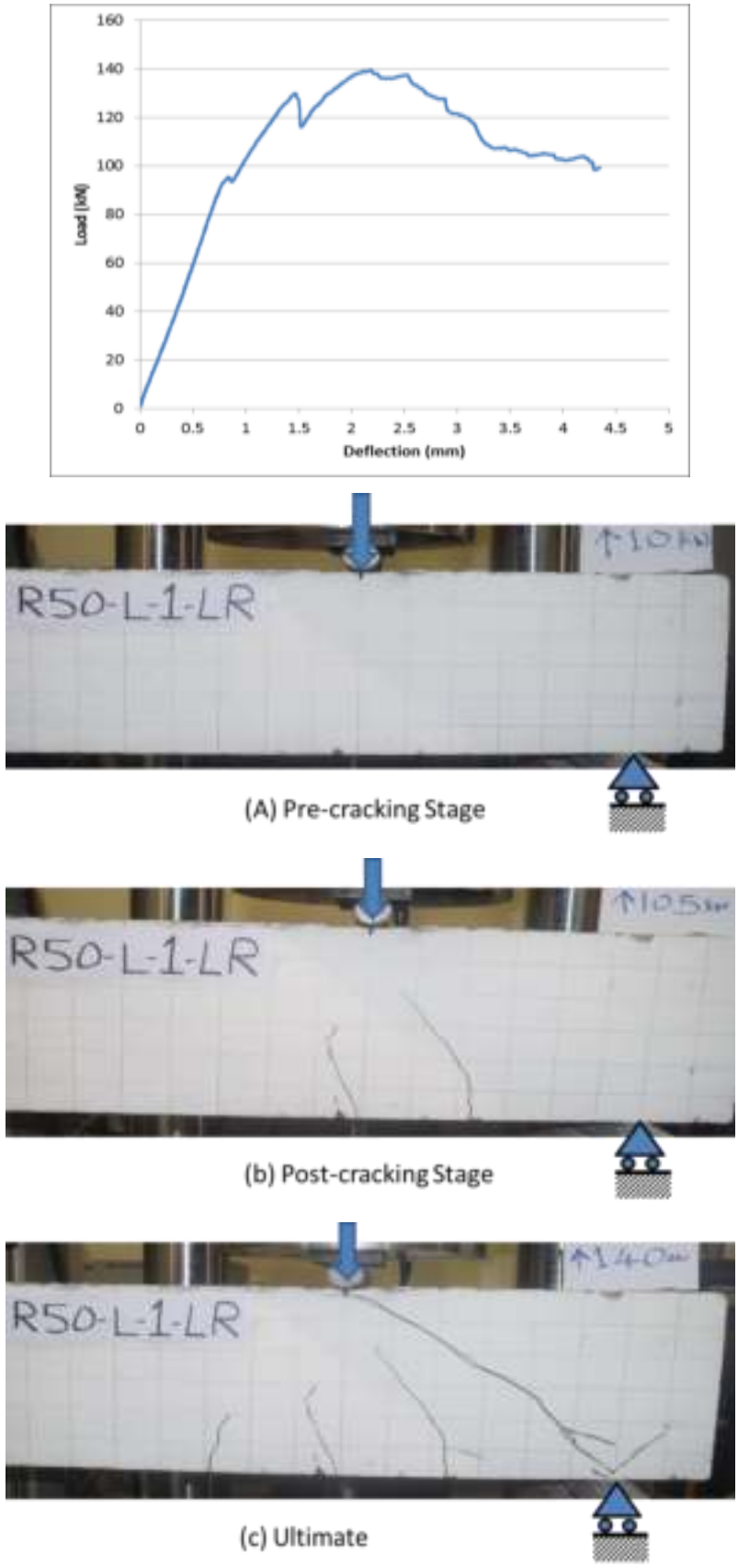

Figure 54: Load- Deflection curve and cracking pattern of beam R50-L-1-LR

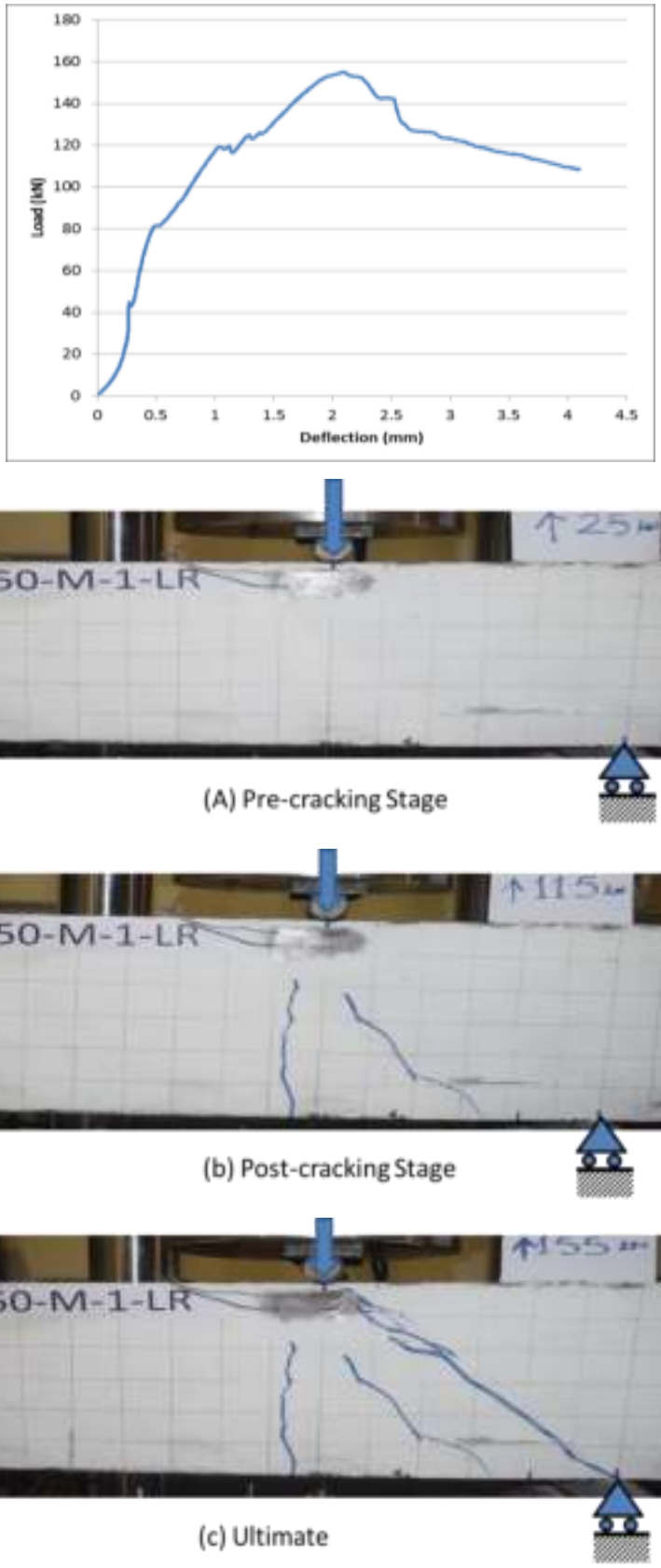

Figure 55: Load- Deflection curve and cracking pattern of beam R50-M-1-LR

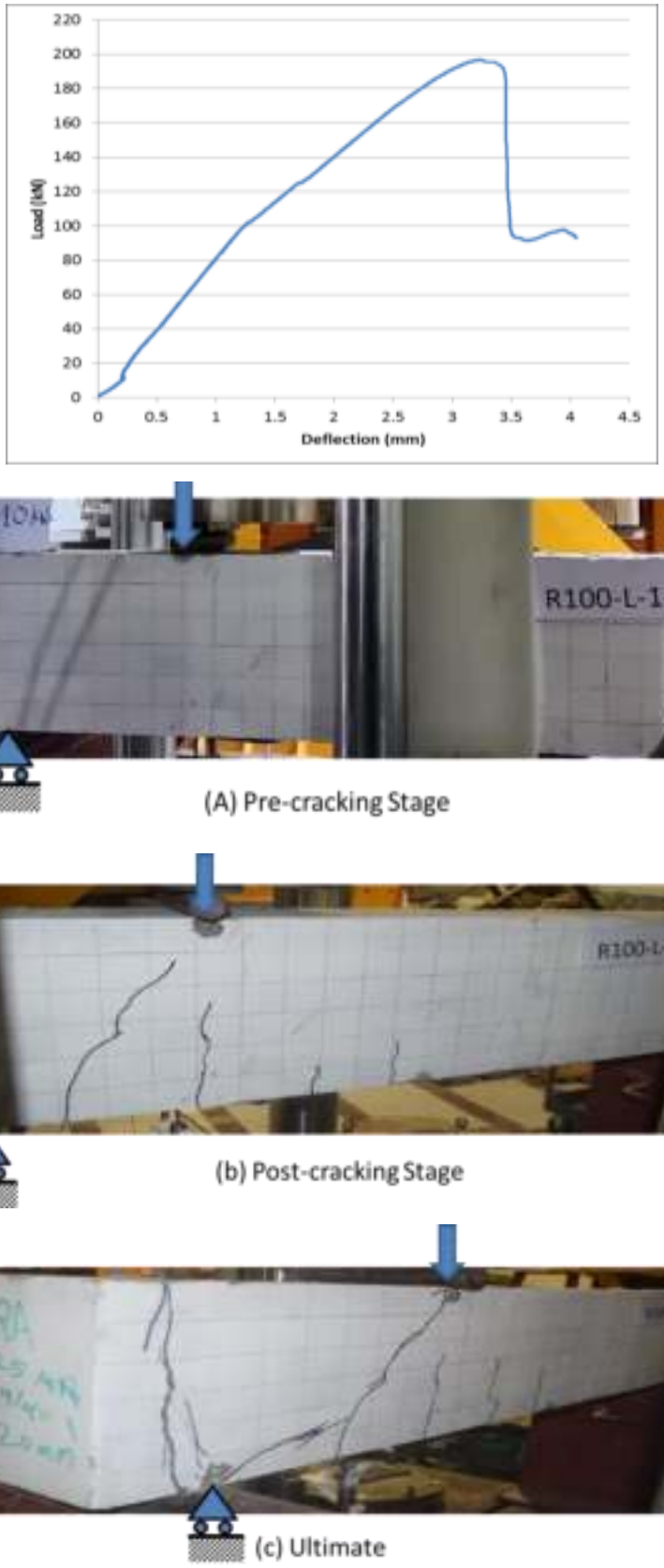

Figure 56: Load- Deflection curve and cracking pattern of beam R100-1-L-HR

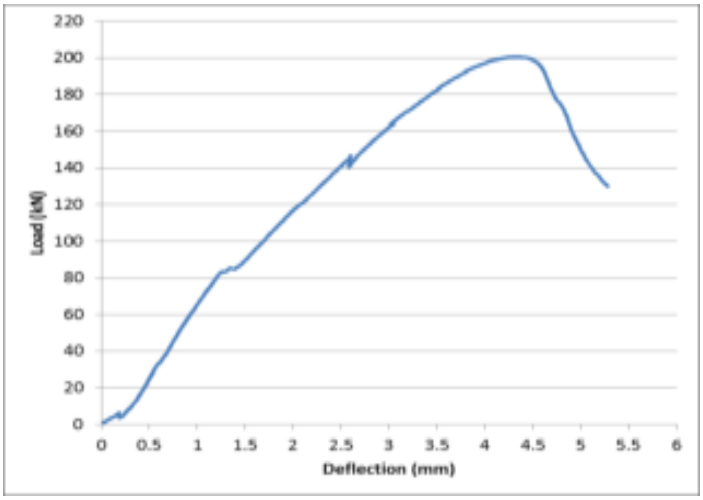

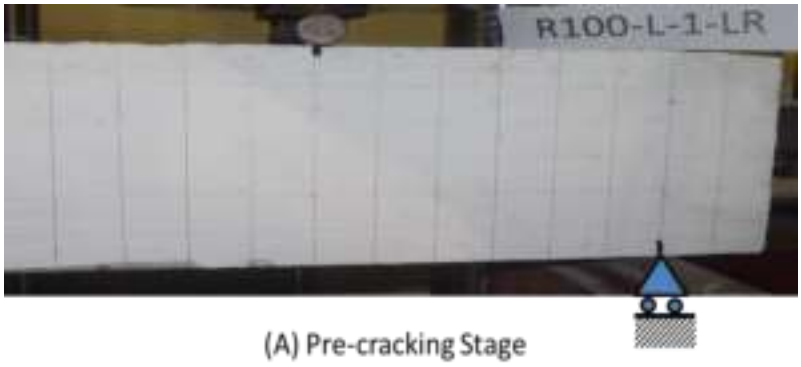

(A) Pre-cracking Stage

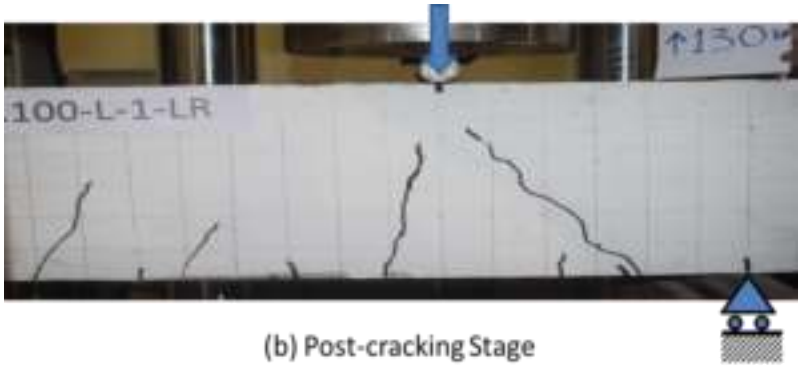

(b) Post-cracking Stage

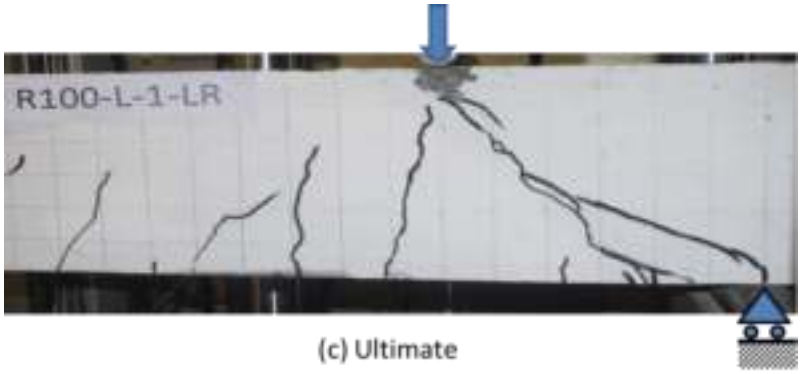

(c) Ultimate

Figure 57: Load- Deflection curve and cracking pattern of beam R100-L-1-LR

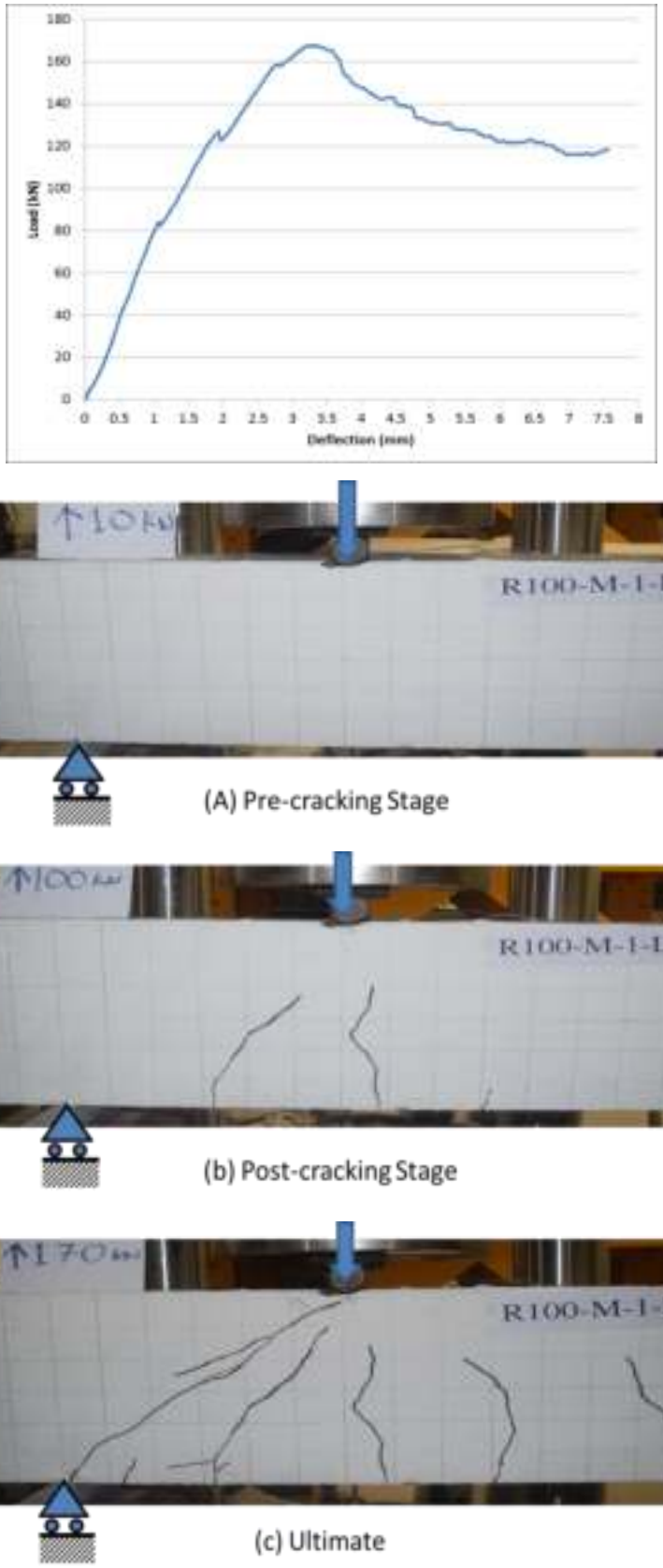

Figure 58: Load- Deflection curve and cracking pattern of beam R100-M-1-LR

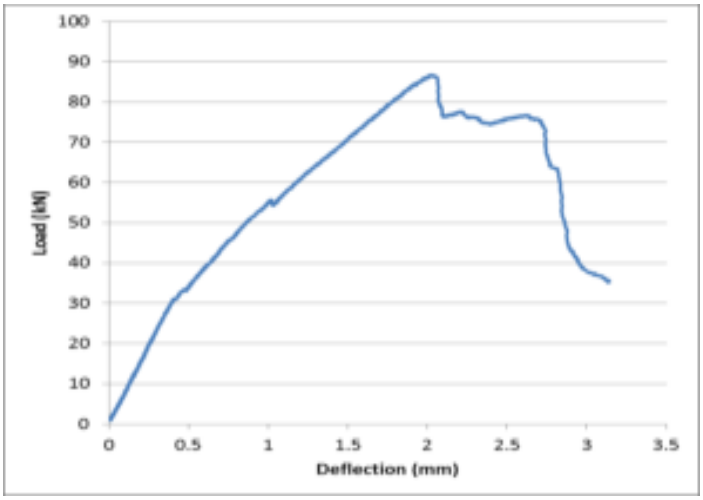

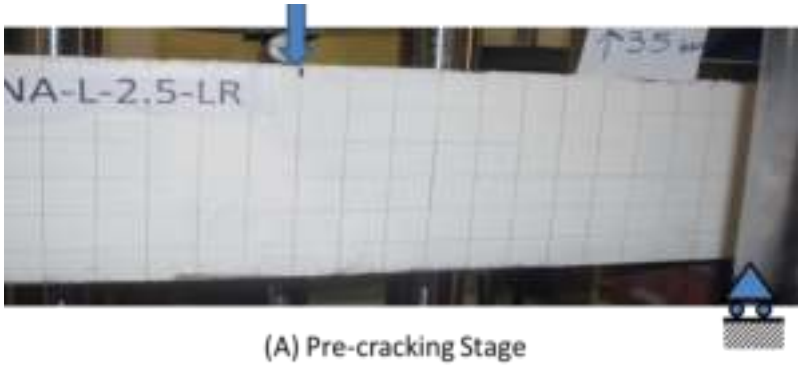

(A) Pre-cracking Stage

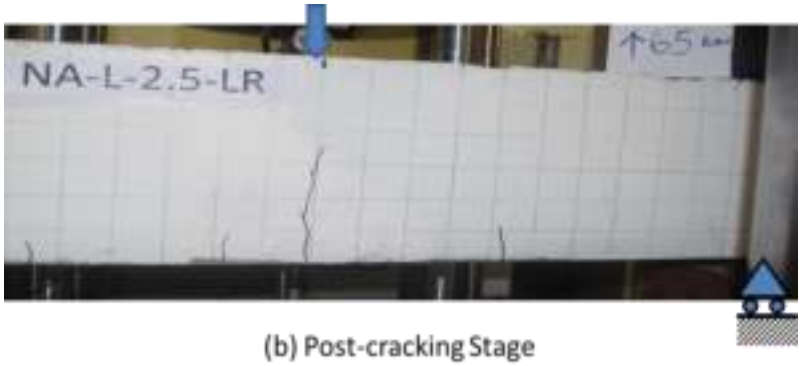

(b) Post-cracking Stage

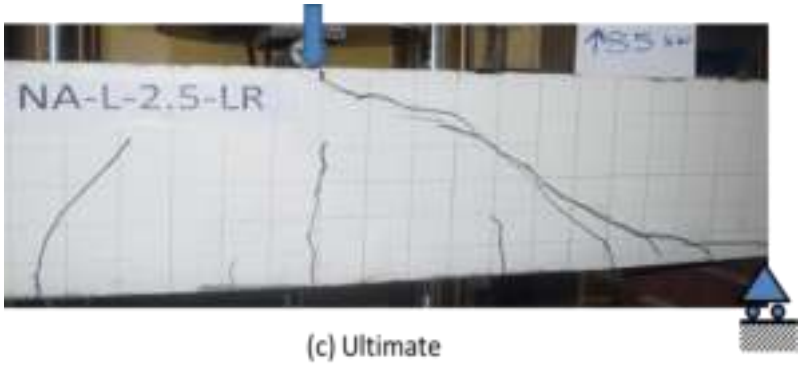

(c) Ultimate

Figure 59: Load- Deflection curve and cracking pattern of beam NA-L-2.5-LR

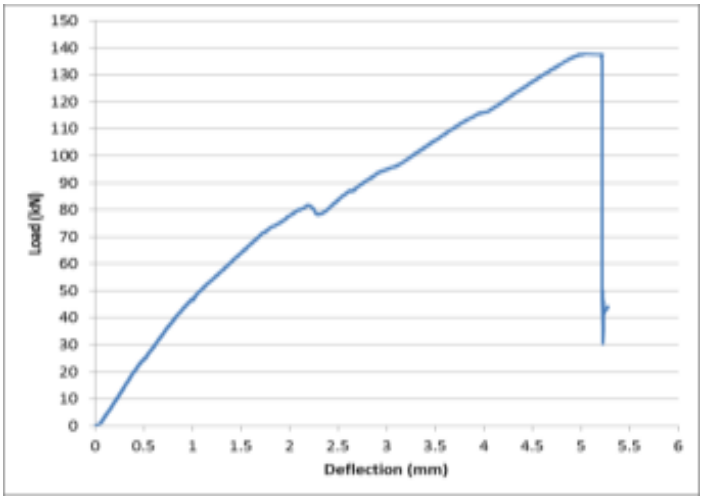

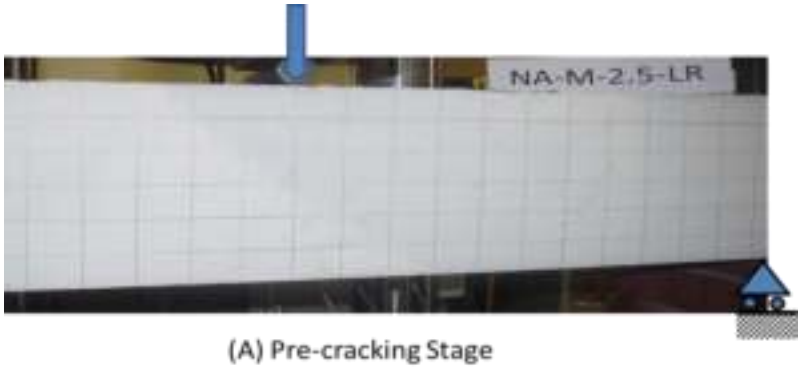

(A) Pre-cracking Stage

(b) Post-cracking Stage

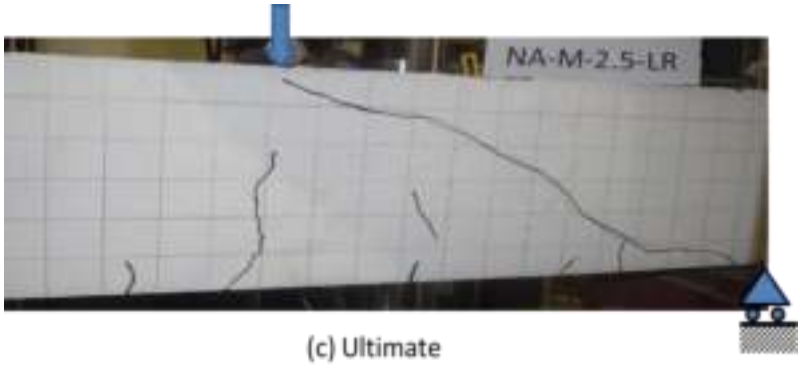

(c) Ultimate

Figure 60: Load- Deflection curve and cracking pattern of beam NA-M-2.5-LR

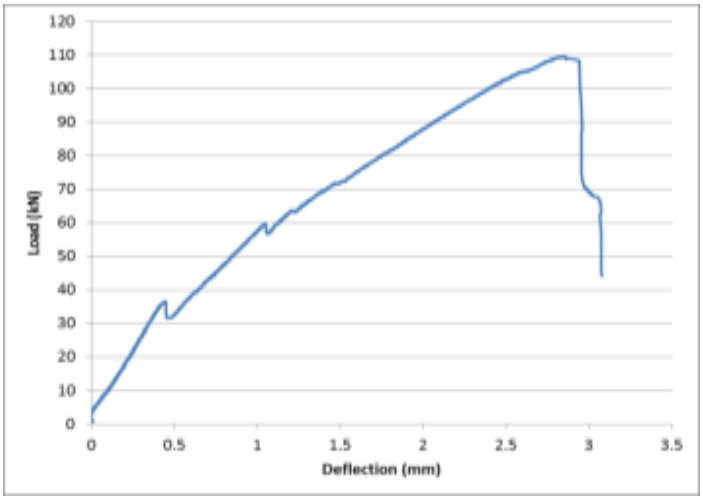

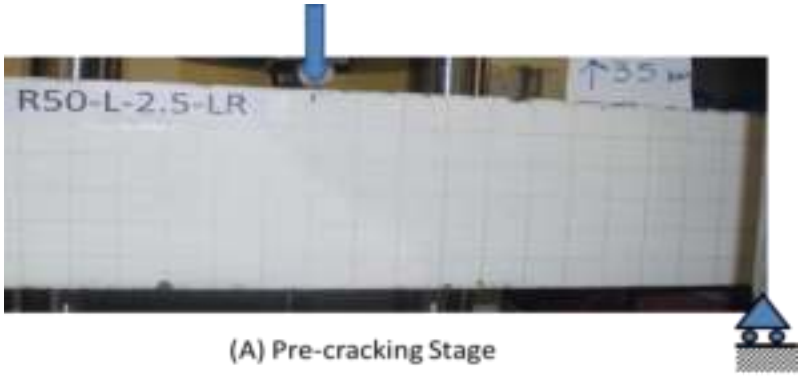

(A) Pre-cracking Stage

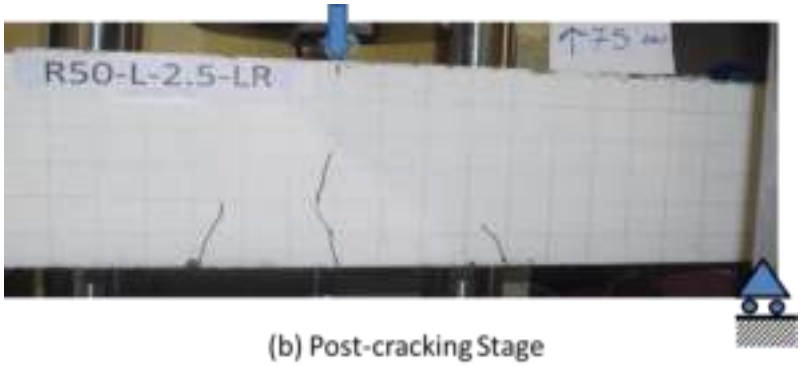

(b) Post-cracking Stage

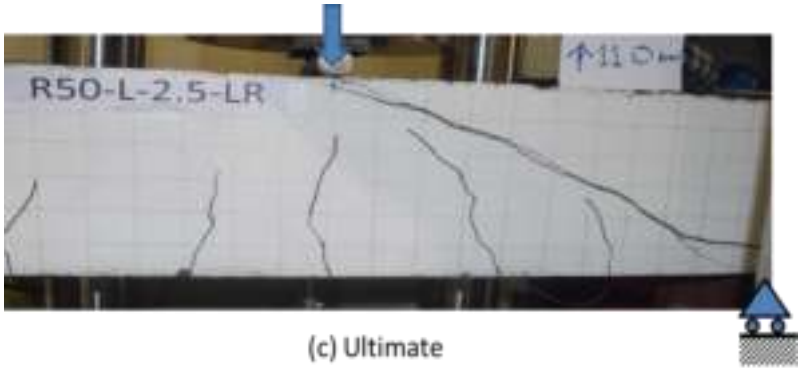

(c) Ultimate

Figure 61: Load- Deflection curve and cracking pattern of beam R50-L-2.5-LR

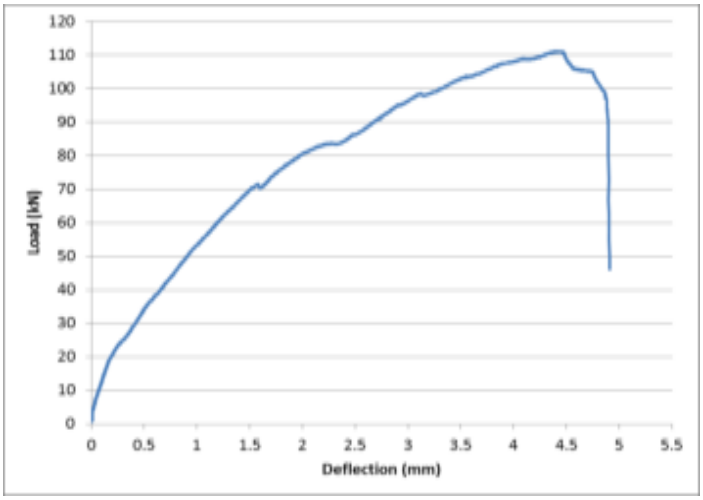

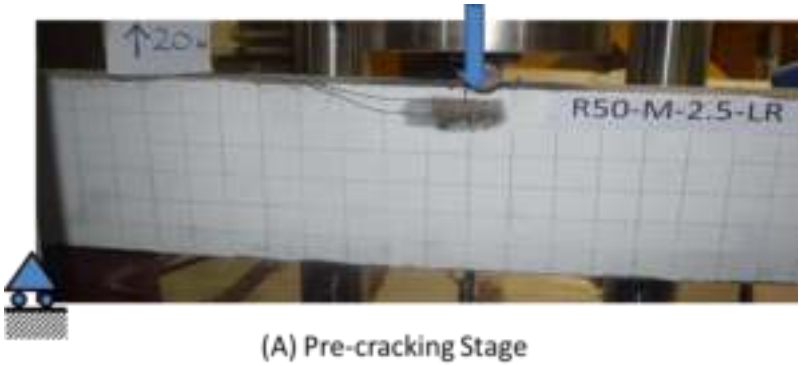

(A) Pre-cracking Stage

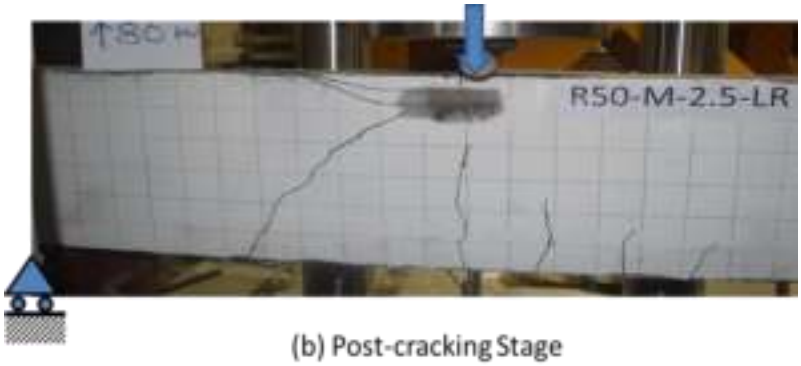

(b) Post-cracking Stage

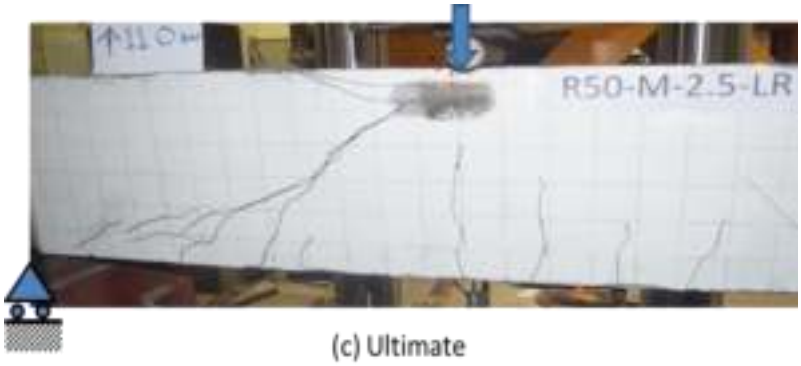

(c) Ultimate

Figure 62: Load- Deflection curve and cracking pattern of beam R50-M-2.5-LR

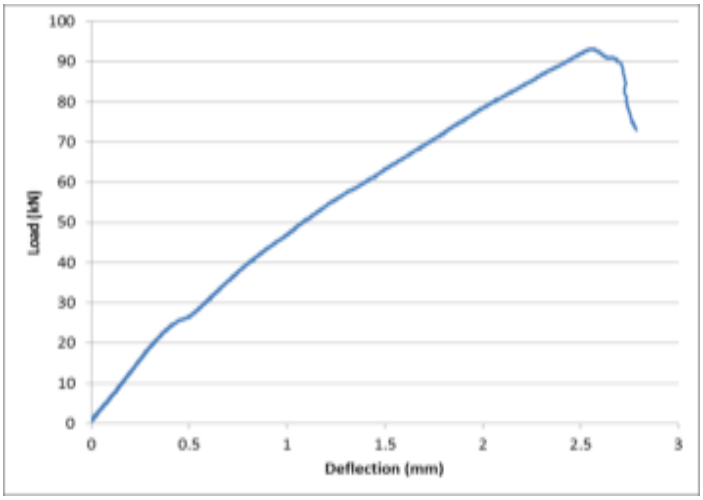

(A) Pre-cracking Stage

(b) Post-cracking Stage

(c) Ultimate

Figure 63: Load- Deflection curve and cracking pattern of beam R100-L-2.5-LR

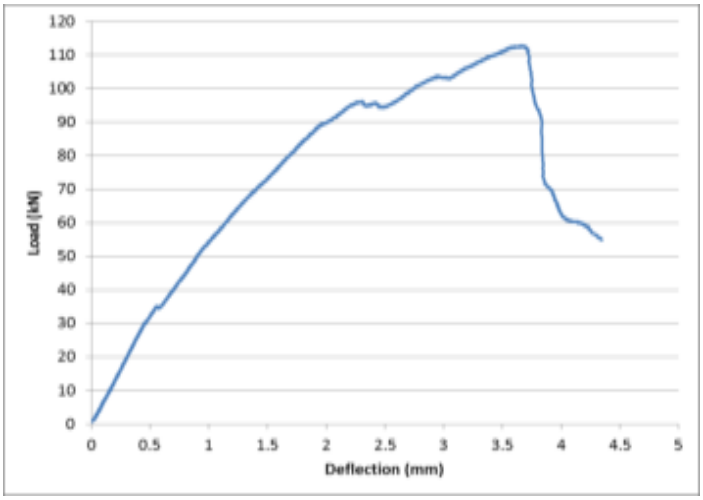

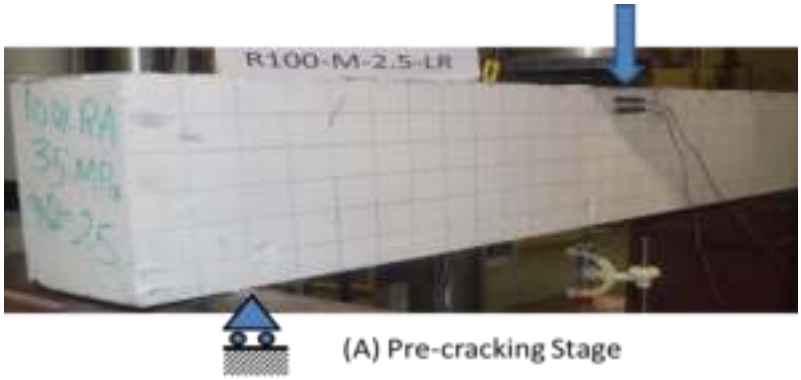

(A) Pre-cracking Stage

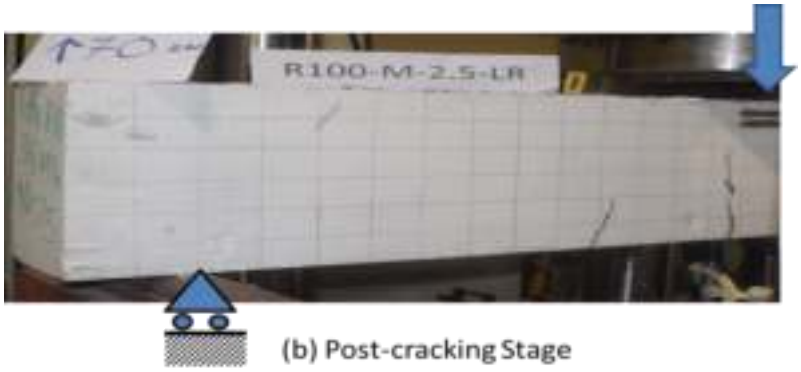

(b) Post-cracking Stage

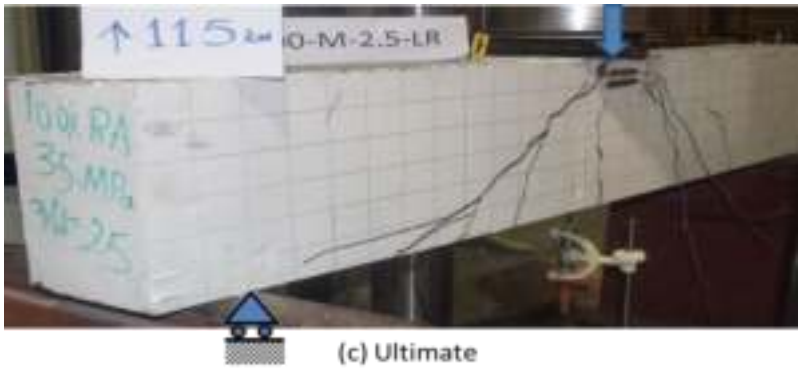

(c) Ultimate

Figure 64: Load- Deflection curve and cracking pattern of beam R100-M-2.5-LR

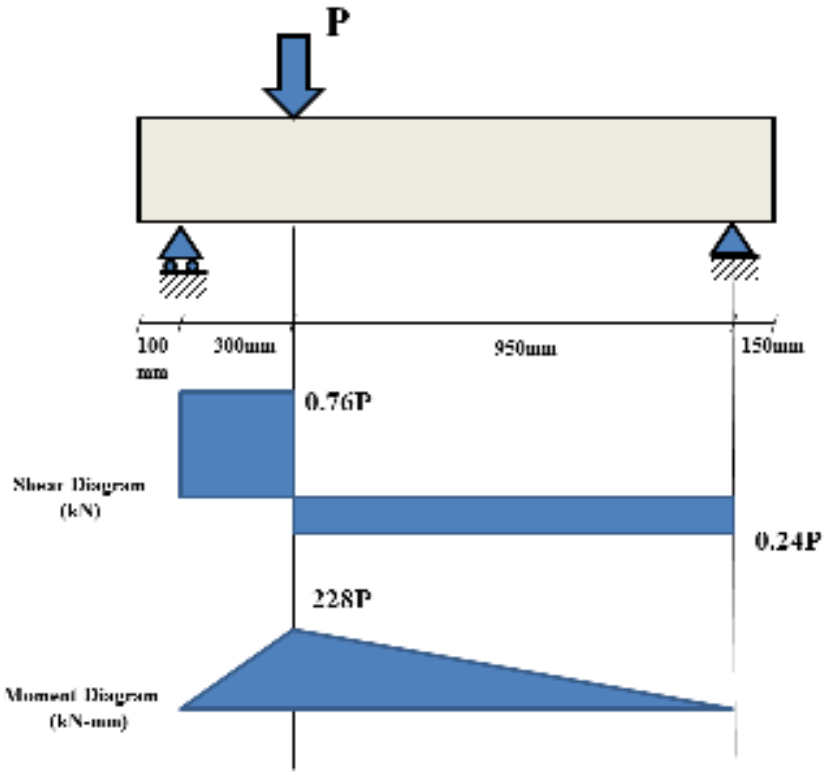

Figure 65: Shear and moment diagram for a beam with *a/d*= 1.15

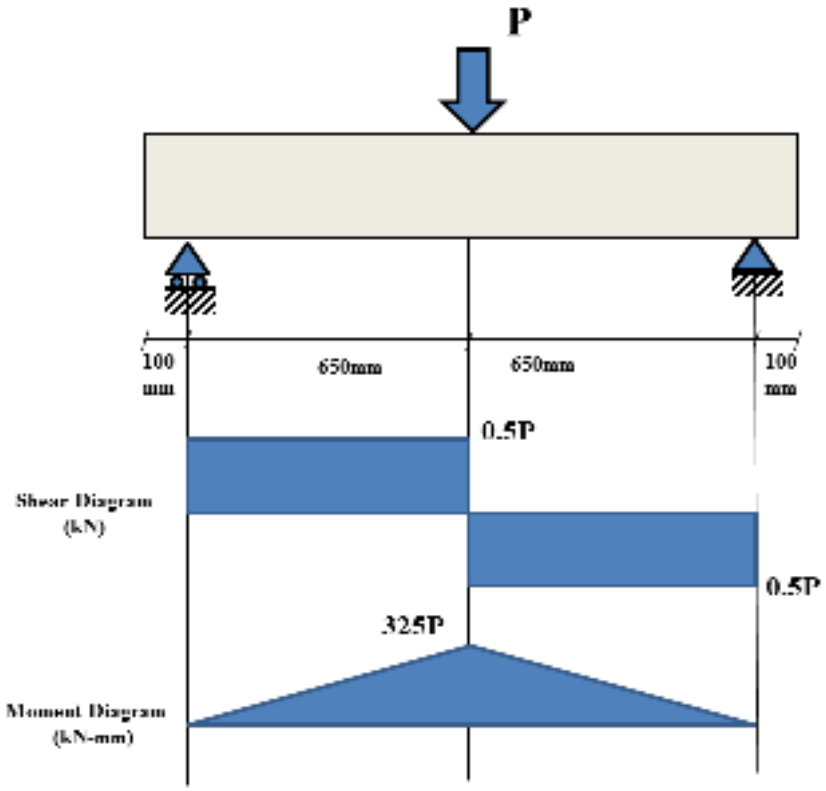

Figure 66: Shear and moment diagram for a beam with *a/d*= 2.5

The numbers in column (P_{max}) were obtained from the UTM output files. Then, depending on the (*a/d*) ratio, V_c was tabulated using the shear diagrams above. Since the critical section in both (*a/d*) ratios is at the location of load application, the values of V_c was calculated at that location. It should be noted that all but two beams were tested at the age of about five months due to logistical issues. The only two beams that were tested at an age of less than five months were R100-M-1-LR and NA-M-2.5-LR. The latter two beams were tested at the age of approximately five weeks.

Table 9: Experimental results of shear strength.

Serial No.	Beam ID	*a/d* ratio	f'_c	Recorded P_{max} (*kN*)	Corresponding V_c (*kN*)
1	NA-L-1-HR	1.15	30.55	212.07	161.17
2	NA-L-1-LR		33.9	190.368	144.68
3	NA-M-1-LR		37.2	227.9	173.20
4	R50-L-1-HR		26.95	141.06	107.21
5	R50-L-1-LR		28.55	139.52	106.04
6	R50-M-1-LR		36	155.14	117.91
7	R100-L-1-HR		31.8	196.845	149.60
8	R100-L-1-LR		29.3	200.745	152.57
9	R100-M-1-LR		36.7	167.9	127.6
10	NA-L-2.5-LR	2.5	33	86.8	43.40
11	NA-M-2.5-LR		43.75	137.82	68.91
12	R50-L-2.5-LR		27.95	109.65	54.83
13	R50-M-2.5-LR		35.55	111.17	55.59
14	R100-L-2.5-LR		31.85	93.329	46.66
15	R100-M-2.5-LR		38.7	112.804	56.40

5.2. Observations from the Experimental Tests

5.2.1. Failure mode of beams. As expected and designed, all the beams failed in shear. As the load increased, flexural cracks started to appear under the loading point where the bending moment in the beam is highest. Gradually, more flexural cracks started to form close to that location, always vertically oriented. After that, shear cracks with angle inclination formed from the locations near the critical support towards the loading point within the instrumented region. These cracks propagated further more with the increase of the load until diagonal tension failure happened. In almost all of the tested beams, the cause of the failure was a major diagonal crack with sudden failure, followed by a drastic decrease in the beam capacity, as shown previously in Figure 50- Figure 64.

5.2.2. Average crack width and inclination. The average shear-crack width was measured using an LVDT positioned on the concrete surface with an angle of 45º as was shown in Chapter 4. Since the actual location and inclination angle of the major shear cracks are very difficult to be determined prior to the test, the LVDTs were often not exactly perpendicular to the shear cracks; hence the measured crack width only gives an idea about the crack size and opening, and can be used for comparative purposes. The data obtained from those LVDTs clearly indicates that the shear cracks start to form after some time from the start of the test, after formation of the flexure cracks. Once the shear cracks started to appear, the average crack width begins to widen as the load increases. When the beam reaches its full capacity and the shear failure mechanism, represented by a diagonal tension failure, takes place, the measured average crack width between two points on the beam surface keeps widening while the beam starts to gradually lose its capacity. The average crack width versus the applied load for some of the tested beams is shown in Figure 67, Figure 68, Figure 69 and Figure 70. For each beam, the average crack width when the beam reaches its maximum load capacity is presented in Table 10, while Table 11 reports the angle of the major shear crack at failure. Figure 71 shows the diagonally oriented LVDT setup to measure the average inclined crack width for a typical beam. Figure 73 shows the orientation and measurement of a typical diagonal shear crack.

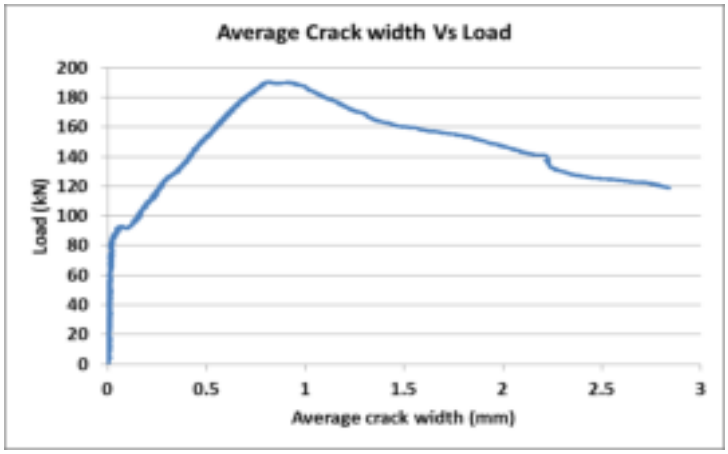

Figure 67: Average crack width versus load for the beam NA-L-1-LR

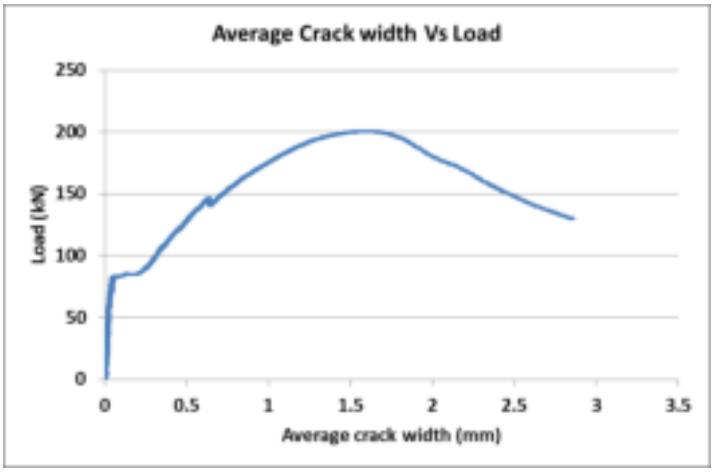

Figure 68: Average crack width versus load for the beam R100-L-1-LR

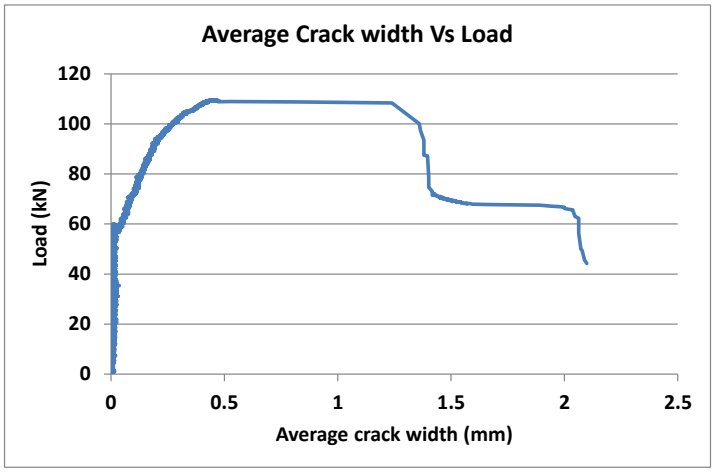

Figure 69: Average crack width versus load for the beam R50-L-2.5-LR

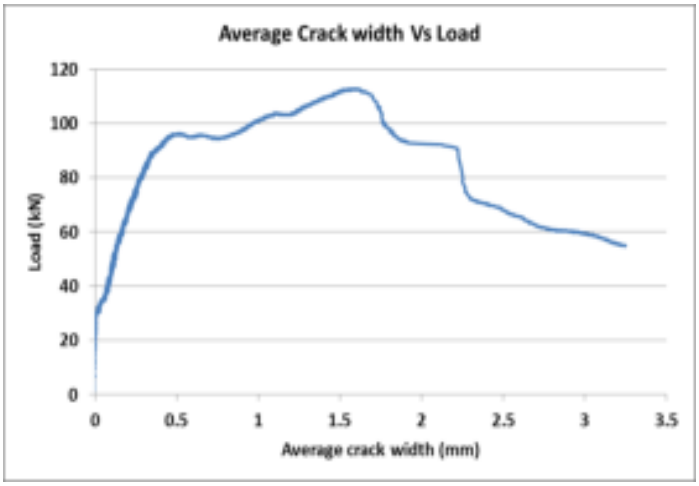

Figure 70: Average crack width versus load for the beam R100-M-2.5-LR

The cracking load at which the first crack appeared was recorded during the test. These first cracks were all flexural cracks in the vicinity of the applied load from the UTM, where the bending moment was largest. The load at which the first shear crack appeared was also recorded during the test. Such a crack occurred in the instrumented region between the applied load and nearby support, in which no stirrups were present.

Table 12 reports the loads and also present the ratio of the first flexure load to the first shear crack load. The average crack width of both beam 100-L-2.5-LR could not be retrieved due to LVDT mechanical failure towards the end of the test; therefore, it is not included in Table 10.

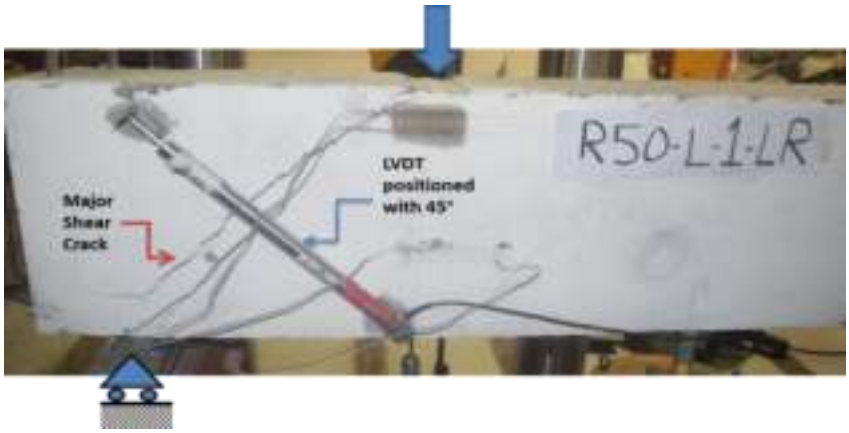

Figure 71: Measuring the average shear-crack width of R50-L-1-LR

Table 10: Average crack width at maximum applied load

Beam ID	Maximum load (*kN*)	Average crack width (*mm*)
NA-L-1-HR	212.07	0.760
NA-L-1-LR	190.37	0.8177
NA-M-1-LR	227.9	1.0052
R50-L-1-HR	141.06	0.6979
R50-L-1-LR	139.52	1.0886
R50-M-1-LR	155.14	1.25
R100-L-1-HR	196.84	0.6406
R100-L-1-LR	200.74	1.6042
R100-M-1-LR	167.9	1.304
NA-L-2.5-LR	86.8	0.4792
NA-M-2.5-LR	137.82	0.7039
R50-L-2.5-LR	109.65	0.4427
R50-M-2.5-LR	111.17	1.4531
R100-L-2.5-LR	93.329	-
R100-M-2.5-LR	112.80	1.5938

As expected, as the amount of flexural reinforcement increases the average crack width due to shear decreases. This finding is true for beams made with concrete from either natural or recycled aggregate. The main reason for this is the dowel action of the flexural reinforcement that helps in arresting the cracks. When the effective flexural reinforcement ratio is somewhat high (ρ=1.6%), the effect of dowel action by such reinforcement on the average crack width is not affected by the type of course aggregate used in the concrete. This is demonstrated in Table 10 by the narrow range of crack width, 0.6406 - 0.760 *mm*, for beams NA-L-1-HR, R50-L-1-HR, and R100-L-1-HR. However, for the beams with low longitudinal steel reinforcement ratio (ρ= 1.03%), the effect of dowel action by such reinforcement on the average crack width is impacted by the type of course aggregate used in the concrete. As the recycled coarse aggregate replacement percentage increases, the average crack width

consistently increases, and this finding is valid for the low and medium strength concrete mixes. This observation is demonstrated in Figure 72.

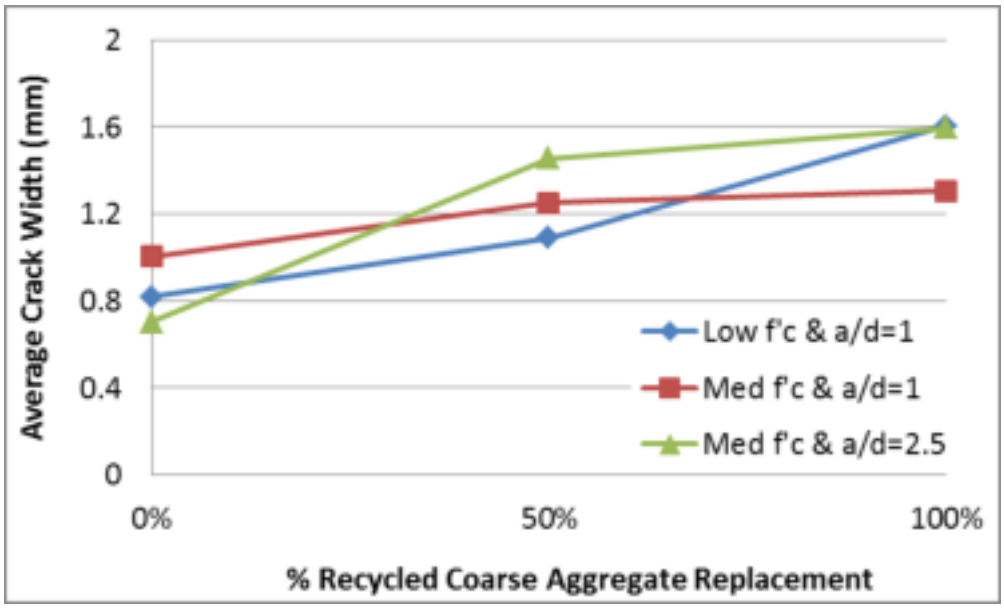

Figure 72: Average shear crack width versus RA% in the mix

The angle of inclination of the major shear crack from a horizontal datum at ultimate for all tested beams varied between 34º and 60º. For the beams with small shear span-to depth ratio (*a/d*= 1), the average angle of inclination of the shear crack was about 45.3º. On the other hand, the average angle of inclination of the shear crack was about 38.3º for the beams with large shear span-to-depth ratio (*a/d*= 2.5). Furthermore, the tested beams with high effective steel reinforcement ratio (ρ=1.6%) showed larger angles (ranging between 50º - 60º) than their counterpart with low reinforcement ratio (ρ=1.03%) which was 40.8º, for the case of *a/d*= 1. Also, RC beams made with NA had somewhat steeper angle of shear crack than those made with RA. For the *a/d*= 1 case, the average angle of the major crack increased with the increase of the coarse aggregate replacement ratio. There was no consistent trend in the average inclination angle for the case of *a/d*= 2.5. However, beams made with NA had somewhat steeper angle of shear crack than those made with RA when *a/d*= 2.5.

Figure 73: Measuring the inclination of the major shear-crack of R50-L-1-LR

Table 11: Inclination angle of the major shear crack at failure

Beam ID	Max Load (*kN*)	Angle of major shear crack (Degree)
NA-L-1-HR	212.07	50
NA-L-1-LR	190.37	40
NA-M-1-LR	227.9	37
R50-L-1-HR	141.06	53
R50-L-1-LR	139.52	41
R50-M-1-LR	155.14	43
R100-L-1-HR	196.84	60
R100-L-1-LR	200.74	37
R100-M-1-LR	167.9	47
NA-L-2.5-LR	86.8	41
NA-M-2.5-LR	137.82	44
R50-L-2.5-LR	109.65	35
R50-M-2.5-LR	111.17	34
R100-L-2.5-LR	93.329	38
R100-M-2.5-LR	112.80	38

The results in Table 12 show, as expected, that the load at first (vertical) flexural crack formation for the beams with low *a/d* ratio is higher than the corresponding load for beams with high *a/d* ratio. This is due to the fact that as the applied load moves away from mid-span, the resulting bending moment decreases; hence, larger load is needed to generate the cracking moment. As for the load at initiation of (diagonal) shear crack, results of the experimental tests demonstrated that as the load moves towards mid-span (*a/d*= 2.5), the load required to cause shear failure is decreased due to presence of significant flexure together with shear force in the region near mid-span.

Table 12: Observed load at the first flexural and first shear crack

Beam ID	First Crack load- L_{Flx-Cr} (kN)	First Shear Crack Load L_{Shr-Cr} (kN)	L_{Flx-Cr} / L_{Shr-Cr}
NA-L-1-HR	50	89	0.56
NA-L-1-LR	40	93	0.43
NA-M-1-LR	35	87	0.40
R50-L-1-HR	55	88	0.63
R50-L-1-LR	50	96	0.52
R50-M-1-LR	49	82	0.60
R100-L-1-HR	48	100	0.48
R100-L-1-LR	45	94	0.48
R100-M-1-LR	45	90	0.5
NA-L-2.5-LR	38	82	0.46
NA-M-2.5-LR	35	55	0.64
R50-L-2.5-LR	40	90	0.44
R50-M-2.5-LR	30	65	0.46
R100-L-2.5-LR	34	90	0.38
R100-M-2.5-LR	38	65	0.58

5.3. Strains

In order to have better understanding of the internal stresses within the tested RC beams, one strain gauge was installed on each of the bottom longitudinal steel rebars (SSG). Moreover, two strain gauges were installed on the surface of the concrete in the compression zone at the loading point beneath each other, one gauge at 20*mm* from the top and another gauge 20*mm* below the first gauge. In few cases one of the steel strain gauges did not work during testing due to various reasons, including high deformations of the beam, mechanical failure of the gauge, etc. From the obtained data we were able to plot the strain in the steel and concrete versus load graphs. The results confirmed that none of the longitudinal steel reinforcement at the bottom of the beam reached a yielding state. Also, the concrete did not fail due to crushing in compression caused by flexure. In other words, the failure mode of the beams was indeed shear failure, not flexure failure, as intended in the study. Figure 74 to Figure 77 depict examples of the strains versus load graphs of different beams. Keeping in mind that the steel yield strength is $\varepsilon_y = 0.003$ and the concrete strain at ultimate compressive capacity is $\epsilon_u = 0.002$.

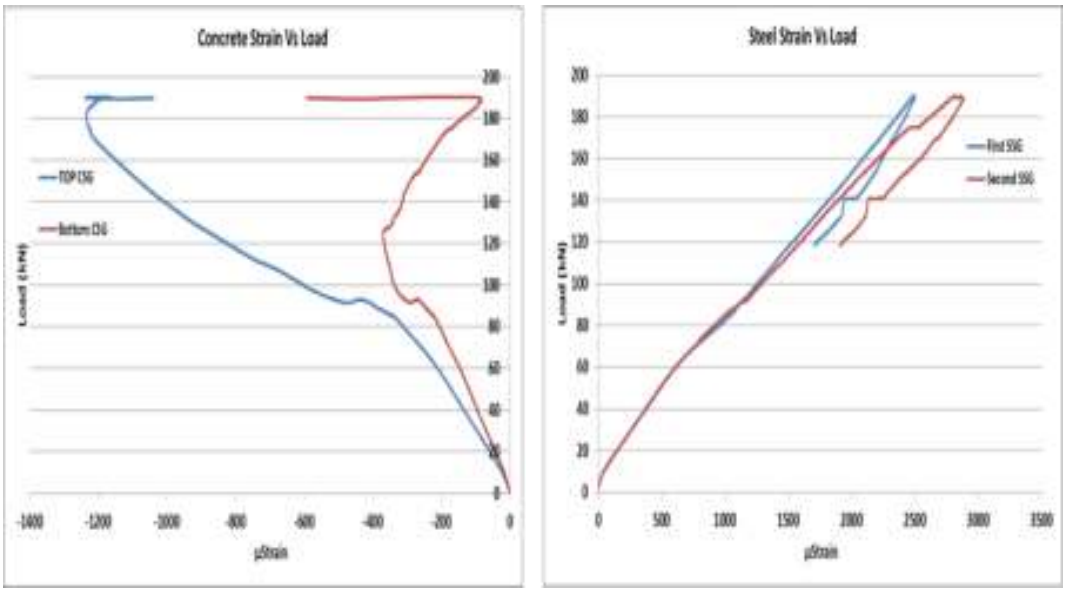

Figure 74: Concrete and steel strains versus load of NA-L-1-LR

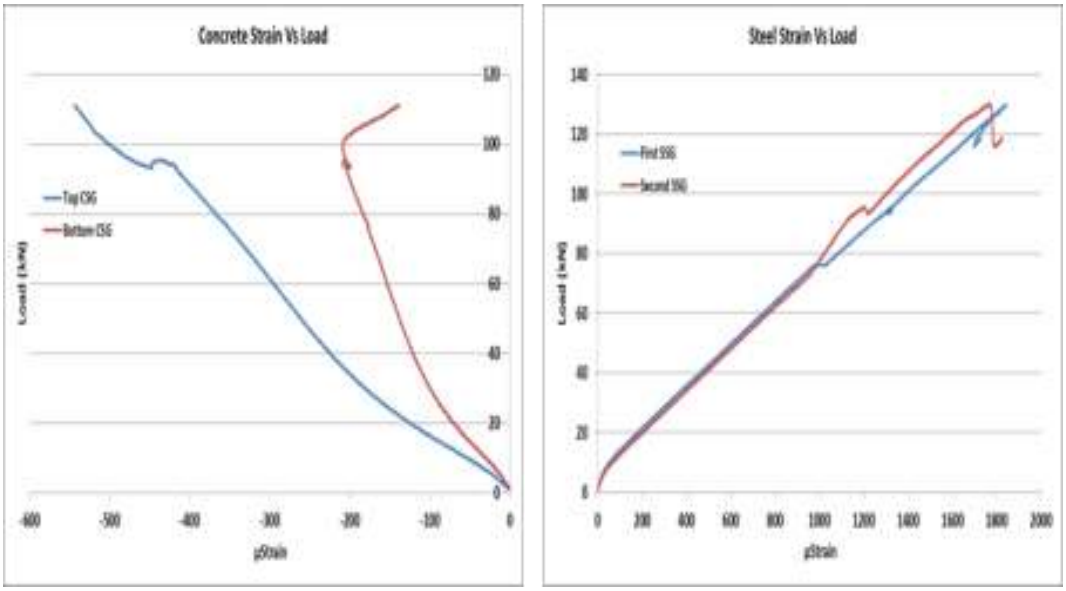

Figure 75: Concrete and steel strains versus load of R50-L-1-LR

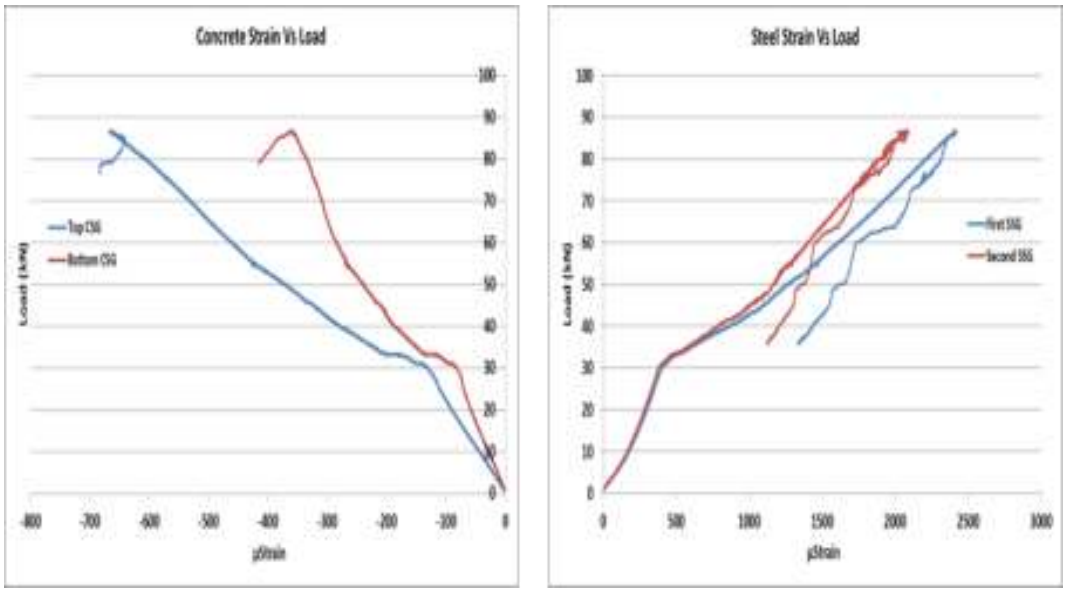

Figure 76: Concrete and steel strains versus load of NA-L-2.5-LR

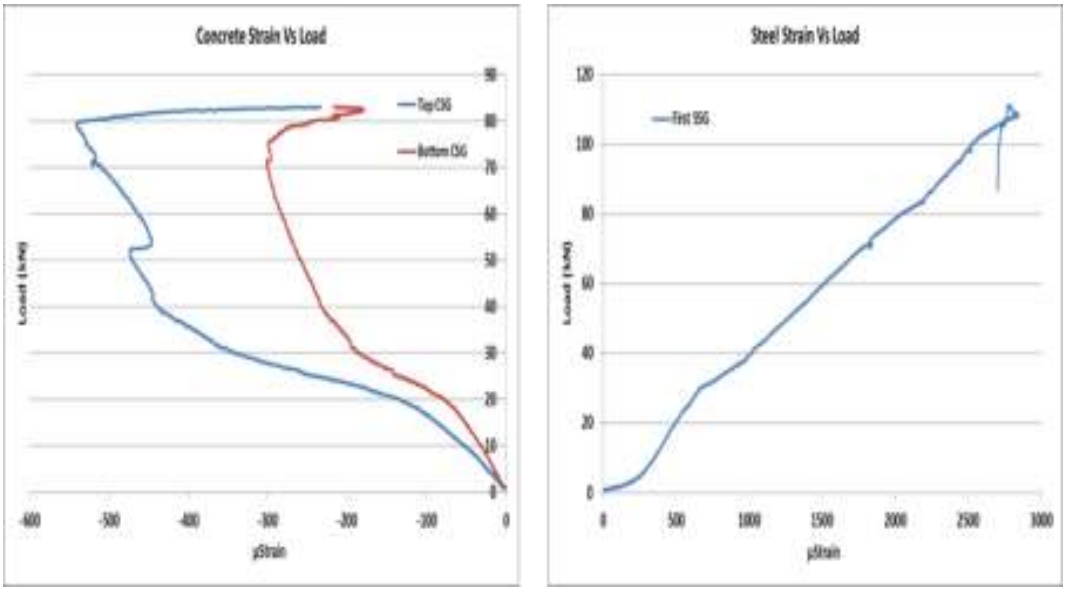

Figure 77: Concrete and steel strains versus load of R50-M-2.5-LR

Chapter 6: Analysis of Results

In this chapter, the experimental results of all beams are compared to the predicted shear strength obtained from international codes and semi-empirical methods, such as MCFT, and theoretical ones, such as fracture mechanics. The effects of different design parameters and material properties on the shear strength are analyzed and discussed in details.

6.1. Predicted Shear Strength

6.1.1. ACI 318. The ACI 318-14 code [56] presents Equation (28) to predict the shear strength provided by concrete in beams.

$$V_c = \left(0.16\lambda\sqrt{f'_c} + 17\,\rho_w \left(\frac{V_u d}{M_u}\right)\right) b_w d \;\leq 0.29\lambda\sqrt{f'_c}\, b_w d \qquad (28)$$

λ: Concrete parameter equal to1.0 for normal weight concrete, 0.75 for all light weight concrete and 0.85 for sand-light weight concrete.

f'_c: Concrete compressive strength (*MPa*)

b_w: Narrowest width of the beam.

$\rho_w = \frac{A_s}{b_w d}$: The flexural steel reinforcement ratio

V_u: Factored shear at the location considered (*N*)

M_u: Factored moment occurring simultaneously with V_u (*N-mm*) and $\left(\frac{V_u d}{M_u}\right) \leq 1$

For the considered RC beams in this study:

$\lambda = 1$, b = 150 *mm*

d = 259 *mm* for beams with ρ=1.03%, and d = 257 *mm* for beams with ρ=1.6%

for load at mid-span: $V_u\, d/M_u = d/a = d/650$

for load near support: $V_u\, d/M_u = d/a = d/300$

Table 13: Predicted shear strength using ACI 318-14 code.

Beam ID	Actual f'_c (MPa)	Predicted values based on ACI 318 (kN)		Actual Values from experimental tests (kN)	
		Shear	Load	Shear	Load
NA-L-1-HR	30.55	43.07	56.68	161.17	212.07
NA-L-1-LR	33.9	42.06	55.35	144.68	190.37
NA-M-1-LR	37.2	43.79	57.61	173.20	227.90
R50-L-1-HR	26.95	41.00	53.95	107.21	141.06
R50-L-1-LR	28.55	39.09	51.43	106.04	139.52
R50-M-1-LR	36	43.17	56.80	117.91	155.14
R100-L-1-HR	31.8	43.76	57.59	149.60	196.85
R100-L-1-LR	29.3	39.52	52.00	152.57	200.75
R100-M-1-LR	36.7	43.53	57.28	127.60	167.90
NA-L-2.5-LR	33	38.42	76.84	43.40	86.80
NA-M-2.5-LR	43.75	43.83	87.65	68.91	137.82
R50-L-2.5-LR	27.95	35.57	71.15	54.83	109.65
R50-M-2.5-LR	35.55	39.77	79.55	55.59	111.17
R100-L-2.5-LR	31.85	37.79	75.58	46.66	93.33
R100-M-2.5-LR	38.7	41.38	82.76	56.40	112.80

6.1.2. CSA 23.3. The National Building Code of Canada for reinforced concrete design [57], denoted by CSA 23.3 (2004), includes two methods for shear design: (a) simplified method, and (b) general method. In this study, the general method is utilized to predict the shear strength of the tested beams because it gives

more accurate results than the simplified method. The general method is based on the Modified Compression Field Theory that was developed by Vecchio and Collins [25] and explained in detail in Chapter 2. Based on this approach, Equation (29) below is used to calculate V_c.

$$V_c = \beta\sqrt{f'_c}\,b_w d_v \tag{29}$$

Where:

$$d_v = max(0.9d, 0.72h) \tag{30}$$

$$\beta = \frac{0.4}{(1+1500\varepsilon_x)}\frac{1300}{(1000+s_{ze})} \tag{31}$$

$$s_{ze} = \frac{35s_z}{15+a_g} \geq 0.85\, s_z \tag{32}$$

$s_z = \min(d_v,$ the maximum distance between layers of distributed longitudinal reinforcement)

$$\varepsilon_x = \frac{M_u/d_v + V_u}{2(E_s A_s)} \tag{33}$$

a_g: The nominal maximum size of coarse aggregate, not less than 20*mm*.

s_{ze}: Equivalent crack spacing parameter

s_z: Crack spacing parameter

Since Equation (29) is implicit because it contains (V) in both sides, it can only be solved iteratively. In other words, V_c is assumed and used to calculate ε_x. Then ε_x is used to find β and ultimately V_c. The convergence happens when the difference between assumed V_c and the calculated V_c is equal to zero. The shear strength results based on the general method is CSA 23.3-2004 are tabulated in Table 14.

Table 14: Predicted shear strength using CSA 2004.

Beam ID	Actual f'_c (MPa)	Predicted values based on CSA 23.3 (kN)		Actual Values from experimental tests (kN)	
		Shear	Load	Shear	Load
NA-L-1-HR	30.55	48.60	63.95	161.17	212.07
NA-L-1-LR	33.9	44.19	58.15	144.68	190.37
NA-M-1-LR	37.2	45.59	59.99	173.20	227.90
R50-L-1-HR	26.95	46.47	61.14	107.21	141.06
R50-L-1-LR	28.55	41.70	54.87	106.04	139.52
R50-M-1-LR	36	45.10	59.34	117.91	155.14
R100-L-1-HR	31.8	49.30	64.87	149.60	196.85
R100-L-1-LR	29.3	42.07	55.35	152.57	200.75
R100-M-1-LR	36.7	45.39	59.72	127.60	167.90
NA-L-2.5-LR	33	36.82	73.63	43.40	86.80
NA-M-2.5-LR	43.75	40.26	80.52	68.91	137.82
R50-L-2.5-LR	27.95	34.91	69.81	54.83	109.65
R50-M-2.5-LR	35.55	37.70	75.40	55.59	111.17
R100-L-2.5-LR	31.85	36.40	72.80	46.66	93.33
R100-M-2.5-LR	38.7	38.73	77.46	56.40	112.80

6.1.3. Response-2000 software package. As mentioned earlier, Response-2000 software was developed at the University of Toronto by Evan Bentz in a project supervised by Professor Michael P. Collins [58]. The software is based on MCFT

which was developed by the same professor. The sections were defined and properties of each beam were input in the software. Moreover, two types of loading increments were used depending on the (*a/d*) ratio. For beams with (*a/d* =1.15) ratio the load increment of '*V*' was 1 *kN* and for '*M*' was 0.3 *kN-m*, while it was 1 *kN* for '*V*' and 0.65 *kN-m* for '*M*' for the beams that has (*a/d*= 2.5). All the results are presented in Table 15. It is worth to mention that the failure of all models using Response-2000 was due to shear which is in agreement with actual beams' failure mode.

Table 15: Results from Response-2000.

Beam ID	Actual f'_c (*MPa*)	Predicted values based on Response 2000 (*kN*)		Actual Values from experimental tests (*kN*)	
		Shear	Load	Shear	Load
NA-L-1-HR	30.55	43.7	57.50	161.17	212.07
NA-L-1-LR	33.9	41.3	54.34	144.68	190.37
NA-M-1-LR	37.2	42.6	56.05	173.20	227.90
R50-L-1-HR	26.95	41.9	55.13	107.21	141.06
R50-L-1-LR	28.55	39	51.32	106.04	139.52
R50-M-1-LR	36	42.2	55.53	117.91	155.14
R100-L-1-HR	31.8	44.3	58.29	149.60	196.85
R100-L-1-LR	29.3	39.4	51.84	152.57	200.75
R100-M-1-LR	36.7	42.2	55.53	127.60	167.90
NA-L-2.5-LR	33	34.9	69.80	43.40	86.80
NA-M-2.5-LR	43.75	37.4	74.80	68.91	137.82
R50-L-2.5-LR	27.95	32.4	64.80	54.83	109.65
R50-M-2.5-LR	35.55	35.1	70.20	55.59	111.17
R100-L-2.5-LR	31.85	33.8	67.60	46.66	93.33
R100-M-2.5-LR	38.7	36	72.00	56.40	112.80

6.1.4. Strut-and-Tie model. The strut-and-tie model is thought by many researchers to resemble the actual behavior of reinforced concrete members in shear. Matamoros and Wong proposed a model to design simply supported beams using a Strut-And-Tie procedure [59], as shown in Figure 78. In this study, their approach is utilized to predict the shear strength of the fifteen tested beams.

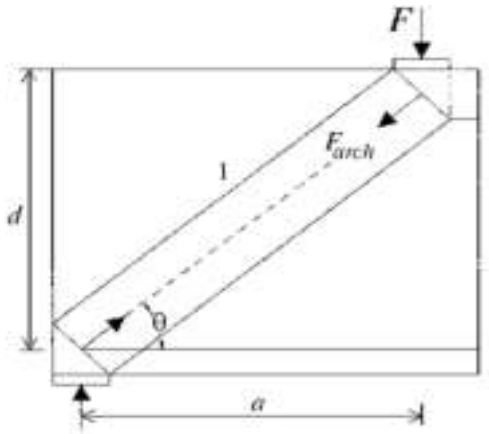

Figure 78: The mechanism of compression strut [59]

For the beams without transverse reinforcement, Equation (34) calculates the strength of the strut based on the geometry of the node at the support and assuming uniform width for the strut.

$$F_{strut} = f'_c A = f'_c(l_b sin\theta + h_a cos\theta)b \quad (34)$$

Where

l_b: the width of the base plate.

h_a: Twice the distance between the centroid of the main reinforcement and the bottom of the beam.

b: thickness of the web.

θ: can be approximated by $tan^{-1}(d/a)$.

C_c is a coefficient that can be obtained by relating the applied force to the strut strength. This coefficient is given in Equation (35):

$$C_c = \frac{P_{max}}{F_{strut}} = P_{max}/f'_c(l_b sin\theta + h_a cos\theta)b \quad (35)$$

They also proposed a lower value expression for the coefficient that includes the shear span-to-depth ratio in Equation (36):

$$C_c = \frac{0.3}{a/d} \leq 0.85\ sin\theta \quad (36)$$

Using Equation (34), Equation (35) and Equation (36), the maximum load was calculated and the results are presented in Table 16.

Table 16: Strut-and-Tie Model results

Beam ID	Actual f'_c (MPa)	Predicted values based on Strut-and-tie (kN)		Actual Values from experimental tests (kN)	
		Shear	Load	Shear	Load
NA-L-1-HR	30.55	103.09	135.65	161.17	212.07
NA-L-1-LR	33.9	115.41	151.86	144.68	190.37
NA-M-1-LR	37.2	126.65	166.64	173.20	227.90
R50-L-1-HR	26.95	90.94	119.66	107.21	141.06
R50-L-1-LR	28.55	97.20	127.89	106.04	139.52
R50-M-1-LR	36	122.56	161.27	117.91	155.14
R100-L-1-HR	31.8	107.31	141.20	149.60	196.85
R100-L-1-LR	29.3	99.75	131.25	152.57	200.75
R100-M-1-LR	36.7	124.95	164.40	127.60	167.90
NA-L-2.5-LR	33	29.09	58.18	43.40	86.80
NA-M-2.5-LR	43.75	38.57	77.14	68.91	137.82
R50-L-2.5-LR	27.95	24.64	49.28	54.83	109.65
R50-M-2.5-LR	35.55	31.34	62.68	55.59	111.17
R100-L-2.5-LR	31.85	28.08	56.15	46.66	93.33
R100-M-2.5-LR	38.7	34.12	68.23	56.40	112.80

6.1.5. Fracture mechanics methods. Researchers came up with models based on the fracture mechanics to calculate the shear strength of RC beams. A model was proposed by Bazant and Yu [42]. The proposed equation, Equation (37), includes the effect of the longitudinal reinforcement, the shear span-to-depth ratio and the maximum size of the aggregate in the mix.

$$V_c = 10\rho^{\frac{3}{8}}\left(1+\frac{d}{a}\right)\sqrt{\frac{f'_c}{1+\frac{d}{f'^{\frac{2}{3}}_c\, 3800\sqrt{d_a}}}}\, b_w d \tag{37}$$

This formula is in the US system units, where d_a is the maximum aggregate size, which is usually considered (0.77 *in* = 20 *mm*). The other symbols were explained earlier. Based on this model the shear strength of the tested beams was evaluated, converted to Metric System and reported in Table 17.

Gastebled and May [43] came up with a different model based on the fracture energy of a tensile crack that causes de-bonding of longitudinal reinforcement from the concrete. The model is described in Equation (38).

$$V_c = \frac{1.019}{\sqrt{d}}\left(\frac{d}{a}\right)^{\frac{1}{3}}\rho^{\frac{1}{6}}\left(1-\sqrt{\rho}\right)^{\frac{2}{3}} f'^{0.35}_c \sqrt{E_s} b_w d \tag{38}$$

Where '*a*' and '*d*' are in meters and f'_c in (*MPa*). E_s is the reinforcement steel modulus of elasticity (*MPa*). The results are shown in Table 18.

Another fracture mechanics model based on fracture energy was proposed by Xu et al. [44]. They claim that their model can predict the shear strength of lightly reinforced slender beams without stirrups. Their proposed model, which is described in Equation (39), is based on the assumption that the release of the longitudinal reinforcement from the surrounding concrete is due to the shear bond failure at the interface of the steel and the concrete.

$$V_c = \frac{1.018}{\sqrt{d}}\left(\frac{d}{a}\right)^{\frac{1}{3}}\rho^{\frac{1}{6}}\left(1-\sqrt{\rho}\right)^{\frac{2}{3}}(0.0255 f'_c + .24) b_w d \tag{39}$$

The predicted shear strengths of the tested beams were calculated and presented in Table 19.

Table 17: Bazant and Yu [42] Model Results

Beam ID	Actual f'_c (MPa)	Predicted values based on Bazant and Yu (kN)		Actual Values from experimental tests (kN)	
		Shear	Load	Shear	Load
NA-L-1-HR	30.55	68.72	90.41	161.17	212.07
NA-L-1-LR	33.9	60.97	80.23	144.68	190.37
NA-M-1-LR	37.2	62.94	82.81	173.20	227.90
R50-L-1-HR	26.95	65.74	86.50	107.21	141.06
R50-L-1-LR	28.55	57.43	75.57	106.04	139.52
R50-M-1-LR	36	62.24	81.89	117.91	155.14
R100-L-1-HR	31.8	69.68	91.69	149.60	196.85
R100-L-1-LR	29.3	57.96	76.26	152.57	200.75
R100-M-1-LR	36.7	62.65	82.43	127.60	167.90
NA-L-2.5-LR	33	60.41	120.82	43.40	86.80
NA-M-2.5-LR	43.75	66.44	132.88	68.91	137.82
R50-L-2.5-LR	27.95	57.00	114.01	54.83	109.65
R50-M-2.5-LR	35.55	61.97	123.95	55.59	111.17
R100-L-2.5-LR	31.85	59.67	119.35	46.66	93.33
R100-M-2.5-LR	38.7	63.78	127.56	56.40	112.80

Table 18: Gastebled and May [43] Model results

Beam ID	Actual f'_c (MPa)	Predicted values based on Gastebled and May (kN)		Actual Values from experimental tests (kN)	
		Shear	Load	Shear	Load
NA-L-1-HR	30.55	54.37	71.55	161.17	212.07
NA-L-1-LR	33.9	53.74	70.71	144.68	190.37
NA-M-1-LR	37.2	55.52	73.05	173.20	227.90
R50-L-1-HR	26.95	52.04	68.47	107.21	141.06
R50-L-1-LR	28.55	50.61	66.59	106.04	139.52
R50-M-1-LR	36	54.88	72.22	117.91	155.14
R100-L-1-HR	31.8	55.14	72.56	149.60	196.85
R100-L-1-LR	29.3	51.07	67.19	152.57	200.75
R100-M-1-LR	36.7	55.25	72.70	127.60	167.90
NA-L-2.5-LR	33	53.24	106.47	43.40	86.80
NA-M-2.5-LR	43.75	58.76	117.52	68.91	137.82
R50-L-2.5-LR	27.95	50.23	100.46	54.83	109.65
R50-M-2.5-LR	35.55	54.64	109.28	55.59	111.17
R100-L-2.5-LR	31.85	52.58	105.16	46.66	93.33
R100-M-2.5-LR	38.7	56.29	112.58	56.40	112.80

Table 19: Xu et al. Model [44] shear strength predictions

Beam ID	Actual f'_c (MPa)	Predicted values based on Gastebled and May (kN)		Actual Values from experimental tests (kN)	
		Shear	Load	Shear	Load
NA-L-1-HR	30.55	68.09	89.59	161.17	212.07
NA-L-1-LR	33.9	67.64	88.99	144.68	190.37
NA-M-1-LR	37.2	70.34	92.55	173.20	227.90
R50-L-1-HR	26.95	64.99	85.52	107.21	141.06
R50-L-1-LR	28.55	63.25	83.23	106.04	139.52
R50-M-1-LR	36	69.36	91.26	117.91	155.14
R100-L-1-HR	31.8	69.16	91.01	149.60	196.85
R100-L-1-LR	29.3	63.87	84.03	152.57	200.75
R100-M-1-LR	36.7	69.93	92.01	127.60	167.90
NA-L-2.5-LR	33	66.90	133.80	43.40	86.80
NA-M-2.5-LR	43.75	75.71	151.42	68.91	137.82
R50-L-2.5-LR	27.95	62.76	125.52	54.83	109.65
R50-M-2.5-LR	35.55	68.99	137.98	55.59	111.17
R100-L-2.5-LR	31.85	65.96	131.91	46.66	93.33
R100-M-2.5-LR	38.7	71.57	143.14	56.40	112.80

6.1.6. Comparing shear strength test results to predictions. To determine the applicability of the current structural design codes provisions and theoretical models available in the literature, the results from the tested beams were related to the predicted shear strength from the aforementioned design codes and models and the ratios are presented in Table 20 and Table 21.

Table 20: Comparison of test and predicted results for *a/d*= 1.15

Beam ID	f'_c	V_{test}/V_{ACI}	V_{test}/V_{CSA}	V_{test}/V_{R2K}	V_{test}/V_{STM}	V_{test}/V_{Bazant}	V_{test}/V_{Gasteb}	V_{test}/V_{Xu}
NA-L-1-HR	30.55	3.7	3.3	3.7	1.6	2.3	3.0	2.4
NA-L-1-LR	33.9	3.4	3.3	3.5	1.3	2.4	2.7	2.1
NA-M-1-LR	37.2	3.9	3.8	4.1	1.4	2.8	3.1	2.5
R50-L-1-HR	26.95	2.6	2.3	2.6	1.2	1.6	2.1	1.6
R50-L-1-LR	28.55	2.7	2.6	2.7	1.1	1.8	2.1	1.7
R50-M-1-LR	36.0	2.7	2.6	2.8	1.0	1.9	2.1	1.7
R100-L-1-HR	31.8	3.4	3.1	3.4	1.4	2.1	2.7	2.2
R100-L-1-LR	29.3	3.8	3.7	3.9	1.5	2.6	3.0	2.4
R100-M-1-LR	36.7	2.9	2.6	3.0	1.0	2.0	2.3	1.8
Average		3.3	3.1	3.3	1.3	2.2	2.6	2.1
Standard Deviation		0.5	0.5	0.5	0.2	0.4	0.4	0.3
COV%		15.5	16.4	16.0	15.2	16.7	15.7	15.5

Table 21: Comparison of test and predicted results for *a/d*= 2.5.

Beam ID	f'_c	V_{test}/V_{ACI}	V_{test}/V_{CSA}	V_{test}/V_{R2K}	V_{test}/V_{STM}	V_{test}/V_{Bazant}	V_{test}/V_{Gastel}	V_{test}/V_{Xu}
NA-L-2.5-LR	33.0	1.1	1.2	1.2	1.5	0.7	0.8	0.6
NA-M-2.5-LR	43.75	1.6	1.7	1.8	1.8	1.0	1.2	0.9
R50-L-2.5-LR	27.95	1.5	1.6	1.7	2.2	1.0	1.1	0.9
R50-M-2.5-LR	35.55	1.4	1.5	1.6	1.8	0.9	1.0	0.8
R100-L-2.5-LR	31.85	1.2	1.3	1.4	1.7	0.8	0.9	0.7
R100-M-2.5-LR	38.7	1.4	1.5	1.6	1.7	0.9	1.0	0.8
Average		1.4	1.5	1.6	1.8	0.9	1.0	0.8
Standard Deviation		0.2	0.2	0.2	0.2	0.1	0.1	0.1
COV%		11.4	12.1	12.6	12.9	12.0	11.9	11.4

From Table 20 and Table 21, it is clear that all the methods that were used to predict the shear strength of the tested beams gave overly conservative results for the case where *a/d*= 1.15, except for the strut-and-tie model which gave very good estimate of the shear strength. In the case where *a/d* = 2.5, the methods that are based on fracture mechanics gave unsafe predictions for one-half of the tested beams. The considered North American codes, e.g. ACI 318 and CSA 23.3, were able to predict the shear strength of beams with *a/d*= 2.5 reasonably well, but failed to do so for the beams with *a/d*= 1.15. It can be concluded that the shear strength of beams made with RA was under-estimated by all methods, except the ones that are based on fracture mechanics.

6.2. Effect of RA Replacement Ratio on Shear Strength

Since the tested beams did not have a constant concrete compressive strength within the two considered categories of low and medium strength, there is a need to normalize the results independent of f'_c. One way to do so for beams not reinforced

with stirrups in the test region is to divide the obtained shear strength, V_c (N), by square-root of f'_c (MPa) since well-established research on the subject has shown that the shear strength of concrete is proportional to this quantity. In order to consider the average shear stress within the cross-section at ultimate, the quantity $V_c/\sqrt{f'_c}$ is further divided by the beam width, b (mm), and effective depth, d (mm). Figure 79 shows the normalized shear strength for all fifteen tested beams.

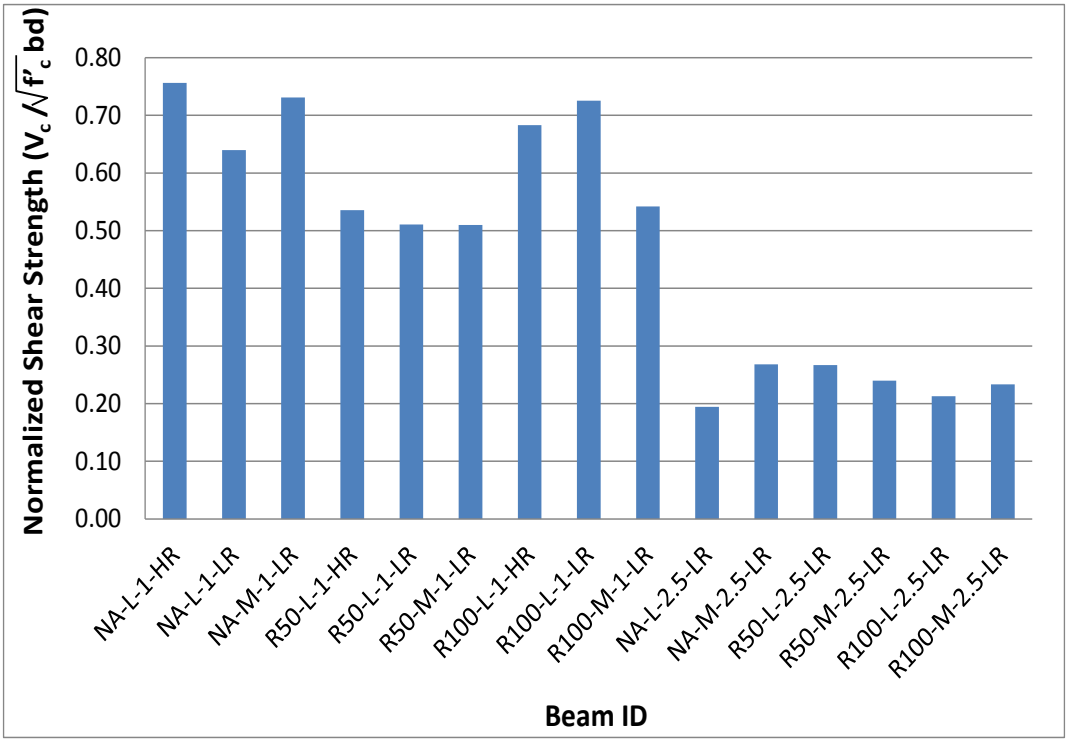

Figure 79: Normalized shear strength for the tested beams

Figure 80 shows the effect of recycled coarse aggregate replacement ratio on the normalized shear strength for all the considered RC beams. In general, the results indicate that the use of locally produced recycled coarse aggregate in beams does not greatly compromise the shear strength of the concrete, especially if the aggregate replacement ratio is 100%. Furthermore, all the recycled aggregate beams that were tested at a shear span-to-depth ratio equal to 2.5 showed close normalized shear strength values to their counterparts that were made with natural aggregate. For the beams with 100% RA, the results did not show a clear trend. For example, there were

three cases in which the NA beams were stronger in shear and two cases in which the RA beams were stronger. As for the beams with 50% RA, all results showed inferior shear strength of such beams when compared with their NA counterparts, except for the case of L-2.5-LR.

Plots of shear strength versus the deflection under the applied load for each group of beams with NA, 50% RA and 100% RA are presented in Figure 81 to Figure 85. In generally, the figures indicate that the beams that were tested at *a/d*= 1 showed somewhat more ductility than the other beams that were tested at *a/d*= 2.5. In the latter case (*a/d*= 2.5), almost all of the beams were not able to sustain any loading once the peak load was reached; thus, failing in a brittle fashion without any warning. Also, beams with 50% RA had less ductility than the ones with NA or 100% RA when the *a/d*= 1. For the case of *a/d*= 2.5 in which beams were subjected to both bending moment and shear, beams with low concrete strength failed when the deflection (2-3 *mm*) was much lower than that for beams with moderate concrete strength (3.7-5.2 *mm*).

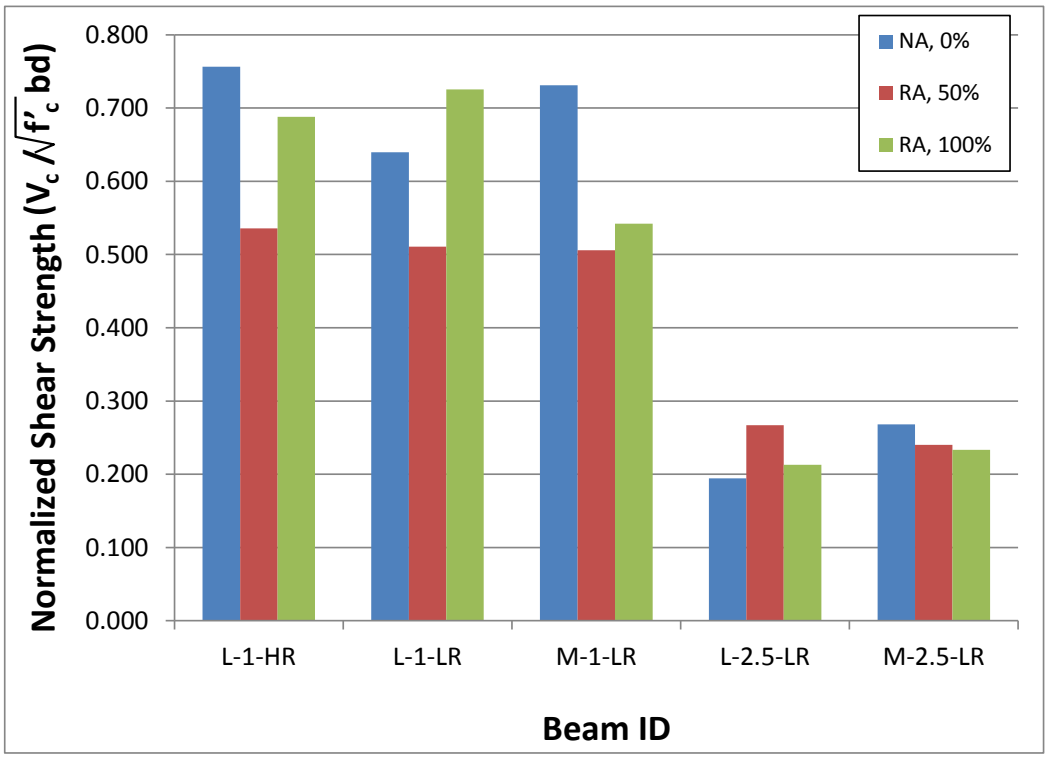

Figure 80: Effect of RA replacement ratio on shear capacity

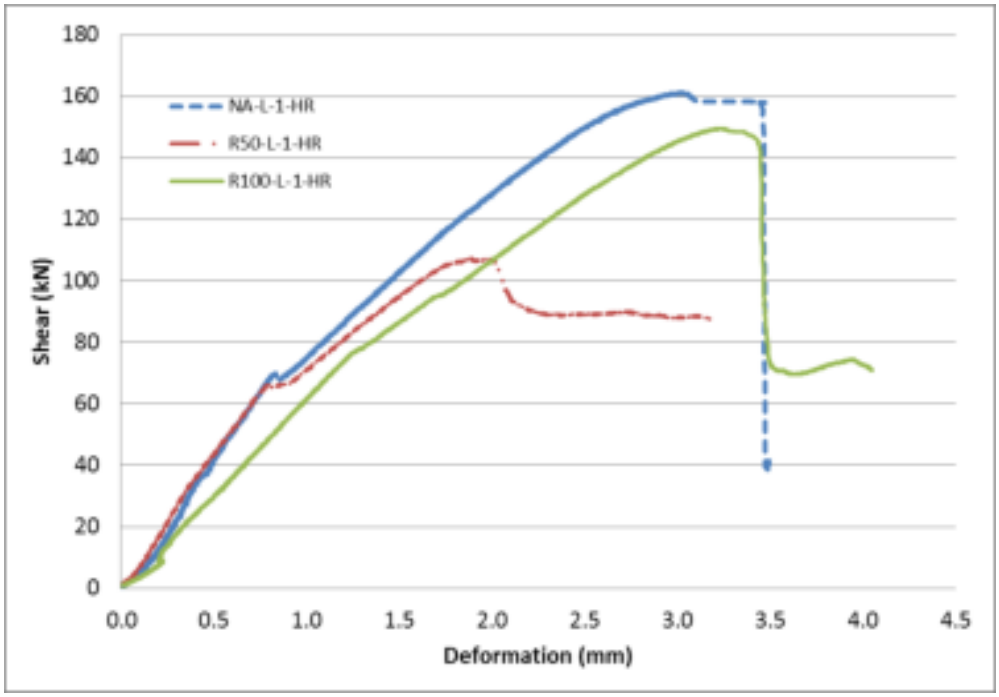

Figure 81: Shear versus deformation of L-1-HR beams

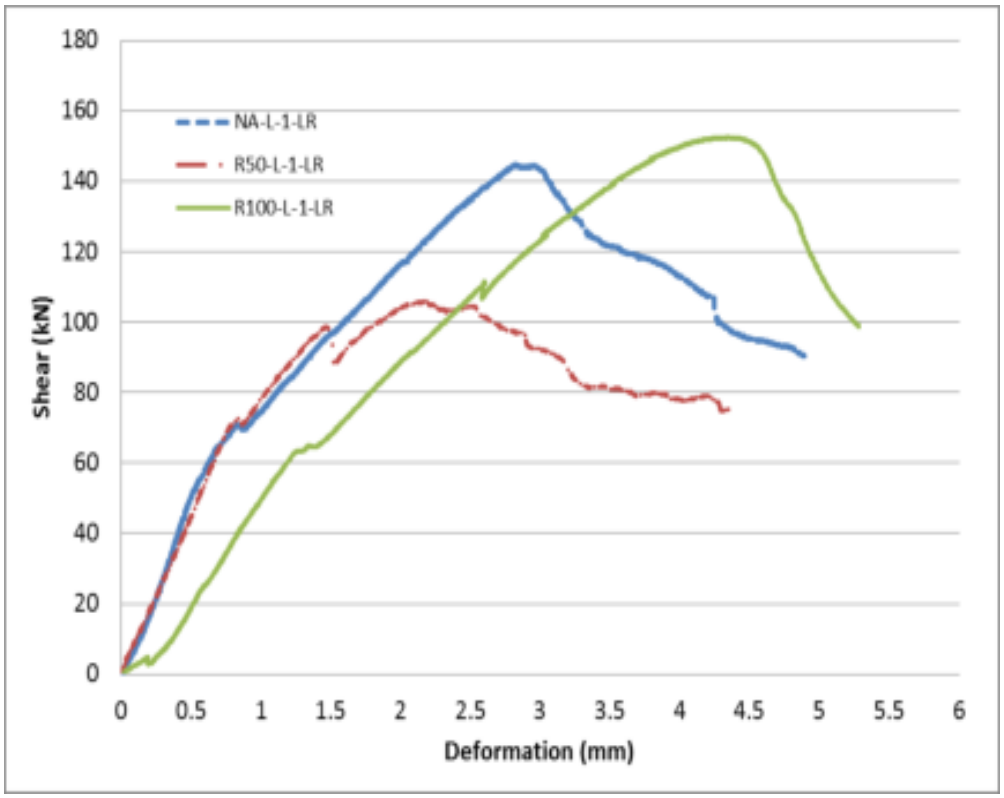

Figure 82: Shear versus deformation of L-1-LR beams

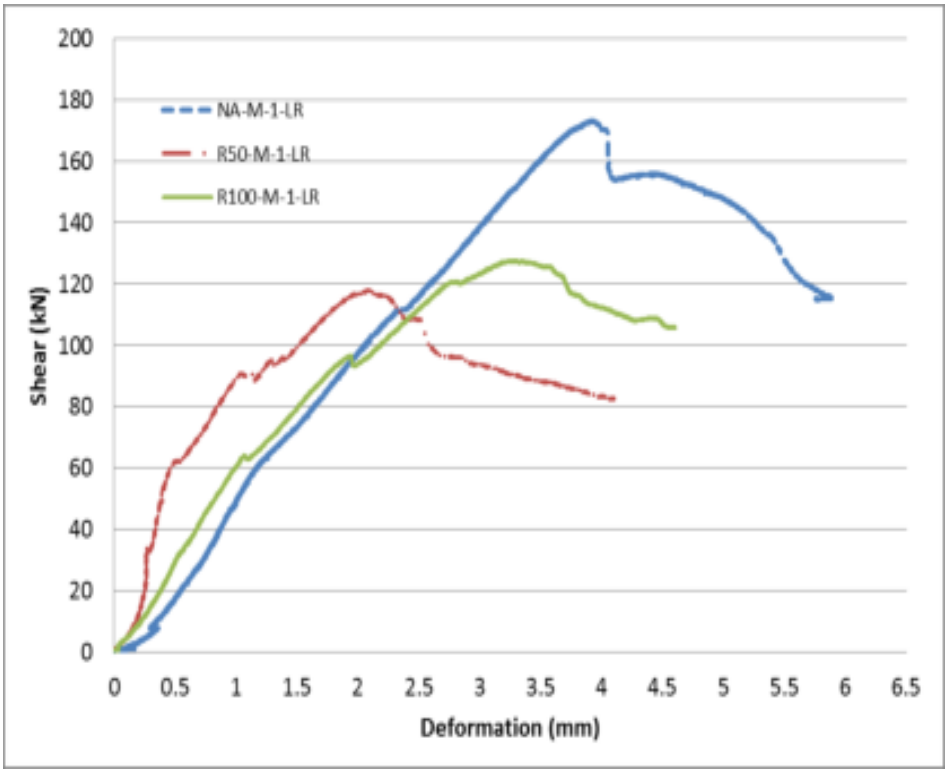

Figure 83: Shear versus deformation of M-1-LR beams

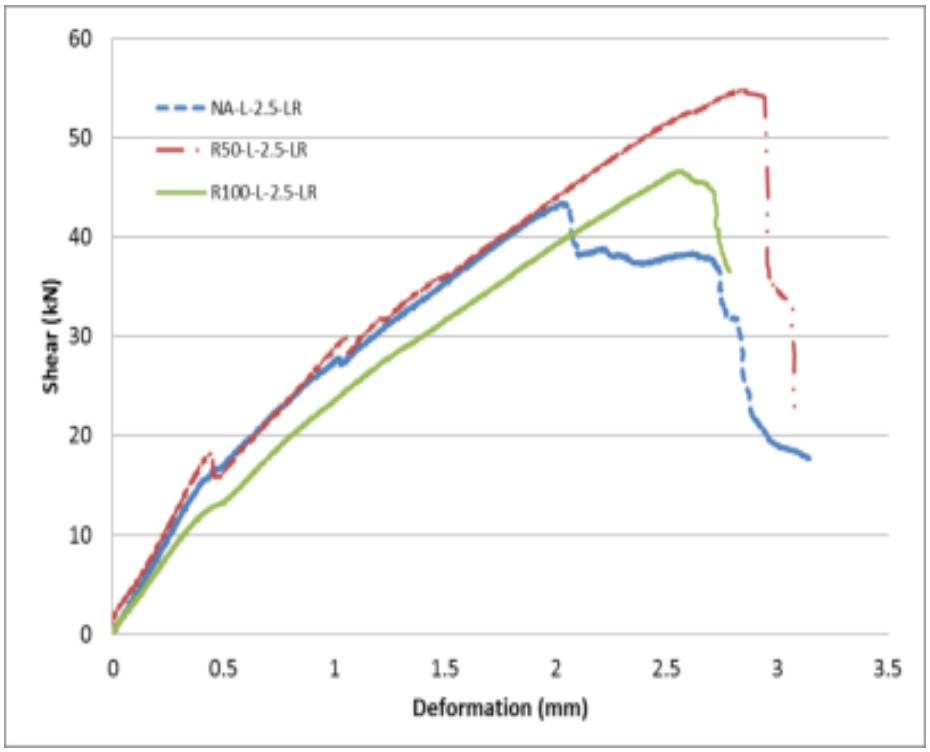

Figure 84: Shear versus deformation of L-2.5-LR beams

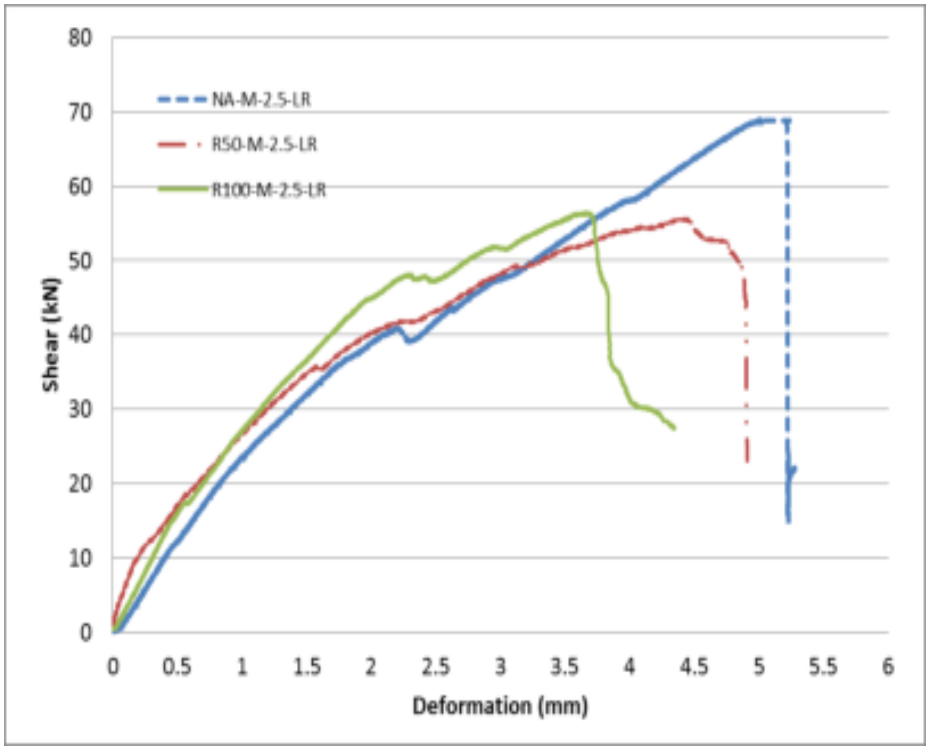

Figure 85: Shear versus deformation of M-2.5-LR beams

Compared with the 50% RA beams, the observed increase in shear capacity of beams made with 100% RA can be attributed to the rough and jagged surface of the recycled aggregate, causing them to have better interlock with each other and bonding with the mortar around them. This was also found by Casuccio et al. [60]. Moreover, it was observed that the shear plane went through the recycled aggregate not around them, proving that the RA had good bonding characteristics although they were somewhat weaker than the NA which were made from lime stone. Figure 86 shows two samples that were taken from a beam made with 100% RA after testing. From the bright white color of the aggregate, one can conclude that the shear plane had cut through the coarse aggregate. The beams that were made with 50% RA achieved more shear capacity than the beams made with NA in the case where *a/d*= 2.5. This indicates that the presence of both rounded natural aggregate with pointed recycled aggregate in the same concrete mix might not give as much high shear strength as a mix with 100% natural aggregate or 100% recycled aggregate, particularly when the *a/d* is small.

Figure 86: Samples taken from beam made with 100% RA

6.3. Effect of Shear Span-to-Depth Ratio on Shear Strength

Existing literature indicates that the span-to-depth ratio has a significant effect on the shear strength of RC beams without stirrups. The smaller the (*a/d*) ratio, the higher the shear strength of a beam is because the bending moment at that location is small and the arching action is more effective when the applied load is near the support. To observe the effect of (*a/d*) ratio in this study, each two corresponding beams are compared together. For example, the beam NA-M-1-LR is compared with the beam NA-M-2.5-LR; where *a/d*= 1.15 in the first beam and *a/d*= 2.5 in the second. Figure 87 depicts the results and presents a comparison between the shear capacities of each two similar beams independent of the concrete strength. Moreover, the shear versus deflection plots of each corresponding beams are presented in Figure 88 to Figure 90. It can be noticed from the results that the shear capacity in beams with *a/d* = 1.15 can be 1.9-3.4 times the shear strength of beams with *a/d*= 2.5. The results showed that the effect of the *a/d* ratio on the shear strength is less dominant in the beams with 50% RA than in the other tested beams.

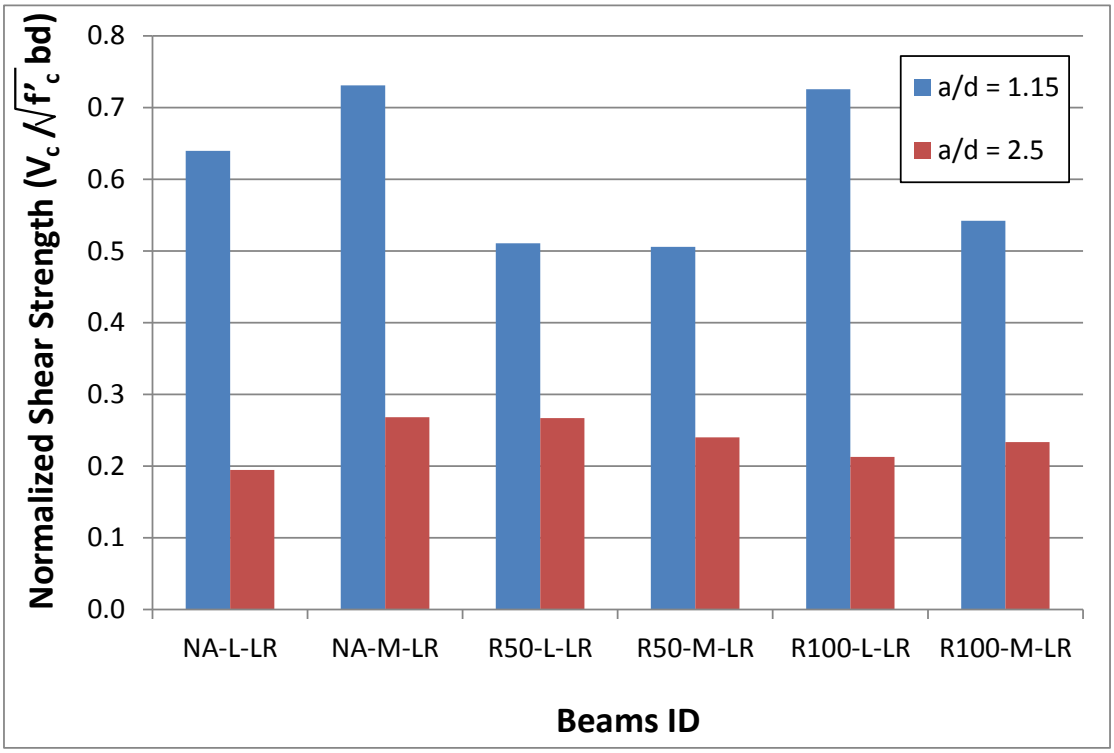

Figure 87: Effect of span-to-depth ratio on the shear capacity

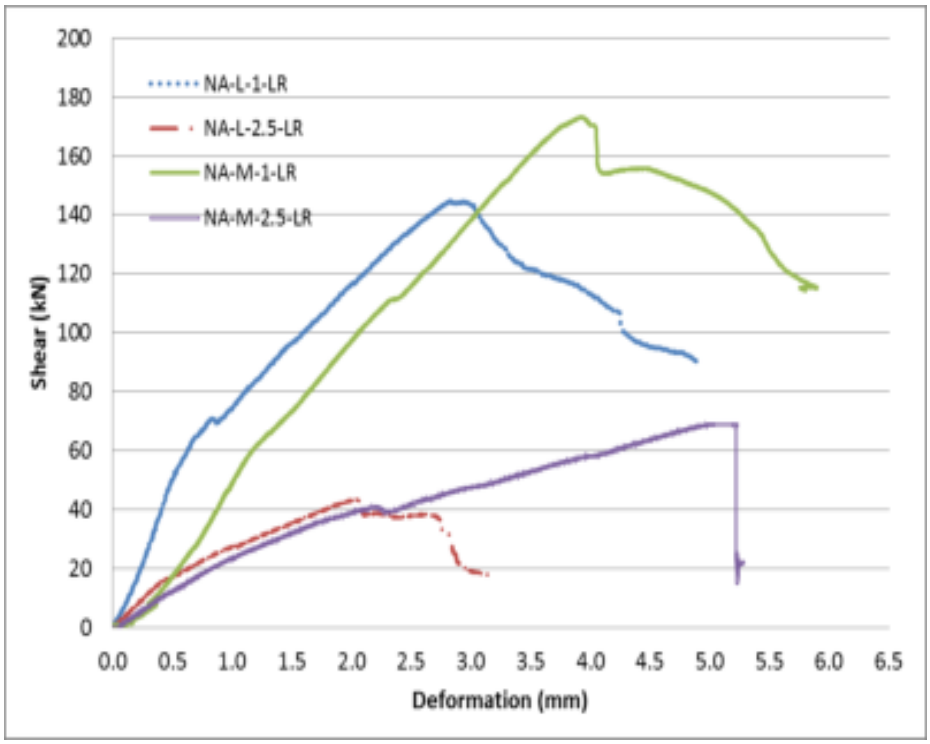

Figure 88: (*a/d*) effect on NA beams for both low and medium f'_c

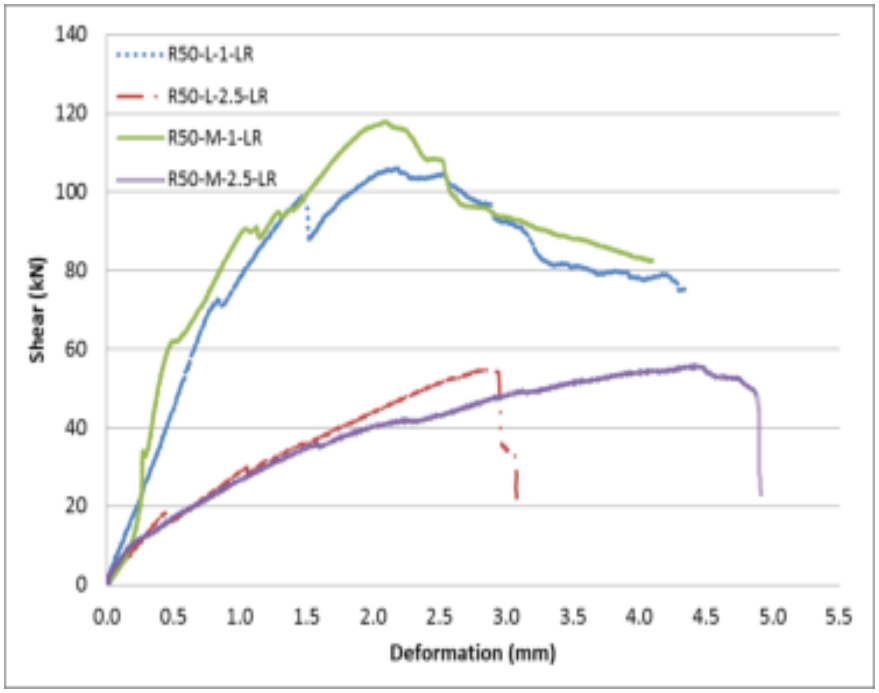

Figure 89: (*a/d*) effect on 50% RA beams for both low and medium f'_c

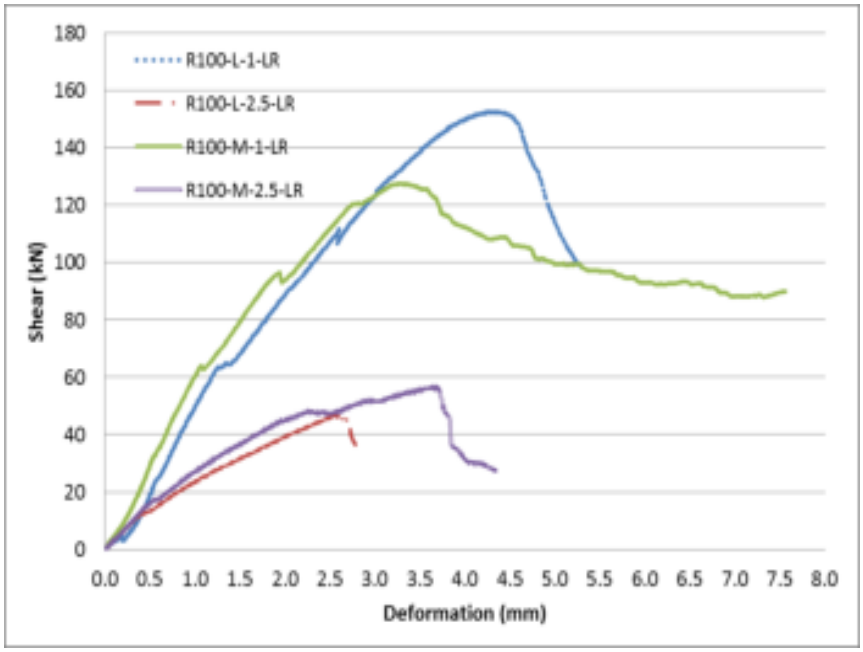

Figure 90: (*a/d*) effect on 100% RA beams for both low and medium f'_c

This increase in shear strength for beams with small *a/d* ratios is recognized by the deep provisions of the ACI 318 code [56]. The strut-and-tie model (STM) is well established model with which it is possible to explain shear behavior of RC deep

beams and shallow beams with shear span-to-total height ratio equal or less than 2. As shown in in Figure 91, the model consists of a strut, diagonal concrete part extending from the load point to the support, which is compressed due to the direct load transfer from the load point to the near support. It also consists of a tie, usually the longitudinal steel reinforcement, which is under tension because it is trying to hold the arch's both ends. Usually, the beams that abide to this model fail in two ways: diagonal tension when the crack reaches the strut and compression failure in the strut [61].

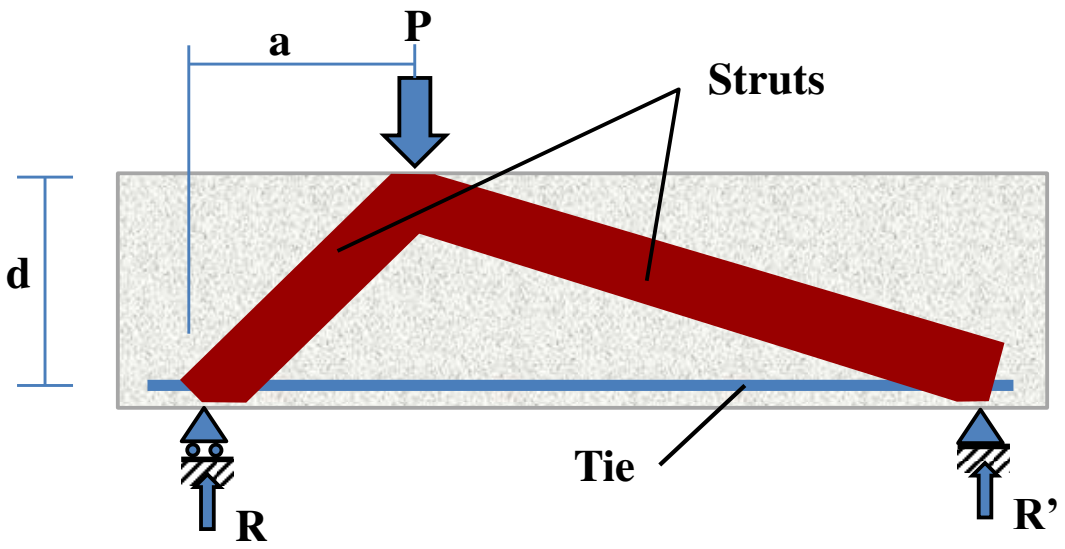

Figure 91: Strut and Tie Model

In this study, all the beams failed due to diagonal tension. For the slender beams, the arching action effect starts to diminish with the increase of (*a/d*) and other factors stated below [62]:

- Shear resistance in the un-cracked concrete: the compression in the un-cracked concrete helps in resisting the shear forces, however, in slender beams this factor contributes very little.
- Interface shear transfer: or as it is usually called the "aggregates interlock" or "friction". The influence of this factor decreases with the

increase in the crack's width, and increases with the increase of the aggregates size.

- Residual tensile stresses: Even though the cracked concrete contribution is usually neglected, the concrete still resists shear when it is cracked, as recognized by the modified compression field theory, especially when the crack width is small. That is because there are still some residual tensile stresses in the crack that are trying to prevent the crack from widening.
- Dowel action: When shear forces cause the concrete to crack, the longitudinal reinforcement crossing the crack will try to hold the crack tight and prevent it from widening. This factor depends on the concrete cover, the size of the flexural reinforcement and the bonding between the surrounding concrete and the reinforcement.

These factors combined produce less resistance to shear compared to the arch action that happens in deep beams. That's why the shear capacity in slender beams with *a/d*= 2.5 is much less than the corresponding deep beams in this study which have *a/d*= 1.15.

6.4. Effect of Concrete Strength on Shear Strength

The contribution of concrete compressive strength to the shear strength of RC beams has been studied for a long time. Higher compressive strength forces the shear plane to go through the aggregates not through the mortar between them; thus, increasing the shear strength of the concrete member. When the strut-and-tie model is used, the compressive strength determines the maximum compression force that the strut can withhold before it fails. More importantly, the concrete compressive strength is the used to derive the tensile strength that the concrete can take using empirical equations. And since the shear failure is a diagonal tension failure, the higher the concrete strength, the more the shear strength is going to be. The ACI 318 includes the concrete compressive strength effect in its shear design guidelines by the term ($0.16\lambda\sqrt{f'_c}$).

In Figure 92, the shear capacity of the tested beams is presented for each pair of beams having similar parameters but different $\sqrt{f'_c}$. In all cases except one, the

higher the compressive strength, the more the shear capacity of the beam is. The only case in which the increase in concrete compressive strength did not cause a rise in the shear capacity was for the pair of beams R100-1-LR. This could be attributed the fact that the beam R100-M-1-LR was tested at age of 5 weeks, where as its counterpart, beam R100-L-1-LR, was tested at the age of 5 months.

Figure 92 also shows that the effect of $\sqrt{f'_c}$ on the shear strength is much more predominant in the beams that were made with NA than in the beams that were made with RA. The reason for this is because it is well established that an increase in compressive strength of concrete with NA causes a direct increase in the shear and tensile strengths of the concrete. This statement is not well established for concrete made with recycled aggregate due to the many variables involved in its production. Therefore, the effect of the compressive strength of concrete made with RA on shear strength is not as dominant as corresponding concrete made with NA.

The shear versus deflection plots of each corresponding beams are presented in figures from Figure 93 to Figure 95. The relationships generally indicate higher stiffness of beams made with NA than corresponding beams with RA.

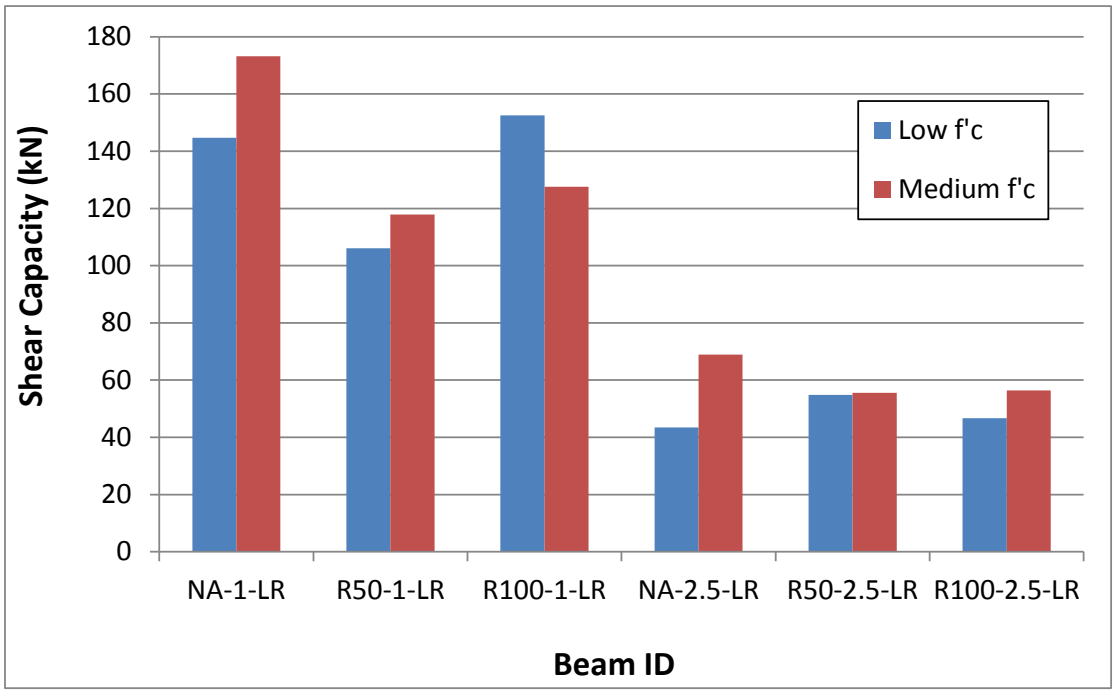

Figure 92: Effect of f'$_c$ on the shear capacity

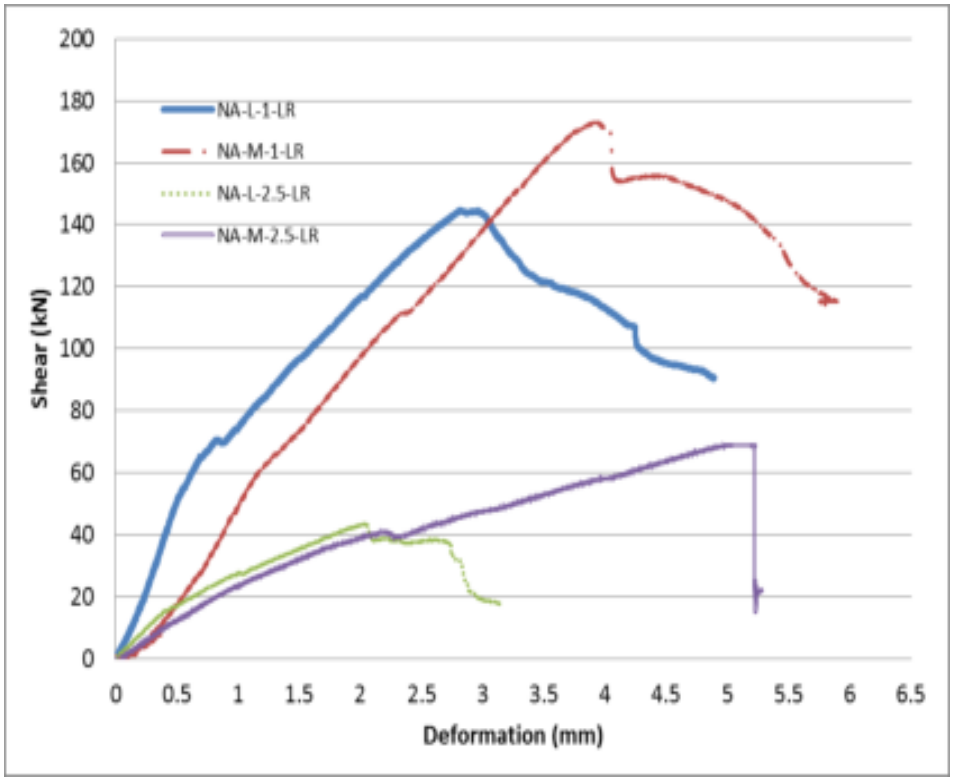

Figure 93: Effect of f'$_c$ on NA beams

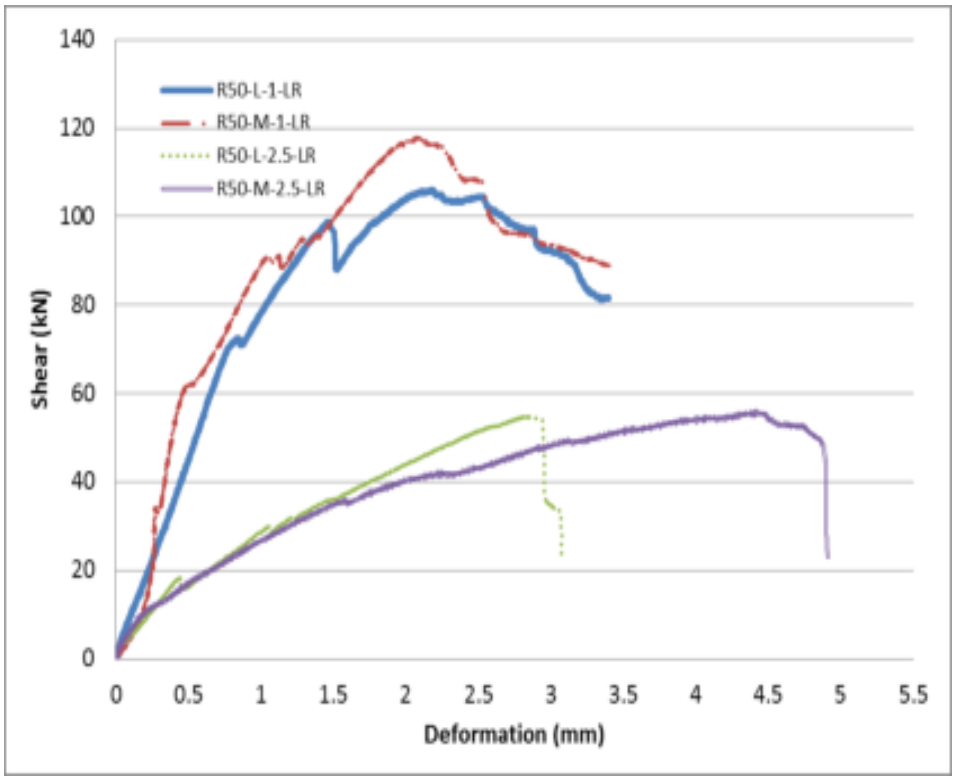

Figure 94: Effect of f'$_c$ on 50% RA beams

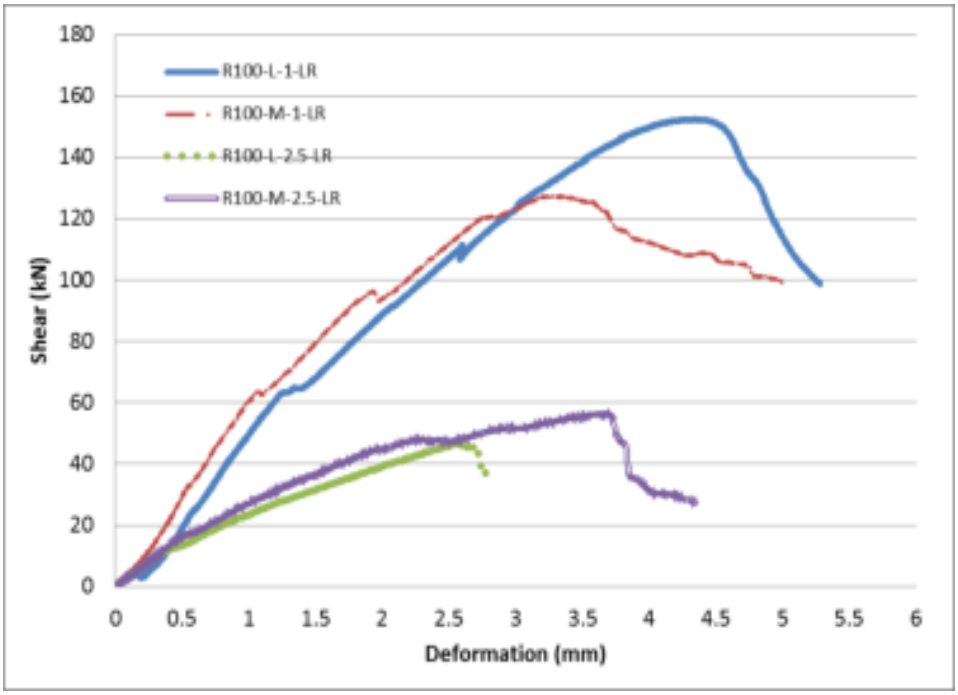

Figure 95: Effect of f'$_c$ on 100% RA beams

6.5. Effect of Longitudinal Reinforcement on Shear Strength

To investigate the effect of the flexural longitudinal reinforcement ratio on the shear strength of RC beams, two reinforcement ratios were used in this study. Three beams were casted with low reinforcement (LR) ratio ($\rho = 1.03\%$), consisting of two No. 12 bars at the bottom, and three similar beams were casted with high reinforcement (HR) ratio ($\rho = 1.6\%$), consisting of two No. 16 bars at the bottom, while keeping all other parameters the same. All of those beams had low target concrete compressive strength and a/d = 1.15. Figure 96 compares the normalized shear strength of each pair of beams having low and high ρ. The shear force versus deflection plots of each corresponding pair of beams are presented in Figure 97 to Figure 99.

It can be deduced from Figure 96 that the normalized shear strength of beams made with NA increased by 15.4% when (ρ) was increased from 1.03% to 1.6%. This is consistent with previous research which shows that dowel action of the flexural reinforcement in resisting shear increases with the increase of area of flexural reinforcement.

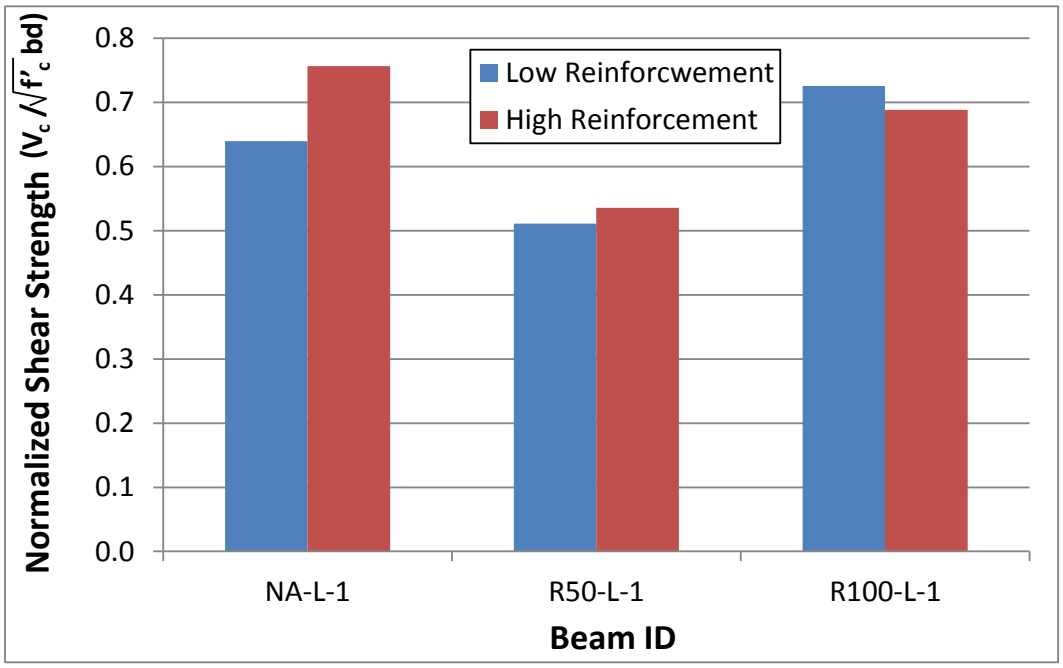

Figure 96: Effect of longitudinal reinforcement ratio on the shear capacity

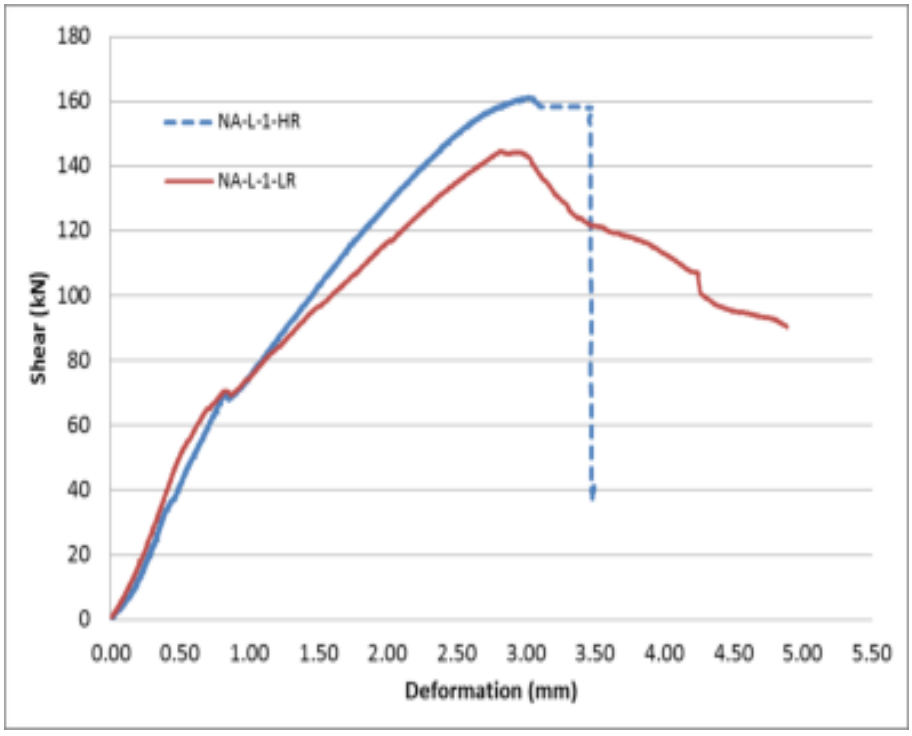

Figure 97: Effect of ρ on NA beams

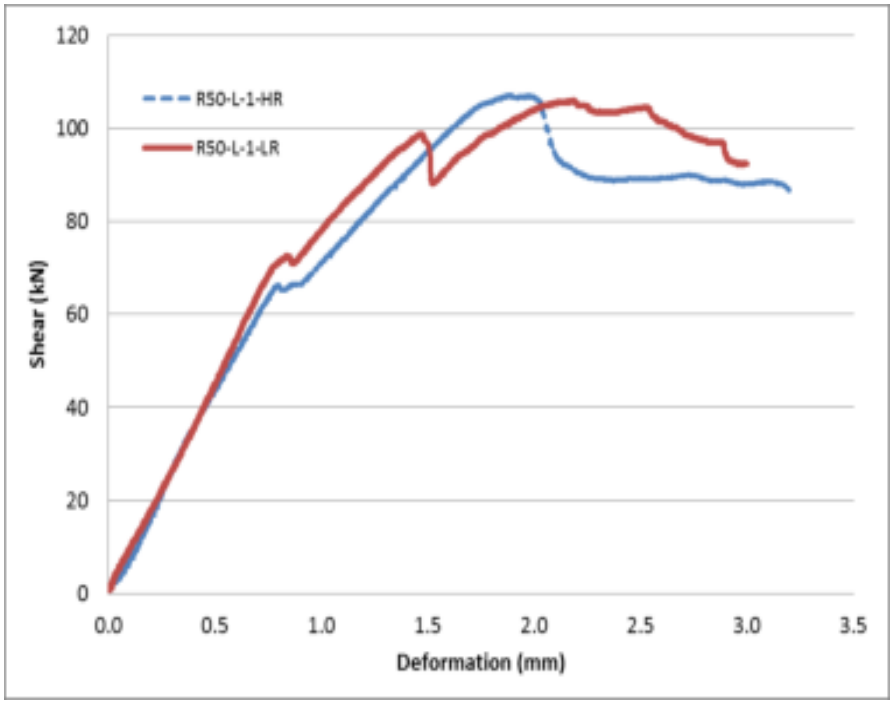

Figure 98: Effect of ρ on 50% RA beams

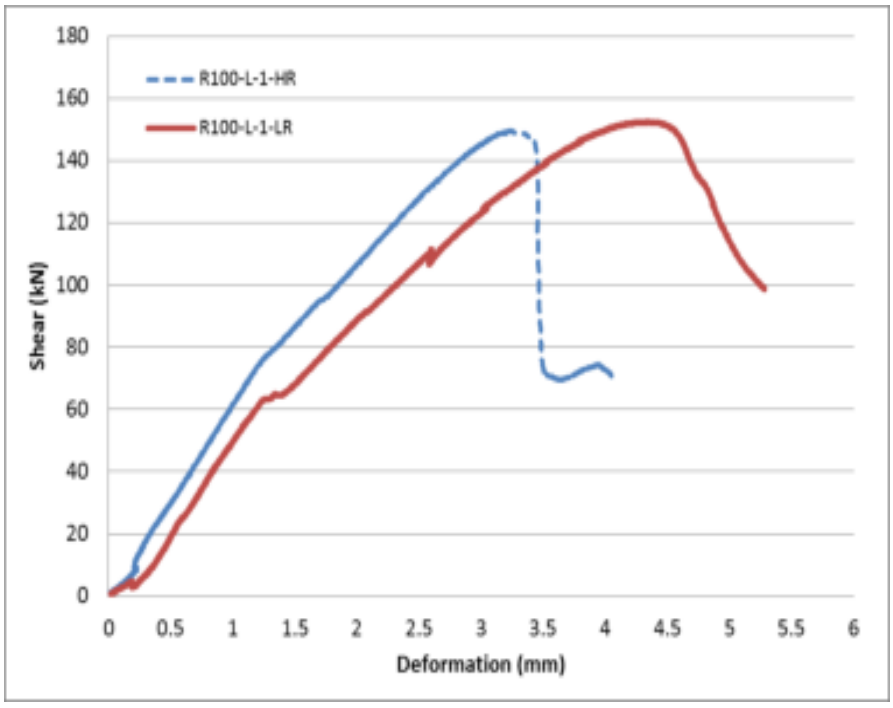

Figure 99: Effect of ρ on 100% RA beams

However, the effect of the flexural reinforcement ratio was not significant in the beams made with concrete utilizing RA, as the shear strength in these cases was slightly improved for the 50% RA beams, and a little reduced for the 100% RA beams. This may be caused by the larger shear crack widths observed in beams made with RA compared with respective beams made with NA, as demonstrated in Figure 73, and possible loss of bond between the concrete and flexural reinforcement in the RA beams at the location of the major shear crack. These two factors reduce the effect of the dowel action due increase in the unsupported length of the rebars in the vicinity of the shear crack.

6.6. Recommendation for Design

Based on this limited study which utilized one batch of recycled coarse aggregate from Beeáh's facility in Sharjah, a factor, (α), is proposed to account for the use of recycled aggregate in the shear simplified equation of the ACI 318 code. The simplified equation, shown as Equation (40) below, already accounts for the use of the light weight aggregate by incorporating the factor λ.

$$V_c = 0.17\lambda\sqrt{f'_c}b_w d \tag{40}$$

The corresponding equation for the shear strength provided by concrete with consideration of the flexural steel reinforcement ratio and *a/d* is shown below:

$$V_c = \left(0.16\lambda\sqrt{f'_c} + 17\,\rho_w\left(\frac{V_u d}{M_u}\right)\right) b_w d \;\leq 0.29\lambda\sqrt{f'_c}b_w d \tag{41}$$

To derive a factor that accounts for the use of recycled coarse aggregate from Bee'h in place of natural aggregate based on the fifteen tested beams in this study, the following conservative approach is utilized:

1- The value of $(V_{test}/\sqrt{f'_c}b_w d)$ is calculated for each beam.
2- The minimum value of $(V_{test}/\sqrt{f'_c}b_w d)_{RA}/(V_{test}/\sqrt{f'_c}b_w d)_{NA}$ for all the tested beams with similar characteristics is calculated. The minimum value is

used because of the limited experimental program of the study and the coarse aggregate was from one batch.

3- The value obtained in Step 3, denoted by α, represents a reduction to expression of V_c, and can be incorporated into Equation (42) and Equation (43) as follows:

$$V_c = 0.17\lambda\alpha\sqrt{f'_c}b_w d \tag{42}$$

$$V_c = \left(0.16\lambda\alpha\sqrt{f'_c} + 17\,\rho_w\left(\frac{V_u d}{M_u}\right)\right)b_w d \;\leq 0.29\lambda\alpha\sqrt{f'_c}b_w d \tag{43}$$

As an example, the first two corresponding beams of 50% recycled aggregate beams will be presented first:

$$\frac{(V_{test}/\sqrt{f'_c}b_w d)_{R50-L-1-HR}}{(V_{test}/\sqrt{f'_c}b_w d)_{NA-L-1-HR}} = \frac{0.5357}{0.7564} = 0.708$$

and so on for all the other RA beams. Figure 100 shows the reduction factor for all the tested beams. Hence,

$$\alpha = Min\left[\frac{0.5357}{0.7564}, \frac{0.5108}{0.6396}, \frac{0.5098}{0.7309}, \frac{0.6829}{0.7564}, \frac{0.7255}{0.6396}, \frac{0.5422}{0.7309}, \frac{0.2670}{0.1945}, \frac{0.2400}{0.2682}, \frac{0.2128}{0.1945}, \frac{0.2334}{0.2682}\right]$$

From the above, the reduction factor α is 0.708, which can be rounded down to 0.70. This factor can be incorporated into the expressions of Equations (42) and (43).

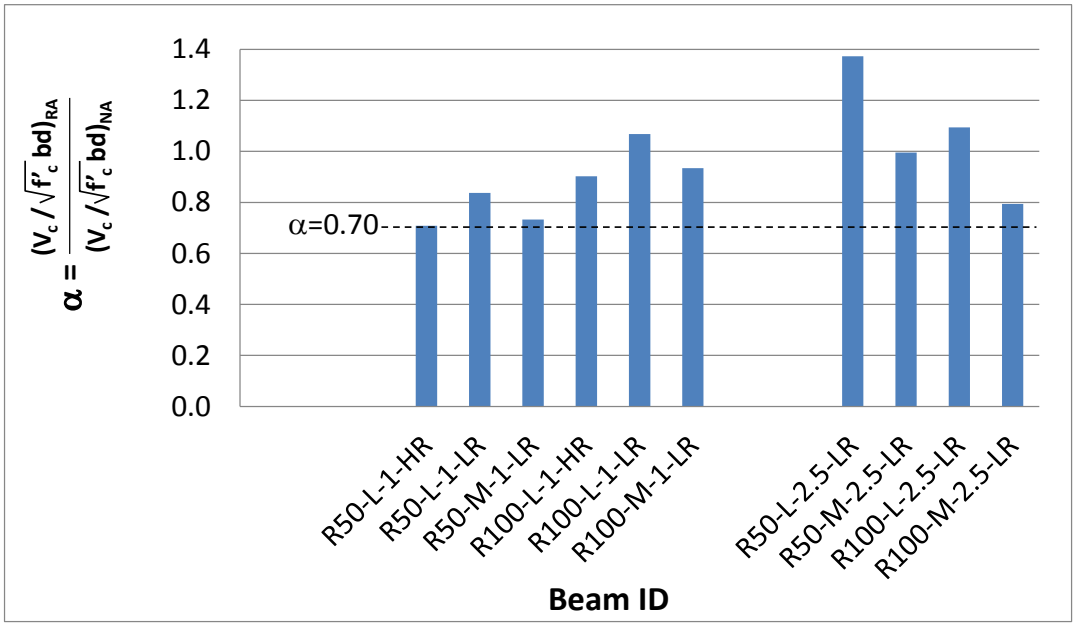

Figure 100: Ratio of recycled-to-natural aggregate shear strength of beams

Chapter 7: Conclusions and Recommendations

7.1. Summary

The Bee'ah's Waste Management Complex in the Emirate of Sharjah, UAE, uses demolition and construction waste (CDW) to produce aggregates that is currently being used primarily in pavements and road works. The purpose of this study is to extend the range of use of such aggregate to structural applications. This study is conducted to investigate the behavior and develop design recommendations for the shear strength of RC beams made with local recycled aggregate from Bee'ah. Fifteen beams were tested experimentally and various parameters were accounted for, such as different concrete compressive strengths, recycled coarse aggregate replacement percentages in the concrete mix, shear span-to-depth ratios and effective flexural steel reinforcement ratios. The theoretical part of the study considers available codified procedures for predicting the shear strength of concrete beams, such as the ACI 318 and CSA A23.3, as well as more thorough and comprehensive methods, such as the strut-and-tie procedure, modified compression field theory and fracture mechanics approach.

7.2. Conclusions

Based on the results of the study, which employed a limited number of beams and one batch of recycled concrete aggregate, the following conclusions are relevant:

1. All the tested beams with NA or RA failed in a brittle fashion once the peak capacity was reached. The mode of failure was due to diagonal tension shear failure. As the recycled coarse aggregate replacement percentage increased, the average shear crack width consistently increased. For the beams with small shear span-to depth ratio, the average angle of inclination of the shear crack was about 45.3º. On the other hand, the average angle of inclination of the shear crack was about 38.3º for the beams with large shear span-to-depth ratio. Also, tested beams made with NA had somewhat steeper angle of shear crack than those made with RA.

2. The ACI 318 and CSA 23.3 shear design provisions for beams without stirrups give reasonable predictions of the shear strength provided by concrete when the shear span-to-depth ratio is large but provide overly conservative estimates when the shear span-to-depth ratio is small. That's why structural concrete design codes recommend the use of the strut-and-tie method for deep beams with shear span-to-thickness ratio less than 2.
3. In general, the Strut-and-Tie model predicted the shear strength of the tested beams with NA and RA much better than the modified compression field theory and the three considered approaches that are based on fracture mechanics.
4. The beams which employed recycled coarse aggregate in the concrete mix showed lower shear strength when the coarse aggregate replacement ratio is 50% and comparable shear strength when the replacement ratio is 100% than corresponding beams made with natural aggregate. All the recycled aggregate beams that were tested at a shear span-to-depth ratio equal to 2.5 showed close normalized shear strengths to their counterparts that were made with natural aggregate. The beams with 100% recycled coarse aggregate replacement often yielded higher shear strength than those with 50% recycled coarse aggregate. This could be attributed to the aggregate interlock along the shear crack due to the rough surface and pointed angles of the recycled aggregate.
5. The influence of the concrete compressive strength on the shear capacity is much more predominant in the beams that were made with natural aggregate than those that were made with recycled aggregate. The reason for this is because it is well established that an increase in compressive strength of concrete with natural aggregate causes a direct increase in the shear and tensile strengths of the concrete. This statement is not well established for concrete made with recycled aggregate due to the many variables involved in its production.
6. The effect of the flexural reinforcement ratio was not as significant in the beams made concrete utilizing recycled aggregate as those made with natural aggregate. This may be caused by the larger shear crack widths observed in the beams made with recycled aggregate compared with respective beams made with natural aggregate, and possible loss of bond between the concrete

and flexural reinforcement in the recycled concrete beams at the location of the major shear crack.

7. Until more tests on shear strength of concrete beams having recycled aggregate from Bee'ah become available, a reduction factor in the order of 30% (i.e. a multiplier equal to 0.7) is suggested to be incorporated into the concrete shear strength equations in the relevant codes.

Overall, the results showed that the shear strength of beams made with locally produced recycled coarse aggregate by Beeáh is dependent on the coarse aggregate replacement ratio. Use of recycled aggregate does not greatly compromise shear strength when compared with equivalent beams having natural aggregate, especially when the coarse aggregate replacement ratio is 100%. Thus, there is potential for using coarse aggregate produced by Beeáh in new concrete mixes for structural application involving shear. As explained throughout the thesis, all of the conclusions included here address RC beams made with recycled coarse aggregate from Beeáh, obtained from one batch.

7.3. Recommendations for Future Research

During the course of the study, it became apparent that structural application of recycled concrete is a wide open field that has many implications. More complicated is the structural shear behavior of reinforced concrete beams made with recycled aggregate. Future research on the subject should consider:

- Different batches of recycled aggregate from the same source.
- Recycled aggregate obtained from different sources.
- Concrete batches utilizing both recycled fine and coarse aggregate
- Beams with different *a/d* ratios from what was tested in this study.
- Different concrete mixes having different W/C ratios and f'_c
- Different cross-sections (e.g. *T, box, I*)
- Different recycled aggregate replacement ratios.
- Different longitudinal reinforcement ratios.
- Beams containing stirrups
- Columns subjected to both axial compressive load plus shear

References

[1] Gulfnews.com. (2015). *UAE economy to grow despite oil prices*. Available: http://gulfnews.com/business/economy/uae-economy-to-grow-despite-oil-prices-minister-1.1481922

[2] Constructionweekonline.com. (2013). *GCC concrete demand to reach $49bn over two years*. Available: http://www.constructionweekonline.com/article-24400-gcc-concrete-demand-to-reach-49bn-over-two-years/

[3] J. de Brito and N. Saikia, *Recycled Aggregate in Concrete*. London, UK: Springer London, 2013.

[4] Bee'ah. (20th, May 2015). *Construction waste recycling*. Available: http://beeah.ae/waste-management-main/#wasterecyclingfacilities

[5] Masaood.com. (2015). *Ready Rocks Quarries*. Available: http://www.masaood.com/content/Ready-Rocks-Quarries

[6] Government-of-Dubai. (2014). *Circular No. 198*. Available: http://www.dm.gov.ae/wps/wcm/connect/9fa0c3ac-9d5f-43a6-bfa0-fa573c344bbf/circular%23198.pdf?MOD=AJPERES

[7] A. D. U. P. Council. (2010). *Estidama Vision*. Available: http://estidama.upc.gov.ae/

[8] Y.-N. Sheen, H.-Y. Wang, Y.-P. Juang, and D.-H. Le, "Assessment on the engineering properties of ready-mixed concrete using recycled aggregates," *Construction and Building Materials,* vol. 45, pp. 298-305, 2013.

[9] V. Radonjanin, M. Malešev, S. Marinković, and A. E. S. A. Malty, "Green recycled aggregate concrete," *Construction and Building Materials,* vol. 47, pp. 1503-1511, 2013.

[10] V. Corinaldesi and G. Moriconi, "Influence of mineral additions on the performance of 100% recycled aggregate concrete," *Construction and Building Materials,* vol. 23, pp. 2869-2876, 2009.

[11] M. Etxeberria, E. Vázquez, A. Marí, and M. Barra, "Influence of amount of recycled coarse aggregates and production process on properties of recycled aggregate concrete," *Cement and Concrete Research,* vol. 37, pp. 735-742, May 2007.

[12] V. Corinaldesi, "Mechanical and elastic behaviour of concretes made of recycled-concrete coarse aggregates," *Construction and Building Materials,* vol. 24, pp. 1616-1620, 2010.

[13] A. S. Abdelfatah and S. W. Tabsh, "Review of research on and implementation of recycled concrete aggregate in the GCC," *Advances in Civil Engineering,* vol. 2011, 2011.

[14] M. P. Collins, D. Mitchell, P. Adebar, and F. J. Vecchio, "A general shear design method," *ACI structural journal,* vol. 93, pp. 36-45, 1996.

[15] R. C. Elstner and E. Hognestad, "Laboratory investigation of rigid frame failure," *Journal of the American Concrete Institute,* vol. 28, pp. 637-678, 1957.

[16] J. A. Ramirez and J. E. Breen, "Review of design procedures for shear and torsion in reinforced and prestressed concrete," The Center1983.

[17] J. A. Ramirez, C. W. French, P. E. Adebar, J. F. Bonacci, M. P. Collins, D. Darwin*, et al.*, "Recent approaches to shear design of structural concrete," *Journal of Structural Engineering,* vol. 124, pp. 1375-1417, 1998.

[18] A. P. Clark, "Diagonal tension in reinforced concrete beams," in *ACI Journal Proceedings*, 1951, pp. 145-156.

[19] A. C. I. Committee, *Building code requirements for reinforced concrete (ACI 318-63)*. Detroit, Mich.: American Concrete Institute, 1963.

[20] A. C. I. Committee, *Building code requirements for reinforced concrete (ACI 318-71)*. Detroit: American Concrete Institute, 1972.

[21] A. C. I. Committee, *Building code requirements for reinforced concrete (ACI 318-77)*. Detroit, Mich.: American Concrete Institute, 1977.

[22] E. d. S. Sanchez Filho, M. d. S. Lima Velasco, H. Silva Filho, and J. Julio, "Effective capacity of diagonal strut for shear strength of reinforced concrete beams without shear reinforcement discussion," *ACI Structural Journal,* vol. 110, pp. 149-149, 2013.

[23] G. Kani, "The riddle of shear failure and its solution," in *ACI Journal Proceedings*, 1964, pp. 441-468.

[24] R. Fenwick and T. Pauley, "Mechanism of shear resistance of concrete beams," *Journal of the Structural Division,* vol. 94, pp. 2325-2350, 1968.

[25] F. J. Vecchio and M. P. Collins, "The modified compression-field theory for reinforced concrete elements subjected to shear," *ACI Journal,* vol. 83, pp. 219-231, 1986.

[26] W. Ritter, "Die bauweise hennebique," *Schweizerische Bauzeitung,* vol. 33 (7) (1899), pp. 59–61, 1899.

[27] M. P. Collins and D. Mitchell, "Shear and torsion design of prestressed and non-prestressed concrete beams," *PCI journal,* vol. 25, pp. 32-100, 1980.

[28] B. Martín-Pérez and S. J. Pantazopoulou, "Effect of bond, aggregate interlock and dowel action on the shear strength degradation of reinforced concrete," *Engineering Structures,* vol. 23, pp. 214-227, 2001.

[29] K.-H. Reineck, "Ultimate shear force of structural concrete members Without Transverse Reinforcement Derived From a Mechanical Model (SP-885)," *Structural Journal,* vol. 88, pp. 592-602, 1991.

[30] J. Schlaich, K. Schäfer, and M. Jennewein, "Toward a consistent design of structural concrete," *PCI journal,* vol. 32, pp. 74-150, 1987.

[31] J. Walraven and N. Lehwalter, "Size effects in short beams loaded in shear," *ACI Structural Journal-American Concrete Institute,* vol. 91, pp. 585-593, 1994.

[32] J.-W. Park and D. Kuchma, "Strut-and-Tie model analysis for strength prediction of deep beams," *ACI Structural Journal,* vol. 104, pp. 657-661,663-666, Nov/Dec 2007.

[33] H. Wagner, "Flat sheet metal girders with very thin metal web," *Z. Flugtechn. Motorluftschiffahrt,* vol. 20, pp. 200-314, 1929.

[34] D. Mitchell and M. P. Collins, "Diagonal compression field theory—A rational model for structural concrete in pure torsion," *ACI Journal,* vol. 71, pp. 396-408, 1974.

[35] M. P. Collins, "Towards a rational theory for RC members in shear," *Journal of the Structural Division,* vol. 104, pp. 649-666, 1978.

[36] B. González-Fonteboa and F. Martínez-Abella, "Shear strength of recycled concrete beams," *Construction and Building Materials,* vol. 21, pp. 887-893, April 2007.

[37] A. B. Ajdukiewicz and A. T. Kliszczewicz, "Comparative tests of beams and columns made of recycled aggregate concrete and natural aggregate concrete," *Journal of Advanced Concrete Technology,* vol. 5, pp. 259-273, 2007.

[38] G. Fathifazl, A. G. Razaqpur, O. B. Isgor, A. Abbas, B. Fournier, S. Foo*, et al.*, "Shear strength of reinforced recycled concrete beams without stirrups," *Magazine of Concrete Research,* vol. 62, pp. 853-856, 2010.

[39] S. Schubert, C. Hoffmann, A. Leemann, K. Moser, and M. Motavalli, "Recycled aggregate concrete: Experimental shear resistance of slabs without shear reinforcement," *Engineering Structures,* vol. 41, pp. 490-497, 2012.

[40] O. C. Lian, L. S. Wee, M. Masrom, and G. C. Hua, "Experimental Study on Shear Behaviour of High Strength Reinforced Recycled Concrete Beam," *Pertanika Journal of Science & Technology,* vol. 21, pp. 601-610, 2013.

[41] M. Arezoumandi, A. Smith, J. S. Volz, and K. H. Khayat, "An experimental study on shear strength of reinforced concrete beams with 100% recycled concrete aggregate," *Construction and Building Material,* vol. 53, pp. 612-620, 2014.

[42] Z. P. Bažant and Q. Yu, "Designing Against Size Effect on Shear Strength of Reinforced Concrete Beams Without Stirrups: I. Formulation," *Journal of Structural Engineering,* vol. 131, pp. 1877-1885, 2005.

[43] O. J. Gastebled and I. M. May, "Fracture mechanics model applied to shear failure of reinforced concrete beams without stirrups," *Structural Journal,* vol. 98, pp. 184-190, 2001.

[44] S. Xu, X. Zhang, and H. W. Reinhardt, "Shear capacity prediction of reinforced concrete beams without stirrups using fracture mechanics approach," *ACI Structural Journal,* vol. 109, pp. 705-713, Sep/Oct 2012.

[45] A. M. Knaack and Y. C. Kurama, "Behavior of reinforced concrete beams with recycled concrete coarse aggregates," *Journal of Structural Engineering,* vol. 12, pp. 401-409, 2014.

[46] V. Prakash, G. Powell, and S. Campbell. (1993, June). *DRAIN-2DX: Static and dynamic analysis of inelastic plane structures.* Available: https://nisee.berkeley.edu/elibrary/Software/DRAIN2DXZIP

[47] M. Arezoumandi, J. Drury, J. S. Volz, and K. H. Khayat, "Effect of recycled concrete aggregate replacement level on shear strength of reinforced concrete beams," *ACI Materials Journal,* vol. 112, pp. 559-568, 2015.

[48] K. Rahal and Y. Alrefaei, "The shear strength of 50 MPa concrete beams made using recycled concrete coarse aggregates," ed: ISEC Press, 2015, pp. p 601-605.

[49] K. Sang-Woo, J. Chan-Yu, L. Jin-Seop, and K. Kil-Hee, "Size effect in shear failure of reinforced concrete beams with recycled aggregate," *Journal of Asian Architecture and Building Engineering,* vol. 12, pp. 323-330, 2013.

[50] Z. H. Deng, Y. Liao, C. L. Meng, and H. F. Yang, "Experimental study on the shearing property of equal strength recycled coarse aggregate concrete," *Applied Mechanics and Materials,* vol. 357, pp. 1420-1427, 2013.

[51] H. Choi, C. Yi, H. H. Cho, and K. I. Kang, "Experimental study on the shear strength of recycled aggregate concrete beams," *Magazine of Concrete Research,* vol. 62, pp. 103-114, 2010.

[52] F. Al-Zahraa, M. T. El-Mihilmy, and T. Bahaa, "Experimental investigation of shear strength of concrete beams with recycled concrete aggregates," *International Journal of Materials and Structural Integrity,* vol. 5, pp. 291-310, 2011.

[53] E. E. Ikponmwosa and M. A. Salau, "Shear capacity of reinforced concrete beams using recycled coarse aggregates," in *TMS 2011 - 140th Annual Meeting and Exhibition*, 2011, pp. 419-426.

[54] W.-l. Wang, S.-c. Kou, and F. Xing, "Deformation properties and direct shear of medium strength concrete prepared with 100% recycled coarse aggregates," *Construction and Building Materials,* vol. 48, pp. 187-193, 2013.

[55] F. Yu and C. Yin, "Study on the recycled concrete beam's shear," in *2015 Seventh International Conference on Measuring Technology and Mechatronics Automation*, 2015, pp. 1087-1090.

[56] A. C. I. Committee, *Building Code Requirements for Structural Concrete (ACI 318M-14)*. Detroit, Mich: American Concrete Institute, 2014.

[57] C. S. Association, *Design of concrete structures*: Canadian Standard Association, 2004.

[58] E. B. Professor Michael P. Collins. (25th, May). *Response-2000 Program*. Available: http://www.ecf.utoronto.ca/~bentz/r2k.htm

[59] A. B. Matamoros and K. H. Wong, "Design of simply supported deep beams using strut-and-tie models," *ACI Structural Journal,* vol. 100, pp. 704-712, 2003.

[60] M. Casuccio, M. C. Torrijos, G. Giaccio, and R. Zerbino, "Failure mechanism of recycled aggregate concrete," *Construction and Building Materials,* vol. 22, pp. 1500-1506, 2008.

[61] J.-w. Park and D. Kuchma, "Strut-and-Tie Model Analysis for Strength Prediction of Deep Beams," *ACI Structural Journal,* vol. 104, pp. 657-661,663-666, Nov/Dec 2007.

[62] A. Shah, "Evaluation of shear strength of high strength concrete beams," PhD Thesis, University of Engineering & Technology Taxila-Pakistan, 2009.

APPENDIX A: Sample Photos from Laboratory Tests

Figure A.1: Beam NA-L-1-HR

Figure A.2: Beam NA-L-1-LR

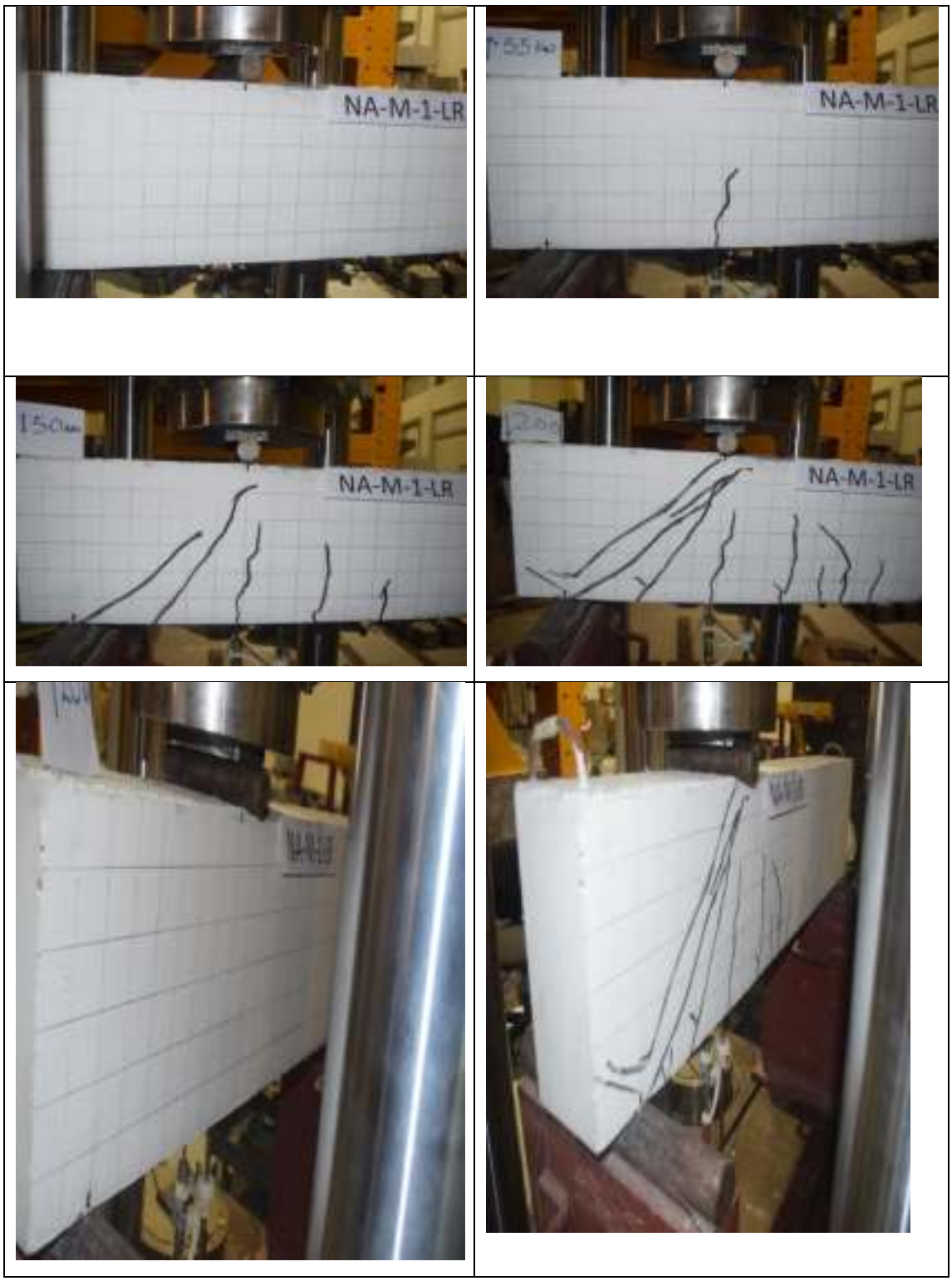

Figure A.3: Beam NA-M-1-LR

Figure A.4: Beam R50-L-1-HR

Figure A.5: Beam R50-L-1-LR

Figure A.6: Beam R50-M-1-LR

Figure A.7: Beam R100-L-1-HR

Figure A.8: Beam R100-L-1-LR

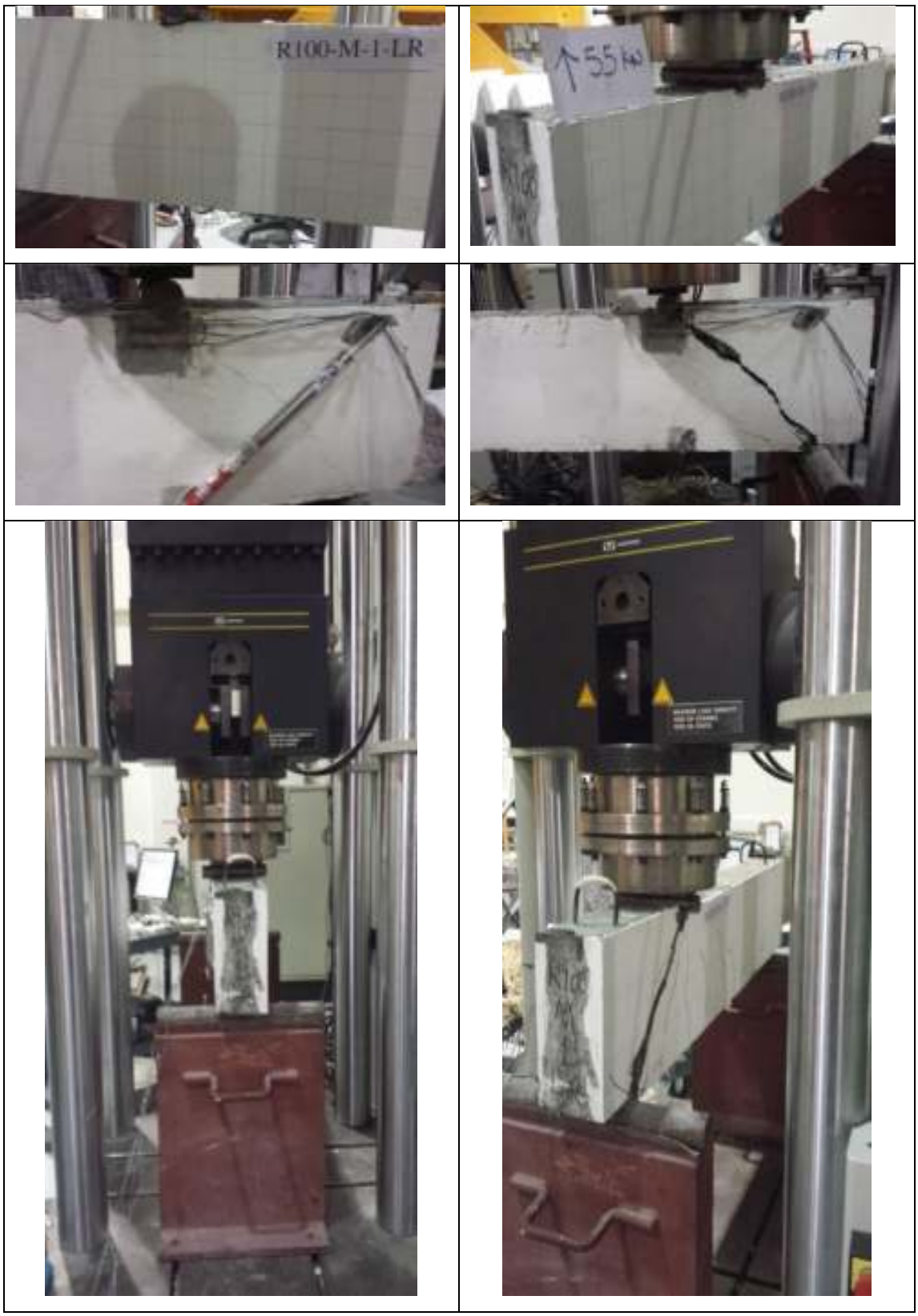

Figure A.9: Beam R100-M-1-LR

Figure A.10: Beam NA-L-2.5-LR

Figure A.11: Beam NA-M-2.5-LR

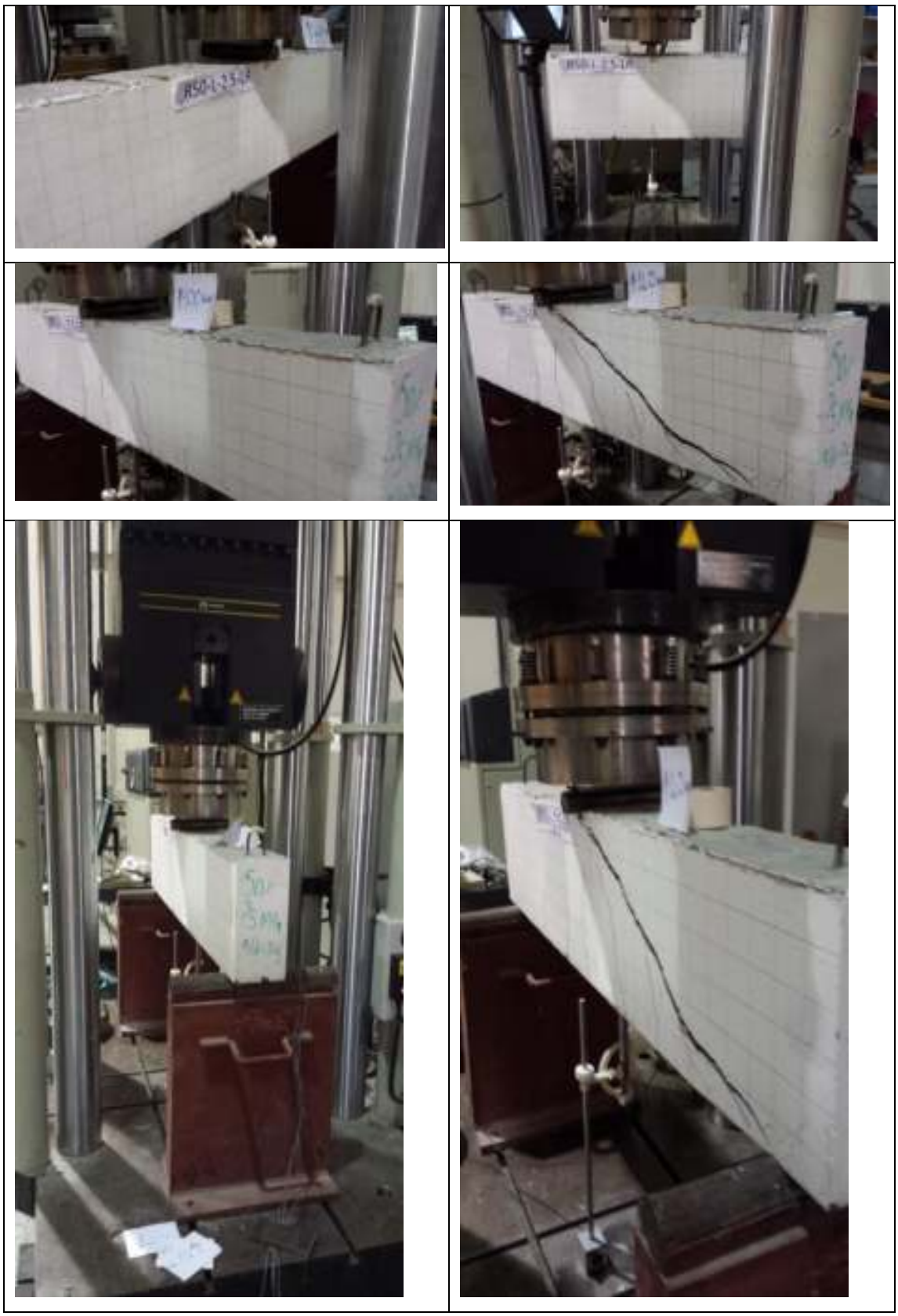

Figure A.12: Beam R50-L-2.5-LR

Figure A.13: Beam R50-M-2.5-LR

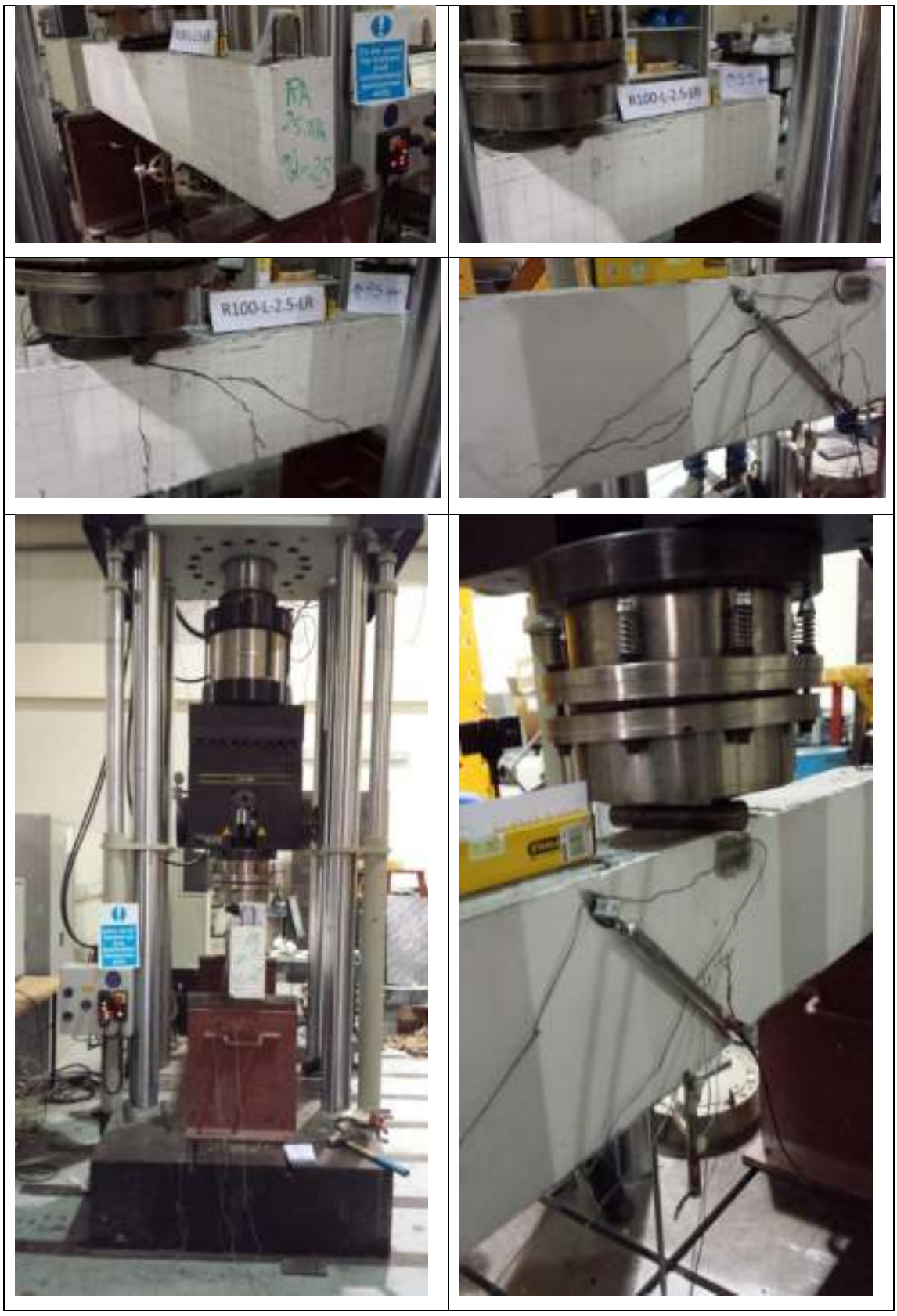

Figure A.14: Beam R100-L-2.5-LR

Figure A.15: Beam R100-M-2.5-LR

APPENDIX B: Sample Calculations

ACI 318-14

Beam NA-L-1-HR

$$V_c = \left(0.16\lambda\sqrt{f'_c} + 17\,\rho_w\left(\frac{V_u d}{M_u}\right)\right) b_w d \;\leq 0.29\lambda\sqrt{f'_c}\, b_w d$$

$$f'_c = 30.55\ MPa$$

$$\rho_w = 0.016$$

d = 259*mm* for beams with ρ=1.03%, and d = 257*mm* for beams with ρ=1.6%

$$\frac{V_u d}{M_u} = \frac{0.76P * 257}{228P} = 0.8567 < 1$$

$$V_c = \left(0.16 * 1 * \sqrt{30.55} + 17 * 0.016 * 0.8567\right) * 150 * 257 = 43074.82\ N$$

$$V_c = 43.07\ kN$$

CSA 23.3-04

Beam NA-L-1-HR

$$\mathrm{V_c} = \beta\sqrt{\mathrm{f'_c}}\,\mathrm{b_w d_v}$$

$$f'_c = 30.55\ MPa$$

$$\mathrm{d_v} = \max(0.9\mathrm{d}, 0.72\mathrm{h})$$

$$\mathrm{d_v} = \max(0.9 * 257, 0.72 * 300) = 231.3\ mm$$

$$\varepsilon_x = \frac{\mathrm{M_u/d_v + V_u}}{2(\mathrm{E_s A_s})} = \frac{228P/231.3 + 0.76P}{2*(200000*628.32)}$$

$$\mathrm{s_{ze}} = \frac{35\mathrm{s_z}}{15+\mathrm{a_g}} = \frac{35*231.3}{15+20} = 231.3 \;\geq\; 0.85\,\mathrm{s_z} = 196.6$$

Assuming P= 63950 N

$$\varepsilon_x = 0.0004442$$

$$\beta = \frac{0.4}{(1+1500*0.0004442)}\,\frac{1300}{(1000+231.3)} = 0.253446504$$

$V_c = 0.253446504\sqrt{30.55} * 150 * 231.3 = 48602.52\ \text{N} = 48.60\ kN$

which can be converted to load (P) again:

P= $V_c/0.76$ = 63950.7 N as assumed.

Response-2000 Software

Beam NA-L-1-HR

Figure B.1: General definition

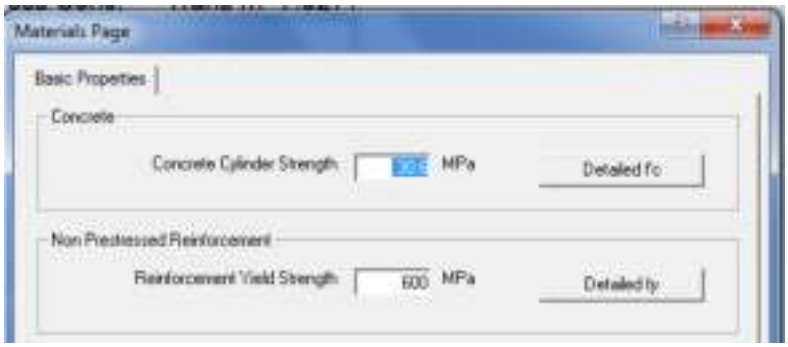

Figure B.2: Material definition

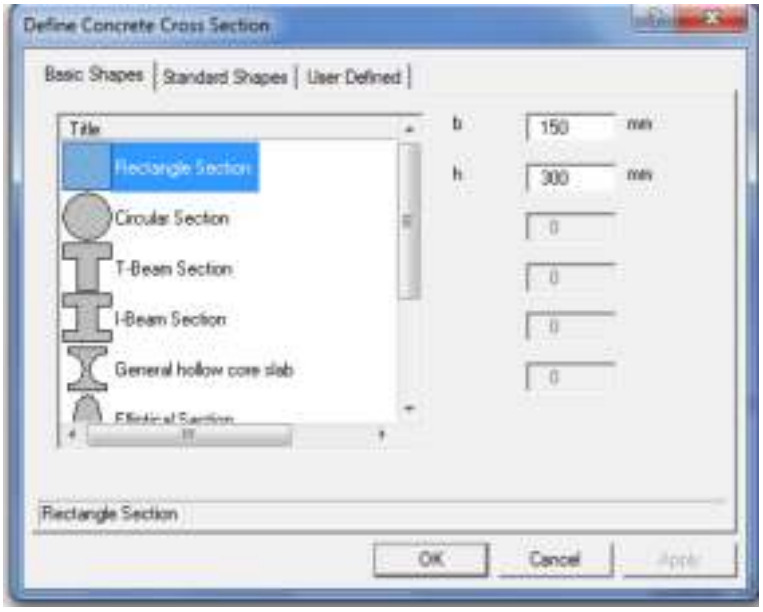

Figure B.3: Cross-section definition

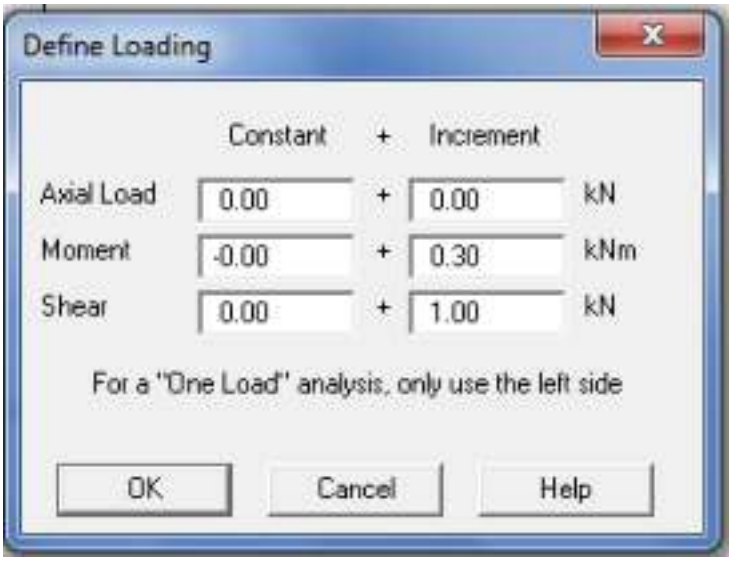

Figure B.3: Loads definition

The results were obtained by using Sectional Response from the menu ‘Solve’. The overall properties of the defined beam are presented in Figure B.4. Results are presented in Figure B.5 utilizing the nine-graph window in the software.

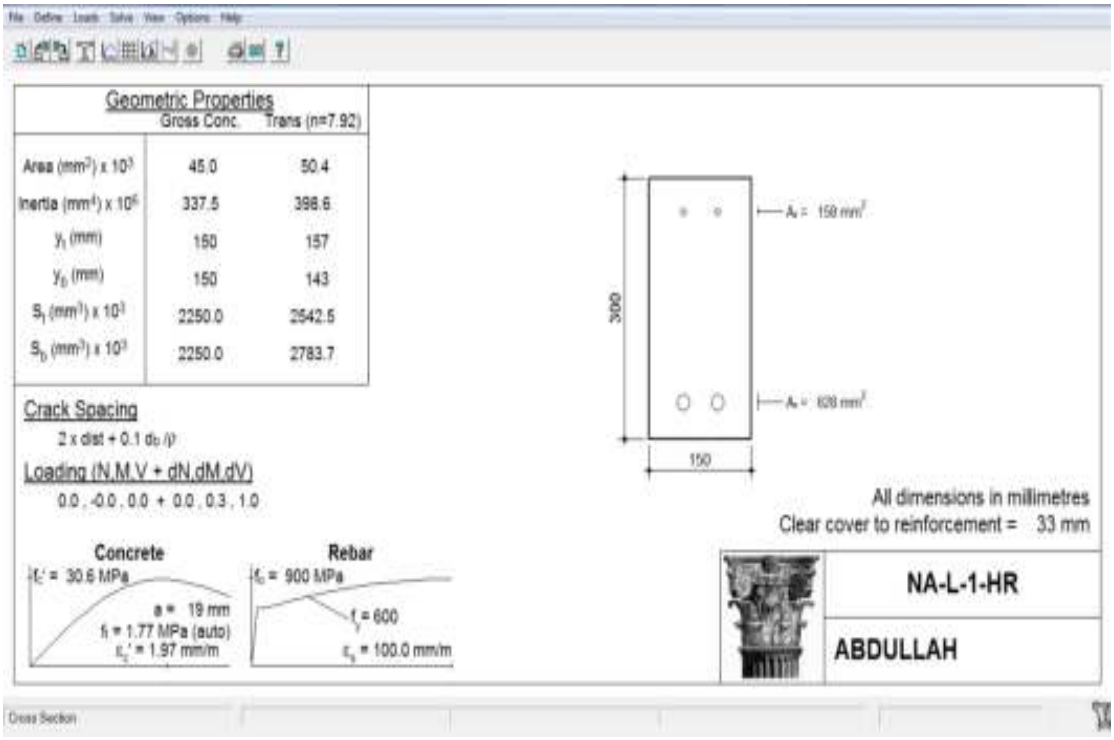

Figure B.4: NA-L-1-HR properties.

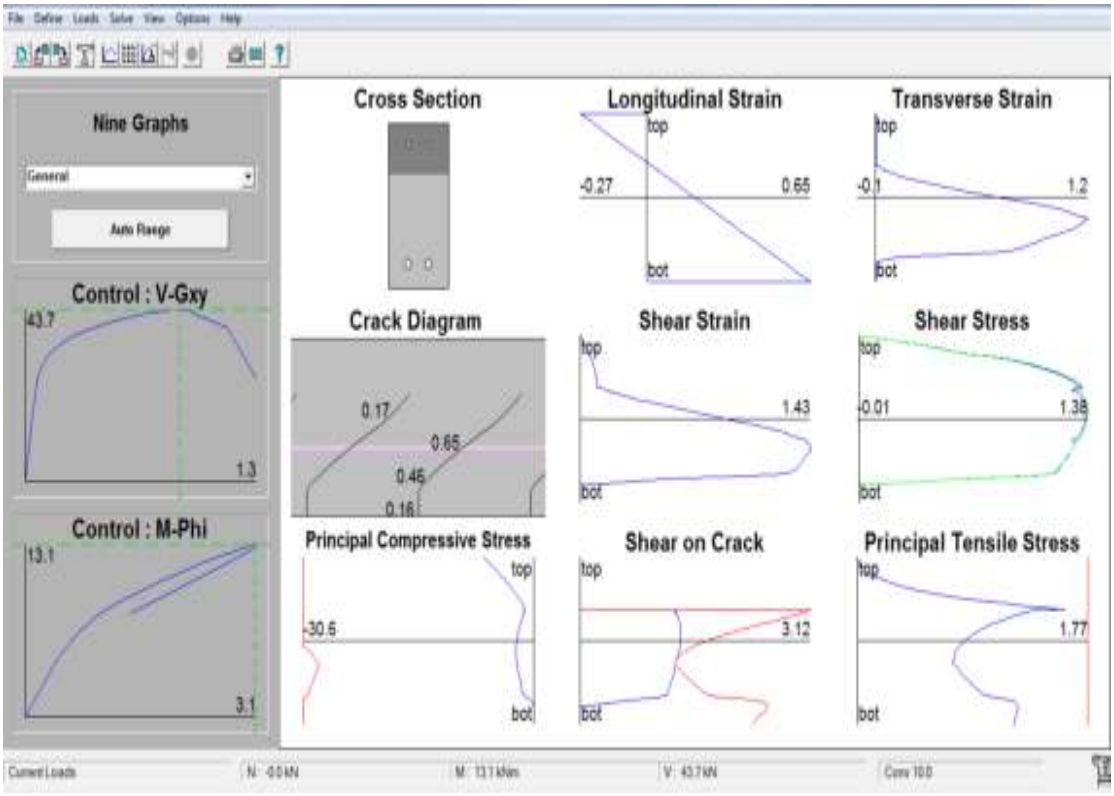

Figure B.5: NA-L-1-HR results

Strut-and-tie model

Beam NA-L-1-HR

$\theta = tan^{-1}(\mathrm{d/a}) = tan^{-1}(257/300) = 40.59°$

$\mathrm{C_c} = \frac{0.3}{\mathrm{a/d}} = \frac{0.3}{300/257} = 0.257 < 0.85\ \sin\theta = 0.553$

$\mathrm{l_b} = 100\ mm$

$\mathrm{h_a} = 2 * 33 = 66\ mm$

$\mathrm{F_{strut}} = \mathrm{f'_c A} = \mathrm{f'_c}(\mathrm{l_b}\sin\theta + \mathrm{h_a}\cos\theta)\mathrm{b}$

$\mathrm{F_{strut}} = 30.55 * \big(100 * \sin(40.59) + 66 * \cos(40.59)\big) * 150 = 527828.71\ \mathrm{N}$

also, $\mathrm{C_c} = \frac{\mathrm{P_{max}}}{\mathrm{F_{strut}}}$, so:

$\mathrm{P_{max}} = \mathrm{C_c} * \mathrm{F_{strut}} = 0.257 * 527828.71 = 135651.98\ N$

thus,

$V_C = 0.76 * \mathrm{P_{max}} = 103095.5\ N = 103.09\ kN$

Fracture Mechanics Method

Beam NA-L-1-HR

1- Bazant and Yu Model

$$\mathrm{V_c} = 10\rho^{\frac{3}{8}}\left(1 + \frac{\mathrm{d}}{\mathrm{a}}\right)\sqrt{\frac{\mathrm{f'_c}}{1 + \frac{\mathrm{d}}{\mathrm{f'_c}^{-\frac{2}{3}}\,3800\sqrt{\mathrm{d_a}}}}}\ \mathrm{b_w d}$$

The units in this expression are in US system units.

$f'_c = 30.55\ MPa = 4430.91\ psi$

a = 300*mm* = 11.8*in*

d= 257mm = 10.1in

$d_a = 20mm = 0.77in$

$$\mathrm{V_c} = 10(0.016)^{\frac{3}{8}}\left(1+\frac{10.1}{11.8}\right)\sqrt{\frac{4430.91}{1+\frac{10.1}{4430.91^{\frac{2}{3}}\,3800\sqrt{0.77}}}}\;5.90551 * 10.1$$

$$\mathrm{V_c} = 15447.8\ \mathrm{lb}$$

$$\mathrm{V_c} = 15447.8 * 4.448222 = 68715.2\ \mathrm{N} = 68.72\ \mathrm{kN}$$

2- Gastebled and May Model

$$V_c = \frac{1.019}{\sqrt{d}}\left(\frac{d}{a}\right)^{\frac{1}{3}}\rho^{\frac{1}{6}}\left(1-\sqrt{\rho}\right)^{\frac{2}{3}}f'^{0.35}_{c}\sqrt{E_s}b_w d$$

where 'a', 'd' and 'b' are in meters and f'_c in (*MPa*). E_s is the reinforcement steel modulus of elasticity (*MPa*)

$$V_c = \frac{1.019}{\sqrt{0.257}}\left(\frac{0.257}{0.300}\right)^{\frac{1}{3}}\ 0.016^{\frac{1}{6}}\left(1-\sqrt{0.016}\right)^{\frac{2}{3}}(30.55)^{0.35}\sqrt{200000} * 0.15 * 0.257$$

$$V_c = 54.37\ kN$$

3- Xu et al. Model

$$\mathrm{V_c} = \frac{1.018}{\sqrt{\mathrm{d}}}\left(\frac{\mathrm{d}}{\mathrm{a}}\right)^{\frac{1}{3}}\ \rho^{\frac{1}{6}}\left(1-\sqrt{\rho}\right)^{\frac{2}{3}}(0.0255\mathrm{f'_c}+0.24)\mathrm{b_w d}$$

$$\mathrm{V_c} = \frac{1.018}{\sqrt{0.257}}\left(\frac{0.257}{0.30}\right)^{\frac{1}{3}}\ 0.016^{\frac{1}{6}}\left(1-\sqrt{0.016}\right)^{\frac{2}{3}}(0.0255 * 30.55+0.24)0.15 * 0.257$$

$$\mathrm{V_c} = \ 68.09\ kN$$

Vita

Abdullah Mohsin Sagher was born in Hama, Syria in May 1988. He moved to United Arab Emirates at the age of eleven years. He studied in local public schools in Abu Dhabi and graduated from Al Mutanabi High school in 2006. He moved back to Syria to study in Al Baa'th University in Homs, and graduated with Bachelor of Science degree in Civil Engineering in July 2011.

Mr. Abdullah moved back to UAE and worked as professional engineer in construction companies before joining the master program in the American university of Sharjah in February 2014. He was awarded a graduate teaching assistantship.